UNIVERSITY OF TUSCIA, ITALY

DEPARTMENT OF ECOLOGICAL AND BIOLOGICAL SCIENCES

(DEB)

PhD course in

Ecology and Sustainable Management of Environmental Resources

Curriculum: Environment, Adaptation and Healthy

XXXI Course

(s.s.d. BIO/11)

Omics profiles of Cancer Stem Cells in Pancreatic ductal adenocarcinoma, an environmental influenced cancer

PhD student

Giuseppina Fanelli

Coordinator of PhD course

Prof.ssa Roberta Cimmaruta

Tutors

Prof.ssa Anna Maria Timperio

Prof. Lello Zolla

A.Y. 2018/2019

Ai miei genitori

Aims

Pancreatic ductal adenocarcinoma (PDAC) is the most common type of pancreatic neoplasm, accounting for more than 85% of pancreatic tumor cases. It is estimated that only 5% to 10% of pancreatic cancer cases are hereditary, and the remaining 90% to 95% are due to environmental risk factors, which are largely modifiable. Among the external factors, nutrition plays a crucial role in the development of cancer. It is been estimated that approximately 50% of pancreatic cancer cases may be attributed to diet. Recently, the frontier of cancer research has shown that energy metabolism, especially lipid metabolism, is significantly elevated during carcinogenesis. The tumor cells increase the uptake of exogenous (or dietary) lipid or activate de novo lipid synthesis in obese individuals. Moreover reactivation of lipid biosynthesis is frequently observed in cancer tissue and these lipid metabolism dysfunctions promote cancer development, invasion and metastasis and lipid synthesis is now known as a feature of many cancer cells. However, despite the growing evidence of the importance of lipid metabolism in cancer biology, the exact role of these metabolic alterations in the development and maintenance of the disease is not fully understood. The complex interaction between oncogenic signaling and lipid metabolism and the broad spectrum of lipid functions at both the cellular and organic levels, underline the importance of a more detailed understanding of alterations of lipid metabolism in cancer. Targeting lipid metabolism can also offer new therapeutic strategies for cancer treatment. Indeed, although targeting tumor metabolism is still in the early days of translation to patients, the improvement of knowledge of deranged metabolic pathways, in particular in cancer stem cells, will accelerate the development of novel therapeutic strategies. It is now universally accepted that metastasis, chemi-resistance and PDAC disease relapse are driven by a subpopulation of highly plastic "stem cells" within the tumor known as cancer stem cells (CSCs). CSCs are small subpopulations of quiescent cells (0.001-0.1%) of cancer cells that are found in the tumor.

The aim of this thesis is to investigate metabolic changes of cancer stem cells (Panc CSCs) of pancreatic ductal adenocarcinoma (PDAC), with particular attention to lipid metabolism.

This study is essentially addressed through "omics" approaches with the purpose of obtaining clearer evidence of the effective involvement of these nutrients in the molecular bases of neoplastic diseases. Moreover in order to develop CSC-targeted therapies, new formulations were investigated demonstrating increases its anti-proliferative activity on pancreatic CSCs. Although targeting tumour metabolism is still in the early days of translation to patients, the improvement of knowledge of deranged metabolic pathways, in particular in cancer stem cells, will accelerate the development of new therapeutic strategies.

Summary

1. Nutrition and cancer

Cancer is a group of over 100 diseases characterized by uncontrolled cell growth as a result of changes in cell genetic information (World Cancer Research Fund, 2007). The development of cancer requires a series of cellular changes. No single gene causes cancer but more factors influence its onset. It is a multi-step process caused by errors accumulated in the genes that control cellular processes. In fact, during the carcinogenesis, a normal cell turns into cancerous acquiring different phenotypic characteristics due to alterations of the genotype. Most cancers become clinically identifiable only years or decades after initial DNA damage. It is now well established that tumors are the combination of both external factors such as the environment and genetics factor (Parsa, 2012). Basically, the incorrect lifestyle and environmental factors are the cause of the development of 90-95% of all tumors (Deng et al., 2016) while the genetic factors represent only 5%.

Among the external factors, nutrition plays a crucial role in the development of cancer (Figure 1). For example, lifestyle-related changes in the body mass index (BMI), a measure of adiposity, are associated with an increased risk of cancer. Excess body weight, both in overweight people (defined as a body mass index [BMI] from 25 to 29 kg/m^2) or obese (BMI of 30 kg/m^2 or higher), is increasingly recognized as an important risk factor for some common cancers (Renehan et al., 2008). In fact, it is estimated that 3.6% of all new cancer cases worldwide, especially liver cancer, pancreatic cancer, non-Hodgkin's lymphoma and myeloma (Calle et al., 2003), are due to excessive adiposity (Goodwin and Chlebowski, 2016). It has also been estimated by the American Institute for Cancer Research and the World Cancer Research Fund that 30-40% of all cancers can be prevented with appropriate diets, physical activity, and proper body weight maintenance (Wolin et al., 2010). Obesity is a state of chronic subclinical inflammation which is a central component of the development and progression of the tumor, as multiple inflammatory cells and mediators are found in the tumor microenvironments, where they can function to support proliferative signaling, activate migration and metastases and promoting angiogenesis (Deng et al., 2016).

Recently, the frontier of cancer research has shown that energy metabolism, especially lipid metabolism, is significantly elevated during carcinogenesis. It is well known that lipid metabolism is a complex physiological process, involving lipid intake, synthesis and transportation, and so on. Lipids are mainly classified into two types: lipoid (e.g. phospholipids, glycolipids and sterols, etc.) and fat, such as triglycerides (TGs), and sterols also including cholesterol, sex hormones and vitamin D, etc.

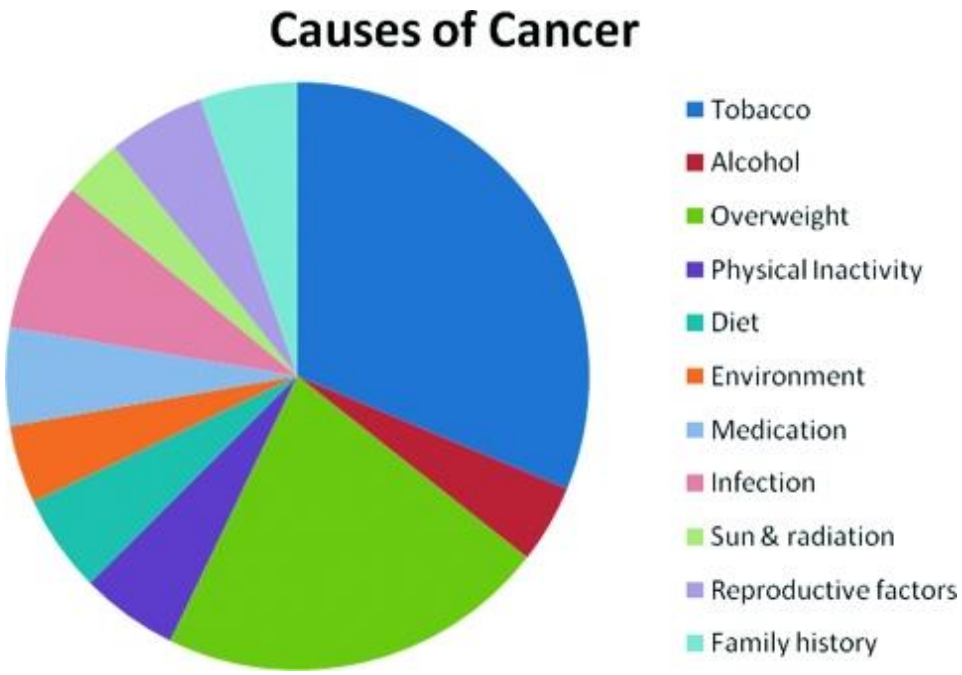

Figure 1: Estimated proportion of cancer in the U.S. that could have been avoided by changes in each category of non genetic cancer causes.

These lipids are digested, absorbed through small intestine, transformed by liver, stored in adipose tissue and subsequently served to other tissues when they are in need. TGs as important energy storage substance play a major role in energy supply, thermoregulation, and organism protection. Additionally, phospholipids as the main components of biofilm structures, they prevent cell membrane from damage, and promote TG metabolism and degradation of deposited cholesterol. Cholesterol is also the basic component of the cell membrane, maintaining the stability of phospholipids bilayer (Long et al., 2018).

The majority of adult mammalian tissues satisfy their lipid requirements through the uptake of free fatty acids (FFAs) and lipoproteins, such as low-density lipoprotein (LDL), from the bloodstream.

Fatty acid (FA) and cholesterol biosynthesis is restricted to a subset of tissues, including liver, adipose and lactating breast tissues. However, reactivation of lipid biosynthesis is frequently observed in cancer tissue (Javier, 2007) and this lipid metabolism dysfunctions promote cancer development, invasion and metastasis through multiple signaling pathways. Tumor cells proliferate rapidly and require a constant supply of lipids for membrane biogenesis and protein modifications. To support these increasing demands, depending on the metabolic status of the host, the tumor cells increase the uptake of exogenous (or dietary) lipid or activate de novo lipid synthesis in obese individuals (Daniëls et al., 2014). Activation of de novo lipid synthesis is now known as a feature of many cancer cells (Figure 2). The most important metabolic alterations in cancer are an increase in glucose uptake and the use of aerobic glycolysis, the so-called the Warburg effect. However, other metabolic processes, including protein, nucleic acid and lipid biosynthesis, are considered as part of the metabolic reprogramming associated with cancer. The alterations of the pathways associated with the synthesis of lipids and cholesterol in tumors are associated with a high expression of fatty acid synthase (FASN). In mammals, FASN is an enzyme that catalyzes the synthesis of endogenous long chain fatty acid. FASN converts diet carbohydrates into long-chain saturated fatty acids through acetyl-CoA, malonylCoA and nicotinamide adenine dinucleotide phosphate (NADPH). Excessive lipids and cholesterol in cancer cells are stored in lipid droplets (LDs), and high LDs and stored-cholesteryl ester content in tumors are now considered as hallmarks of cancer aggressiveness (Beloribi-Djefaflia et al., 2016). Moreover, accumulation of energy-rich lipids could provide cancer cells with energy during times of nutrient depletion (Baenke et al., 2013).

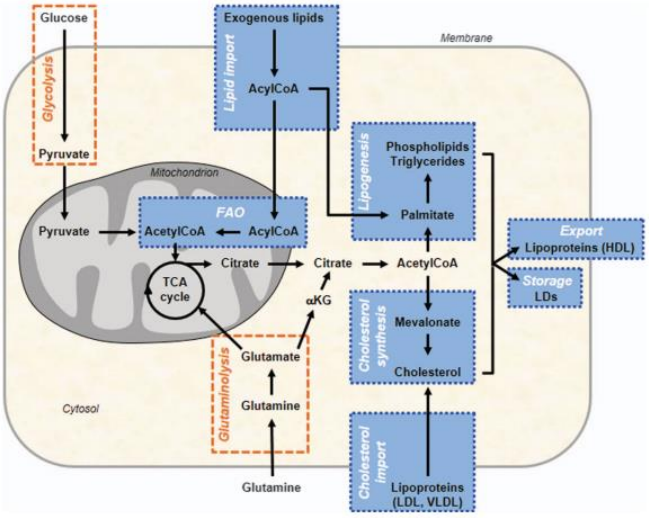

Figure 2: A simplified map of the main altered lipid metabolic pathways in cancer cells. Lipid metabolic network (blue) includes import/export and catabolic pathways (FAO) as well as de novosynthesis pathways, such as lipogenesis (that is, synthesis of TGs and PLs) and cholesterol synthesis.

Due to the diversity of their biological roles, lipids contribute to different aspects of the biology of tumors, such as growth, energy and redox homeostasis, as well as the spread of tumor cells to form distant metastases (Figure 3).

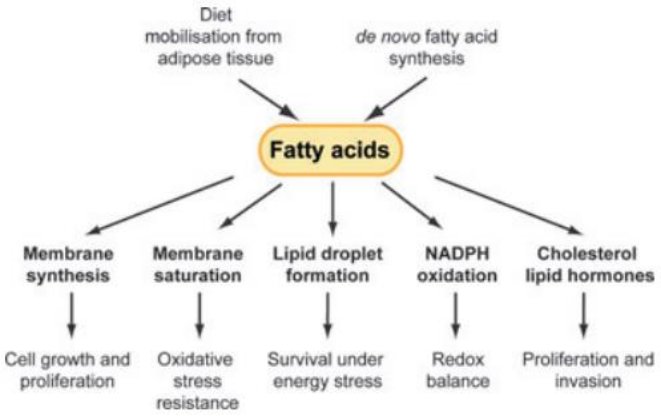

Figure 3. Lipids can promote different aspects of cancer development. Stimulation of fatty-acid synthesis by oncogenic signalling nand increased mobilization from adipose tissue as a consequence cachexia increase the availability of lipids in cancer cells. These may contribute to several aspects of the tumour phenotype, such as growth and proliferation, survival under oxidative and energy stress, support of a high-glycolytic rate by promoting redox balance and stimulation of signalling pathways that lead to proliferation and invasion.

However, despite the growing evidence of the importance of lipid metabolism in cancer biology, the exact role of these metabolic alterations in the development and maintenance of the disease is not fully understood. The complex interaction between oncogenic signaling and lipid metabolism and the broad spectrum of lipid functions at both the cellular and organic levels, underline the importance of a more detailed understanding of alterations of lipid metabolism in cancer. Targeting lipid metabolism can also offer new therapeutic strategies for cancer treatment (Santos and Schulze, 2013).

2. The omics sciences

Omics sciences, are the set of disciplines that study molecular mechanisms within cells. These "omics" technologies, increasingly used in the last two decades (Boja et al., 2014) have made it possible to clarify the different aspects of cells, improving the knowledge in molecular biology technologies.

The 'omics' science include four general areas: genomics, transcriptomics, proteomics and metabolomics. In fact the word omic is often used as a suffix, and the related prefix specifies the aspect of molecular biology that is investigated. For instance, genomics refers to a discipline that analyses the function and structure of genomes (the complete set of DNA within a single cell of an organism), while proteomics refers to the study of proteome, i.e. the whole set of proteins in an organism. However, while changes observed in the transcriptome or in the proteome do not always correspond to phenotypic alterations (increases in mRNA levels do not always correlate with increases in protein levels (Gygi et al., 1999), and once translated a protein may or may not be enzymatically active (Sumner et al., 2003), measurement of the metabolites or lipid synthesized by a biological system, constitutes an important complement to assess genetic function (Villa boas et al., 2005). Indeed metabolites and lipids, although chemically and physically diverse (e.g., molecular weight, polarity, acidity, stability, and function), represent the phenotypic state of a biological system (Ulmer et al., 2015).

In the related fields of proteomics, metabolomics and lipidomics, analysis with liquid chromatography combined with mass spectrometry (LC-MS) is becoming increasingly important as it improves the efficiency, sensitivity and reliability of targeted and non-targeted analyzes. Mass spectrometry (MS) represents a universal, sensitive tool that can be used to characterize and quantify a large number of compounds in a biological sample (Kaddurah-Daouket et al., 2008). By combining MS with liquid chromatography, molecular identification and quantification of polar, less-polar, and neutral metabolites can be achieved, even when they are present at relatively low concentrations levels and in a complex matrix (Villa boas et al., 2005) MS measure the mass-to-charge ratios (m/z)

of ions in order to determine their molecular weight (MW). This process involves several steps:

- ✓ The sample is delivered to the mass spectrometer via a chromatographic device (e.g. LC column)
- ✓ Ionization and vaporization of molecules into gas-phase ions by the ionization source;
- ✓ Ion separation by their m/z values via magnetic or electric fields through a component, namely mass analyzer;
- ✓ Detection of the separated ions as electric charge obtaining signals proportional to the abundance of each species and a plot of ion-abundance against m/z represents a ‘‘mass spectrum’’ (Griffiths and Wang, 2009) where in the x-axys represents m/z values, whereas the y-axis indicates total ion counts.

In many configurations, additional tandem MS analyses (MS/MS) are feasible. In the MS/MS mode, the instrument uses the first mass analyzer to select a single ion that is subsequently fired into a collision cell, where it collides with gas molecules such as argon (*e.g*., collision-induced dissociation, CID) causing the ion fragmentation.

As this extraordinary analytical technology can provide key information about analytes, including their structure, purity, and composition, mass spectrometric techniques are increasingly becoming accepted as a routine diagnostic tool in clinical laboratories (Tenori et al., 2012) as well as in industry and research field for various purposes such as drug discovery, diagnostics and bio-analyses (Di Girolamo et al., 2013).

2.1 Metabolomics

Metabolomics is the science that studies all metabolites (<1 kDa molecules) within a biological system. The metabolome represents the entire set of metabolites that belong to a wide variety of different classes, such as amino acids, lipids, organic acids, nucleotides, etc. (Dettmer et al., 2007) Metabolites are extremely diverse chemical compounds ranging from ionic inorganic species to hydrophilic carbohydrates, volatile alcohols and ketones, amine and non-amine organic acids, hydrophobic lipids and complex natural products (Villa boas et al., 2005). Being the intermediates or products of biochemical

reactions, the metabolites play a very important role in linking the different pathways that operate within a living cell. The level of the metabolites is determined by the concentration and properties of the enzymes, and their level is, therefore, a complex function of many different regulatory processes within the cell (Villa boas et al., 2005). Moreover metabolite distributions are subject to high temporal-spatial (circadian fluctuations) and biological variability (diet dependent) (Vigneau-Callahan et al., 2001). Metabolites are important indicators of physiological or pathological states: changes in metabolism result in alterations in the abundance of metabolites (Kobayashi et al., 2013) and elucidating the metabolomic changes that occur in a particular disease can provide information for the identification of biomarkers for a disease and help to understand its occurrence and progression (Nicholson and Wilson, 2003). Therefore, the metabolomics can improve the diagnosis of the disease and the understanding of pathological mechanisms (Tomita et al., 2012), becoming a useful tool for the identification of new biomarkers. It's able to act as an instrument early diagnostic (Nishiumi et al., 2010), using biofluids such as urine, blood and cells, as well as predicting treatment response and survival. Metabolomics, or metabolome analysis, involves two approaches, metabolite profiling and metabolic fingerprinting (Dettmer et al., 2007). In metabolite profiling, the selected metabolites in a particular environment are identified, and then, a quantitative or semi-quantitative assessment is performed. This approach is useful for understanding known metabolic pathways and biological alterations. On the other hand, metabolic fingerprinting is used to initially examine how metabolite patterns change in response to various stimuli, for example, diseases, toxic exposure, or environmental changes (Nishiumi et al., 2010). MS-metabolomics has the potential to generate novel noninvasive diagnostic tests, and provides a unique insight into established and novel metabolic pathways, while being simple and cost-effective yet retaining high sensitivity and specificity characteristic (Zhang et al., 2015). Mass spectrometry based small molecule profiling in conjunction with multivariate data analysis approaches is a powerful tool for analysis of the metabolome in disease making more realistic the possibility of a personalized medicine (Kaur et al., 2012): metabolomics become a tools for discover biomarkers that can reach the clinic to diagnose health, disease or the outcome of pharmacological treatment.

2.2 Lipidomics

Lipidomics is one of the prominent areas of metabolomics. Lipidomics can be defined as the comprehensive identification and quantification of all lipid molecular species in a biological system (Griffiths and Wang, 2009). Lipids are classes of molecules thought to be very important, not only as energy source or constituents of biological membrane, but also as functional molecules concerning the many regulation steps in biological process (Taguchi et al., 2000). Lipids are essential cellular constituents that have multiple distinct yet critical roles in cellular function. First, the majority (by mass) of cellular lipids form a membrane bilayer whose integrity and physical characteristics are vital for life processes. Second, lipids provide an appropriate hydrophobic environment for membrane protein function and interactions. Third, cellular lipids serve as reservoirs for energy storage, which can be rapidly accessed at times of demand. Finally, membrane lipids are the source of lipid second messengers generated by the actions of a variety of intracellular enzymes (Han and Gross 2004). Cellular lipids can be roughly classified into three large groups including non-polar lipids, polar lipids, and metabolites based on their relative polarities of the head group regions and/or their relative mass content (Han and Gross 2004):

- Non-polar lipids include predominantly cholesterol and cholesterol esters as well as TAGs
- Polar lipids are predominately comprised of phospholipids, sphingolipids (SLs) and glycolipids (GPLs). Based on different types of polar head groups, chain length of FAs, number of acyl-chains, degree of saturation in the acyl-chain, and number of double bonds, GPLs can be differentiated into several subclasses [24]: phosphatidic acid (PA), phosphatidylcholines (PC), phosphatidylethanolamine (PE), phosphatidylglycerol (PG), phosphatidylinositol (PI) and the last is phosphatidyloserine (PS). The polar lipids (GPLs, LPLs and SLs) are so involved in critical cell functions and they are the principal lipid class studied in lipidomic research. Bio-membranes are particularly rich in PC and PE. Similarly, SLs are essential bioactive compounds of cellular membrane, with important biological functions.

Based on the nature of the covalent linkage of polar moieties to ceramide (i.e.,N-acylsphingosine) the SLs include ceramides, cerebrosides, gangliosides, sphingomyelins (SMs) and sulfatides (STs). SL structure is formed by a sphingoid base backbone; the head group attached to the primary hydroxyl group, N-acyl group and sphingoid-base backbone determines a change in structure of SLs.

- The last group of lipids are lipid metabolites, which are derived by enzymatic action on ‘‘parent’’ lipids or their precursors. Metabolites can either be anabolic or catabolic in nature. Although this group of lipids are only a few percent of total common metabolites include long chain acyl-CoAs, long chain acylcarnitines, nonesterified fatty acids (NEFA), fatty acid esters, ceramides, lysolipids, eicosanoids, DAGs, sphingosine-3-phosphate, etc. Many of the metabolites are biologically active second messengers.

Lipidomics is focused on the identification of alterations in lipid metabolism and lipid-mediated signaling processes that regulate cellular homeostasis during health and disease. The research in lipidomics identifying and quantifying the lipids within the cell delineates the biochemical mechanisms through which the lipids interact with each other and with crucial proteins associated with the membrane. The usual strategy is to perform a lipid extraction with chloroform and methanol based on the Folch or modified method of Bligh and Dyer, and analyse the crude extract by ES-MS (Griffiths and Wang, 2009). Through the detailed quantification of a cell’s lipidome (e.g., lipid classes, subclasses, and individual molecular species), the kinetics of lipid metabolism, and the interactions of lipids with cellular proteins, lipidomics has already provided new information on the status of health and illness (Han and Gross 2004). Lipidomics is an emerging approach in tumor characterization for detecting and classifying neoplastic cells or tissues, as well as differentiating between a neoplasmic and normal environment. Moreover, this approach allows the evaluation of anticancer treatment, in terms of responsivity or resistance, and can be applied to the discovery of new tumor biomarkers. Integration of lipidomic strategies in cancer research could generate new opportunities to obtain insights into diagnosis, prognosis and prediction of tailored therapies (Perrotti et al., 2016).

3. Pancreatic ductal adenocarcinoma (PDAC)

Pancreatic cancer is one of the most lethal malignancies (Xie and Xie, 2015) and represents one of the leading causes of cancer related deaths world wide, reflected by an incidence of 277,668 new cases and almost the same mortality rate (266,029 cases) (Di Gangi et al., 2014). Pancreatic ductal adenocarcinoma (PDAC) is the most common type of pancreatic neoplasm, accounting for more than 85% of pancreatic tumor cases. In the USA, PDAC is the fourth most common cause of cancer (Giovannetti and Giaccone, 2014): there were an estimated 53,670 new diagnoses of PDAC in 2017 with 43,090 PDAC related deaths over the same year (Hosein and Beg, 2018). PDAC is the only cancer with increasing mortality rates for both men and women. Despite its low incidence rate, less than 2% of new cancers, it is among the leading causes of cancer related mortality as the vast majority of patients present with locally advanced or metastatic disease. PDAC is an epithelial tumor that arises from the cells of the pancreatic duct or ductules, for which it is named. In health, the pancreatic duct(s) serve as the conduit through which digestive enzymes and bicarbonate ion produced in acinar cells reach the small intestine. Ductal cells and acinar cells together represent the "exocrine" pancreas, from which the vast majority of pancreatic neoplasms arise (Stark and Eib, 2015).

The pancreas is divided into the following anatomic regions: the uncinate process, the head, the body, and the tail. In the context of PDAC, the anatomy may be simplified into two groups, namely the head of the pancreas (including the uncinate process) and the body/tail. Approximately, 60-70% of PDAC arise from the head of the pancreas, whereas 20-25% from the body/tail (Stark and Eib, 2015). The dramatic clinical course of PDAC is the result of the invariable metastatic behavior demonstrated along the progression of this malignancy. The 5-year survival rate for all stages of PDAC is only 8% (Giovannetti et al., 2017). Unfortunately PDAC is projected to become the 2nd leading cause of cancer death worldwide by 2030 surpassing colorectal cancer and breast cancer. (Rahib et al., 2014).

These awful statistics are partly attributed to the fact that 53% of pancreatic cancers are diagnosed metastatic and 28% with loco-regional disease, with survival rates of 2% and 11%, respectively (Sheahan et al., 2018). Metastasis is the spread of cancer cells from the primary tumor to distant sites. Cancer cells invade through their surrounding tissue (invasion), enter the bloodstream, either directly or through the lymphatic system (intravasation), migrate throughout the body and extravasate from the bloodstream into secondary sites (extravasation) (Steeg, 2016). The final step in this cascade is the acquired ability of micrometastatic deposits to form macroscopic metastases, a process often named colonization, and outgrow in organs at distant sites (McAllister and Weinberg, 2014). Metastasis is the leading cause of death in cancer patients especially in PDAC, where the dimension, number and growth rate of metastases have been correlated to worse outcome (Iacobuzio-Donahue et al., 2009), and explain why PDAC is one of the few cancers for which survival has not improved substantially over nearly 40 years. Indeed there has been little progress in the detection or treatment of this malignancy and it is still marked by a dismal prognosis with less than 10% of patients surviving 5 years after diagnosis (Hosein and Beg, 2018).

The poor prognosis of PDAC is related to several factors. First, no sensitive methods for screening are available in order to improve early detection in high-risk groups (Bruenderman and Martin, 2015). The use of imaging studies (e.g., abdominal Computed tomography (CT)), is inadequate because these techniques do not reliably detect pancreatic tumors <1–2 cm in size, so, at the moment, there is no effective method for early detection (Di Gangi et al., 2014). Furthermore there aren't a disease-specific biomarkers. Among the main biomarkers used there are:

- tumor markers: CA 19-9, CA-242, CA-50, CEA, CEACAM1,MIC1, MUC1, alpha-fetoprotein, DU-PAN-2 mAb, alpha4GnT;
- apoptosis markers: NF-kB, hTert and CK-19;
- cytokines, such as IL-8;
- adhesion molecules: ICAM-1, MMP-2, MMP-9; and, growth and angiogenesis factors, such as EGFR, IGFBP-1

Unfortunately, none of these markers has achieved sufficient levels of sensitivity and specificity to be recommended for screening asymptomatic patients in the general population, so the search for new biomarkers that would allow early detection of disease is still an open issue (Giovannetti et al., 2017). Various "omics" technologies (transcriptomics, proteomics, metabolomcs) have been used for biomarker discovery of pancreas cancer (Kaur et al., 2012) however as described below, metabolomics results to be particularly helpful in improving prognosis and therapy of PDAC, because it allows detection of metabolites that are involved in early and progression of disease.

Second, clinical presentation typically occurs very late in the history of the disease: the symptoms are often vague and nonspecific until the cancer has reached an advanced stage, making early detection extremely difficult. PDAC occurs over an extended period of time, and likely follows a stepwise progression similar to other carcinomas (colorectal carcinoma, in particular). This progression is characterized by the transition of a normal pancreatic duct to a pre-invasive precursor which can ultimately develop into an invasive PDA (Stark and Eib, 2015). Indeed histopathological studies on pancreatic neoplasms have identified three major precursor lesions, which have the potential to evolve into highly malignant and invasive pancreatic cancer (PDAC): pancreatic intraepithelial neoplasia (PanIN), mucinous cystic neoplasms (MCN), and intraductal papillary mucinous neoplasms (IPMN). PanIN is the most common precursor pancreatic lesion (Xie and Xie, 2015). Moreover patients with pancreatic cancer usually have generic symptoms and are often difficult to diagnose at an early stage (Ansari et al., 2012).

The most common symptoms of PDAC are pain and weight loss, and the most common clinical sign is jaundice. More specifically, one study reported the following frequency of sign and symptoms in patients with PDAC, in descending order (Porta et al., 2005):

- Weakness/fatigue (asthenia): 86%
- Loss of appetite (anorexia): 85%
- Weight loss: 85%
- Abdominal pain: 79%
- Dark urine: 59%
- Jaundice: 56%

- Nausea: 51%
- Back pain: 49%
- Diarrhea: 44%
- Vomiting: 33%

Signs and symptoms are often related to the location of the tumor. In general, tumors arising from the head of the pancreas come to clinical attention earlier than tumors arising from the body and tail, as the head of the pancreas contains the common bile duct. A tumor that obstructs the common bile duct leads to the phenomenon known as "painless jaundice" as bile constituents accumulate in the blood, often prompting an imaging study that will reveal the underlying tumor. In contrast, tumors of the body and tail do not produce jaundice, and therefore most often come to clinical attention later once weight loss and/or pain become apparent (Stark and Eib, 2015).

Finally, despite the approval of novel chemotherapeutic regimens, which led to a slight improvement of overall survival (OS), surgical resection remains the only potentially curative option for PDAC, but it is only possible in a small subset of patients (Chakraborty and Singh, 2013). Once a diagnosis of PDAC is confirmed or highly suspected, it is established if the tumor is potentially resectable, borderline resectable pancreatic cancer (BRPC), or unresectable, which exhibit venous involvement of superior mesenteric vein/portal-vein (SMV/PV) and gastroduodenal artery encasement, locally advanced and metastatic (Adamska et al., 2018). A tumor that is considered as resectable, is suitable for surgery with curative intent. Unfortunately, at the time of diagnosis, less than 20% of patients have a resectable tumour. For PDAC located in the head of the pancreas, a pancreaticoduodenectomy (also known as a "Whipple" procedure) is the only surgery of choice (Figure 4). The Whipple procedure is performed safely with perioperative mortality around 2% when performed by a surgeon in a high-volume center. However, between 30-40% of patients will endure a major complication, most commonly pancreatic fistula or delayed gastric emptying (Stark and Eib, 2015).

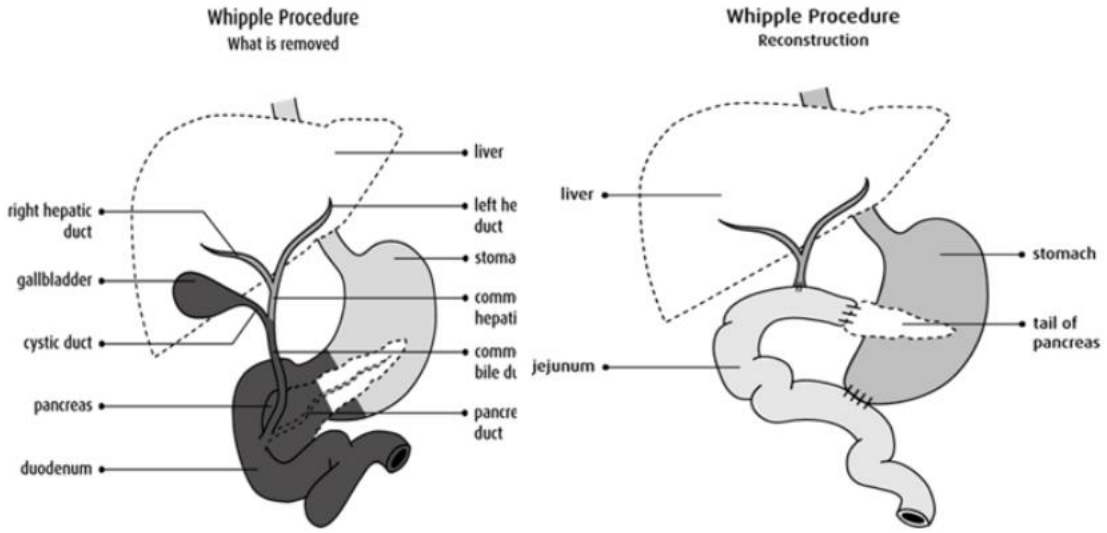

Figure 4: standard whipple procedure

Most patients are instead diagnosed with advanced-stage disease, characterized by infiltration of lymph-nodes and vasculature as well as metastasis to 2–3 distant organs (around 50% of diagnosed patients present with metastatic disease) such as liver, lungs and peritoneum (Iacobuzio-Donahue et al., 2009).

At this stage of the disease, retroperitoneal and perineural infiltration, haematogenic dissemination and angioinvasion are observed. In particular, cancers of the body and tail of the pancreas are often detected at the late stage and they usually present major vessels involvement, such as hepatic artery or celiac axis. Therefore, even despite the lack of metastasis, they are usually classified as unresectable. Furthermore, tumour heterogeneity and plasticity cause PDAC to develop chemoresistance (Adamska et al., 2018). The median survival of patients undergoing curative resection is significantly longer than for those with unresectable pancreatic cancer.

Over-activation of many signaling pathways involved in growth and proliferation, as well as altered expression of tumor suppressor genes, are regularly detected in PDAC, influencing cell proliferation, survival and invasion. The broad repertoire of genetic and metabolic remodeling allows PDAC to survive under harsh conditions and increases proliferative ability. Furthermore, recent analysis of gene expression and activity allowed

for classification of observed mutations into four distinct phenotypic subtypes that are defined as squamous, pancreatic progenitor, immunogenic and aberrantly differentiated tumor histopathological features and correlates with different prognosis. Classification of diagnosed patients into one of these four subtypes may provide substantial prognostic value and may be of great therapeutic relevance, allowing for more personalized treatments. Additionally, a dense, diffuse stroma called desmoplasia, is formed around the tumour, contributing to its resistance and influencing tumour progression and invasion. Physiologically, pancreatic stroma is essential to maintain pancreatic tissue homeostasis, as reflected by reciprocity among the cells in the pancreas and the surrounding microenvironment via communication with each other and the extracellular matrix (ECM) through junctions, receptors, hormones, and other soluble factors. Also, normal stroma may protect non-malignant pancreatic cells from developing into malignant cells (Xie and Xie, 2015). Tumor stroma comprises heterogeneous cellular and non-cellular components such as fibroblasts, blood vessels, immune cells, pancreatic stellate cells (PSCs), and the extracellular matrix (ECM) (Sunami et al., 2018). Stroma compartments can make up over 90% of the tumor mass, which drives the hypoxic tumor microenvironment. The pancreatic stellate cells (PSCs) have a key role in stroma formation. In addition to endogenous quiescent PSCs, bone marrow may also contribute to the population of activated PSCs. PSCs are involved in tumor growth, invasion, metastasis and resistance to radiochemotherapy (Ansari et al., 2012) hence alterations of the stroma are actively involved in pancreatic cancer development and progression. Several studies have supported the suppressive impact of normal stroma on pancreatic cancer.

Because effective systemic therapy capable of controlling the aggressive pancreatic cancer biology, is currently lacking, the need for a better understanding of detailed mechanisms underlying pancreatic cancer development and progression is vary urgent (Xie and Xie, 2015).

3.1 Risk factor

PDAC is associated to several risk factors, both inherited and non-inherited, and the characterization of these may contribute to an early diagnosis and identification of new biomarkers.

3.1.1 Inherited risk factors

Similar to other cancers, both activation of oncogenes and inactivation of tumor suppressor genes play key role in PDAC pathogenesis. The most frequent genetic alterations documented in PCs, including PDAC, are presented in Table 1. Approximately 5–10% of individuals with PDAC report a family history of the disease (Shi et al., 2009). *MYC*, proto-oncogene and major regulator of transcription in growing cells, controls several metabolic processes such as: gycolysis and glutaminolysis; nucleotide biosynthesis; lipid biosynthesis, and mitochondrial biogenesis. Furthermore, *MYC* stimulates glutamine uptake and metabolism. Mutations in four driver genes (*KRAS, P16/CDKN2A, TP53* and *SMAD4*) were well described as the most frequently altered genes in PDAC; activating mutations in the *KRAS* gene occur in the early stages, followed by inactivating mutations in the cyclin dependent kinase inhibitor 2A (*CDKN2A)* gene and in the *TP53* and *SMAD4* genes in the late stages of pancreatic carcinogenesis. Mutations of oncogenic *KRAS* occur almost universally in PDAC patients. Ras is a guanine nucleotide-binding protein that acts as a binary switch to activate several important cellular signaling pathways. Normally, Ras is loaded with GDP and is inactive until acted upon by guanine exchange factors (GEFs) that are under the control of receptors for a variety of growth factors, cytokines, and other signaling molecules. GEFs exchange GDP to GTP allowing Ras to be active and able to stimulate downstream pathways. Downstream signaling pathways, stimulated by active Ras, which are important in cell growth, differentiation and cell survival include phosphoinositide 3-kinase, mitogen-activated protein kinase (MAPK) and Ral (Philip et al., 2013). The consequence of *KRAS* mutations is among others, the constitutive activation of the Ras/MAPK signaling pathway, resulting in uncontrolled cellular proliferation (Bailey et al., 2016). Mutations in the *CDKN2A* gene are identified in up to 90% of PDACs, resulting in the loss of the p16 protein (Bailey et al., 2016, Hidalgo, 2010,

Yachida et al., 2016). This protein is widely known as an essential regulator of the G1/S checkpoint. Therefore, *CDKN2A* mutations lead to the disruption of the G1/S checkpoint machinery and to corresponding increase in cell proliferation. About 75% of PDACs have inactivating mutations in the TP53 gene involved in the regulation of bioenergetic homeostasis and lipid metabolism in both normal and cancer cells. The p53 inactivation allows cells to bypass cell cycle checkpoints and evade apoptotic signals and it also contributes to genomic instability. Furthermore, mutations in the SMAD4 gene are detected in 30–50% of pancreatic tumors, leading to the aberrant activity of the transforming growth factor beta (TGFβ) signaling pathway (Bailey et al., 2016, Hidalgo 2010). Genomic analyses revealed that aberrations that fuel PDAC tumorigenesis and progression, such as SMAD4 loss, are also implicated in metastasis (Giovannetti et al., 2017).

Oncogene/tumor suppressor	Metabolic pathway	Enzyme
MYC	Glucose transport	GLUT1
	Glycolysis	Hexokinase 2
		Phosphohexose isomerase
		Phosphofructokinase 1
		Aldolase A
		3-phosphoglyceraldehyde dehydrogenase
		Phosphoglycerate kinase
		Phosphoglycerate mutase
		Enolase 1
		Pyruvate kinase 2
		Lactate dehydrogenase A
	Regulation of PDH	Pyruvate dehydrogenase kinase 1
	Glutamine transport	Glutamine transporters ASCT2 and SN2
	Glutaminolysis	Glutaminase 1
	Serine hydroxymethyltransferase	
	Pyrimidine synthesis	
	Aminoacids metabolism	CAD
		Ornithine decarboxylase
	Lipogenesis	Fatty acid synthase
p53	Glucose transport	GLUT1
	Glycolysis	Hexokinase 2
		Fructose-2,6-bisphosphatase
		Phosphoglycerate mutase
	Oxidative phosphorylation	Cyrochrome c oxidase
	Glutaminolysis	Glutaminase 2
	Pentose Phosphate Pathway	Glucose-6-phosphate dehydrogenase
	Regulation of PDH	Pyruvate dehydrogenase kinase 1
	Krebs cycle	Aconitase
KRAS	Glucose transport	GLUT1
	Glycolysis	Hexokinase 2
		Phosphofructokinase 1
		Lactate dehydrogenase A
	Pentose phosphate pathway	Transketolase
	Hexosamine synthesis	Phosphohexose aminotransferase
	Glutaminolysis	Glutamate dehydrogenase
		Aspartate transaminase
Akt/PTEN	Glucose transport	GLUT1
	Lipogenesis	FASN

Table 1: Oncogenes and tumor suppressor genes, whose products participate in regulation of cancer cells metabolism.

All these genetic events, combined with accompanying histopathological alterations, suggest a sequential transformation roadmap of pancreatic cancer from normal pancreatic epithelium to increasing grades of pancreatic intraepithelial neoplasia to, ultimately, invasive pancreatic adenocarcinoma (Xie and Xie, 2015). Reactivation of developmental pathways, such as hedgehog, notch and wnt/β-catenin, may be crucial for the development of PDAC (Ansari et al., 2012).

3.1.2 Non-inherited risk factors

It is estimated that only 5% to 10% of pancreatic cancer cases are hereditary, and the remaining 90% to 95% are due to environmental risk factors, which are largely modifiable (Salem and Mackenzie, 2018).

The incidence of PDAC is strongly age-dependent; the median age for diagnosis of pancreatic cancer is 71, with 75% of cases diagnosed between the ages of 55 and 84. The median age for death as a result of pancreatic cancer is 73 years old. Smoking, alcohol, obesity, diet, and physical inactivity have been the most studied, and numerous studies have shown them to be associated with increased risk.

Cigarette smoking is the leading preventable cause of PDAC and is believed to account for 20% of PDACs (Blackford et al., 2009). Smoking shows a dose related effect, and smokers display an increased risk of PDAC by 25% compared to non-smokers. Chronic pancreatitis increases the risk of PDAC, with a cumulative risk of 4% after 20 years in young adults with high BMI, but can also influence the prognosis of patients with PDAC especially at an older age. However, diet may have the largest attribution of cases; it is been estimated that approximately 50% of pancreatic cancer cases may be attributed to diet (Table 2). Cancer cells do utilize food-derived FAs for synthesis of phospholipids required for cell proliferation and lipid signaling. This corroborates well with the evidence that a high dietary intake of fat constitutes potential risk factor of some malignancies (Zaidi et al., 2013). Moreover, there is growing evidence that obesity, associated with elevated blood concentrations of FAs, modulates the risk and prognosis of certain cancers. These findings suggest that, apart from lipogenesis, cancer cells can utilize FAs present in blood (derived from VLDL and chylomicrons or from adipose tissue) for their growth. Furthermore, apart from inhibition of lipogenesis, also reduced

dietary lipid digestion and absorption, and decreased lipoprotein lipase and FAs uptake seem to be necessary for the control of cancer growth (Swierczynski et al., 2014).

Two lipid compounds, fatty acids and cholesterol, have received much research attention for their potential impact on a variety of disease processes. With respect to pancreatic cancer, chronic and excessive consumption of dietary fat may lead to hypertrophy and hyperplasia in pancreatic tissue. As dietary fat enters the duodenum, cholecystokinin is released and stimulates the secretion of lipase enzymes from the pancreas. An excess, however, may lead to hypertrophy or hyperplasia in the pancreas in order to keep up with the demand for digestive enzymes (Woutersen et al., 1999). This, in turn, may render pancreatic tissue more susceptible to carcinogens. Additionally, a high intake of fat may promote excess bile acid secretion, which has been shown to stimulate the release of COX-2, an eicosanoid producing enzyme that has been found to be over-expressed in pancreatic tumors (Tucker et al., 2004). Evidence for a biological connection between cholesterol and pancreatic carcinoma is more sparse, but some researcher indicate that higher total cholesterol levels may be associated with increased pro-inflammatory cytokines and inflammation which plays a role in pancreatic carcinogenesis (Salem and Mackenzie, 2018).

Nutrient	Potential link to pancreatic cancer	Association with pancreatic cancer risk
Vitamin C	Boosts immune function Antioxidant Prevents DNA damage [10]	Significant reduced risk *(remained significant only in case control studies after stratification)* Mixed results for serum vitamin C
Folate	Methyl donor Prevent DNA double strand breaks [20] Deficiency may lead to aberrant methylation of tumor suppressor or oncogenes [21].	Inverse association for dietary folate and total folate *(remained significant only in case-control studies)* No association for supplemental folate Non-significant U-shaped association for serum folate
Vitamin E	Chain breaking antioxidant [28] Growth inhibitory effect of pancreatic cancer cells in vitro [29,30]	Reduced risk *(borderline significant association after stratification for cohort studies)* Non-significant inverse association for plasma vitamin E
Vitamin A (Retinoids and Carotenoids)	Vitamin A may mechanically reprogram pancreatic cancer stellate cells [36] β-carotene has pro-vitamin A capacity. Other carotenoids have antioxidant and anti-inflammatory properties [37].	Inverse association for Vitamin A and carotenoids in general *(no association after stratification for cohort studies)* Possible inverse association for lycopene, β-carotene, and β-cryptoxanthin after stratification by carotenoid type Inverse association for the highest plasma levels of β-carotene and zeaxanthin
Vitamin D	Activates genes involved in cell transformation: proliferation, apoptosis, differentiation [41]. Modulates the immune system [42].	No association for dietary intake or serum levels of 25-OH D3
Selenium	Component of antioxidant enzymes [52].	Significant inverse association *(only significant in case control studies)*
Lipids	Chronic and excess dietary fat may lead to pancreatic hypertrophy [55]. Saturated fat associated with insulin resistance [57]. Higher Cholesterol increases pro-inflammatory cytokines [59].	No association for total fat, saturated fat, monounsaturated fat Possible inverse association for polyunsaturated fat, particularly DHA Increased association for cholesterol *(only significant in case control studies)*

Table 2: associations between nutrients and pancreatic cancer risk

3.2 Therapy

As mentioned before, treatment options for pancreatic ductal adenocarcinoma are rather limited and highly depend on the disease stage (Figure 5). Currently, chemotherapy is indicated in the treatment of PDAC in all cases and represents the main option for patients with advanced and metastatic tumours. although the duration and type of chemotherapy depends on the goals of therapy. Radiation, in combination with chemotherapy, is another option for unresectable, metastatic cancer (Le et al., 2016). Nonetheless, the effects achieved by both approaches are mainly a mildly increased survival rate and lowered cancer-related symptoms. Moreover, due to elevated toxicity, combination chemotherapy, which is associated with slightly better outcomes, is limited only to patients with a good performance status (PS). For patients that have undergone surgery, adjuvant chemotherapy is given post-operatively and has been shown to impart a survival advantage when compared to surgery alone (Stark and Eib, 2015).

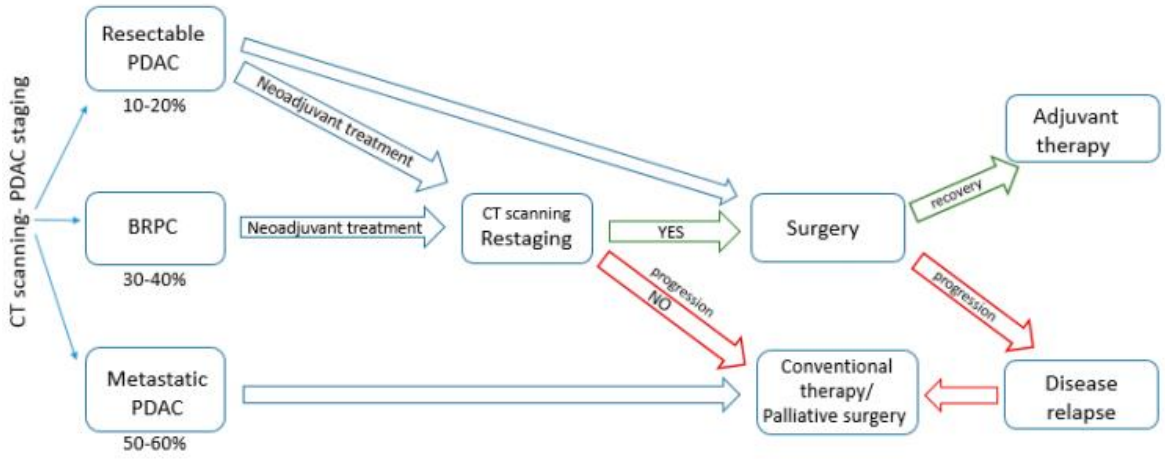

Figure 5: possible treatment of pancreatic cancer depending on PDAC staging.

The current agents that are the standard of care in this setting are gemcitabine or a combination of 5-flurouracil plus leucovorin (FOLFIRINOX). The gemcitabine is the most effective single agent in the palliation of advanced PDAC, where it has been shown to improve clinical symptoms and modestly extend survival (Adamska et al., 2018).

However, large percentage of pancreatic cancers is resistant to gemcitabine. In these patients the pancreatic cancer stroma plays critical roles in gemcitabine resistance of pancreatic cancer, indeed multiple components such as abnormal vasculature and myofibroblasts, are believed to contribute to chemoresistance (Xie and Xie, 2015). Hence, despite Gemcitabine is preferred, it is far from being the gold standard, since the overall patient-survival rate is unacceptably low.

Recently, based on the proven advantageous and synergistic activity of its particular components, a multidrug combination (irinotecan, oxaliplatin, fluorouracil, and leucovorin) called FOLFIRINOX has been shown to be an effective first line therapy, especially for patients with metastatic pancreatic cancer. Clinical trials have thus shown that FOLFIRINOX has a greater efficacy, but with profound limitations due to systemic toxicity and neurotoxicity (Le et al., 2016). The data from trials with FOLFIRINOX and gemcitabine show that good performance status patients can reach one-year survival rates in the range of 40%–50% (Giovannetti et al., 2017). New regimens are urgently needed to push forward survival of advanced PDAC patients. Improvement in the field of targeted, more personalized therapies is of high importance. In this way liquid chromatography and mass spectrometry -based small molecule profiling is a powerful tool for interrogations of the tumor metabolome and complements the goals of personalized medicine.

3.3 Metabolomics of PDAC

Unfortunately there are no effective methods for pancreatic cancer early detection. CA19-9, which is usually used as a tumor marker, is unsuitable for the early detection of pancreatic cancer (PC) due to the low sensitivity for resectable stages of disease. Other biomarkers such as Carcinoembryonic Antigen (CEA) or cell surface associated mucin 1 (MUC-1) have also shown promise for detecting pancreatic cancer by sampling the circulation, but they have suffered from the same lack of specificity and sensitivity that prevent them from being routinely recommended for patients (LaConti et al., 2015). Imaging examinations are not cost effective and cannot discriminate pancreatic cancer from benign pancreatic diseases such as tumor-forming pancreatitis. Endoscopic examinations are not appropriate for screening because of their low throughput and the high risk of complications (Kobayaski et al., 2013). Metabolomics (metabolome analysis) may be an useful tool for the identification of novel biomarkers capable of acting as an early diagnostic tool. Metabolomics, which is the endpoint of the Omics cascade and therefore the last before the phenotype, is the comprehensive study of low molecular weight metabolites (typically 1000 Da) in biofluids and other complex matrices, and the metabolome represents the metabolite profiles of the cellular processes in a cell, tissue, organ, or organism. Changes in metabolism result in alterations in the abundance of metabolites, and elucidating the metabolomic changes that occur in a particular disease will increase our understanding of it (Kobayaski et al., 2013). As mentioned before, carcinogenesis involves significant changes in cellular metabolism, especially in carbohydrate, lipid, nucleic acid, and amino acid metabolism so that metabolomic technologies have recently developed rapidly and have been used for biomarker discovery of pancreas cancer. These technologies, which are typically based on nuclear magnetic resonance analysis (NMR), gas chromatography mass spectrometry (GC-MS), liquid chromatography mass spectrometry (LC-MS), and capillary electrophoresis mass spectrometry (CE-MS), have been well-documented in the literature and have been applied to various research fields including the medical one. In particular electrospray ionization (ESI) is a popular choice as ion source in MS-based applications in PC research (Bi et al., 2013). When combined with LC, it shows good sensitivity and a high dynamic range

and versatility, but also provides soft ionization conditions, giving access to the molecular mass of intact molecules from complex mixtures and advances in the identification of metabolites in a variety of clinical specimens. Pancreatic tumor can represent a rich source for the discovery of biomarkers with appreciable specificity and sensitivity. The use of metabolomics-based approaches providing access to biochemical-phenotype information can offer an opportunity for non-invasive screening of early tumor-associated perturbations in the cellular metabolism (Di Gangia et al., 2014) and for distinguishing between pancreatic cancer (pancreatic ductal adenocarcinoma (PDAC)) and other disorders such as chronic pancreatitis (CP) (Mayerle et al., 2018). The levels of a number of phospholipids as well as Glycocholic acid, N-palmitoyl glutamic acid, Hexanoylcarnitine phenylacetylglutamine (PAGN) and chenodeoxyglycocholate were altered in PDAC blood compared to CP (Lindahl et al., 2017). A number of studies used metabolomics profile of serum/plasma, urine and other biological fluids (such as bile and saliva) cell culture or tissue extract, as a diagnostic tool for pancreatic cancer investigation. Indeed, although PC is characterized by several oncogenes and tumor-suppressor genetic aberrations (e.g., K-Ras and p53-protein mutation), which lead to uncontrolled proliferation and are responsible for enhanced cancer cell survival, by modulating downstream signaling pathways (MAPK and PI3K mTOR pathways), these genetic aberrations are also closely involved in modulating the main metabolic pathways (glycolysis, amino acid metabolism and different biosynthetic pathways). Different classes of compounds (e.g., amino acids, organic acids, sugars, and fatty acids) were analyzed and identified in PC as metabolites with a relevant significance in the development and the progression of the disease (Di Gangia et al., 2014). The vast majority of clinical research has been carried out on urine and serum samples. The pathogenesis of pancreatic disease causes significant decreases in the serum levels of amino acids and fatty acids in pancreatic cancer (valine, n-caprylic acid, threonine, nonanoic acid, methionine, asparagine, glutamine lysine, histidine, and tyrosine) (Kobayaski et al., 2013). It is well known that the uptake and the catabolism of aminoacids and fatty acids are improved to support rapid cell proliferation in cancer tissues, and these decreases may be explained as a result of enhanced usage in tumors. Patients with pancreatic disease are also troubled by malnutrition because of pancreatic endocrine and exocrine insufficiency. So there is the possibility that decreases in their

serum-metabolite levels may also reflect malnutrition (Di Gangia et al., 2014). A comparison of the serum metabolites between pancreatic cancer patients and healthy volunteers identified 18 metabolites significantly changed in PC (Table3) (Nishiumi et al., 2010), as well as a significant increase in choline and taurine, which are indicators of cancer and immune system responses, respectively, in PC patients (Itoi et al., 2017).

Metabolites	Fold-induction	P-value
Lactic acid	1.48	0.00011
Glycine	0.76	0.033
Urea	0.80	0.0028
Octanic acid	0.73	0.00055
Glyceric acid	0.53	0.00063
Decanoic acid	0.76	0.016
Thiodiglycolic acid	6.27	<0.00001
7-hydroxyoctanoic	1.38	0.00025
Lauric acid	0.76	0.047
Asparagine	1.35	0.013
Aconitic acid	1.54	0.030
Homogentisic acid	1.26	0.031
Myristic acid	0.77	0.073
Palmitic acid	0.79	0.032
N-acetyltyrosine	1.57	0.026
Uric acid	0.61	0.0029
Margaric acid	0.80	0.018
Steric acid	0.74	0.0034

Table 3: Comparison of the serum metabolites between pancreatic cancer patients and healthy volunteers (Nishiumi et al., 2010).

The untargeted metabolomics study performed on urine by Napoli and co-workers (Napoli et al., 2012), confirmed the association of the metabolites produced in ketogenesis (e.g., acetoacetate) with the disease, as well as a decreased level of citrate, which has often been correlated with a down-regulated TCA cycle as a consequence of the so-called ‘‘Warburg effect’’ (Di Gangia et al., 2014). Unger et al (Unger et al., 2018) used a high resolution mass spectrometry based global tissue profiling approach in conjunction with multivariate analysis for developing a classification algorithm that would predict early stage PC with high accuracy. Briefly, they used a least squares discriminant analysis (PLS-DA) model (Metaboanalyst 3.0) for discriminating colorectal cancer (CRC), pancreatic lesions (PL), and pancreatic ductal adenocarcinoma (PDAC) and identified 6 metabolites (5-hydroxytryptophan, LysoPE (18:2), PC (16:0/16:0), PC (18:0/22:4), PE (17:0), and SM (d18:1/16:0)) significantly associated with early stage

PDAC as compared to the benign pancreatic disease group (Figure 6). Also serum citrate could be used to differentiate between mice with precursor lesions of PDAC and mice with normal pancreas. Indeed, citrate was found increased in the circulation of mice with PDAC lesions compared to mice with normal pancreas, and it was related to the increase in citrate synthase expression in diseased pancreatic ducts, such an observation reported and was also seen in an analysis of data generated with human samples (LaConti et al., 2015). Other metabolites significantly identified as altered in pancreas tumor tissue by using tandem mass spectrometry were shown in Figure 7. The down regulation of citric acid cycle intermediates succinate and malate may have an overall impact on the energy metabolism of the cell, while lower levels of uridine,5'-uridine monophosphate (5'-UMP) and 5'-adenosine monophospahte (5'-AMP) could reflect rapid turnover of these nucleotides in the tumor tissue (Kaur et al., 2012)..

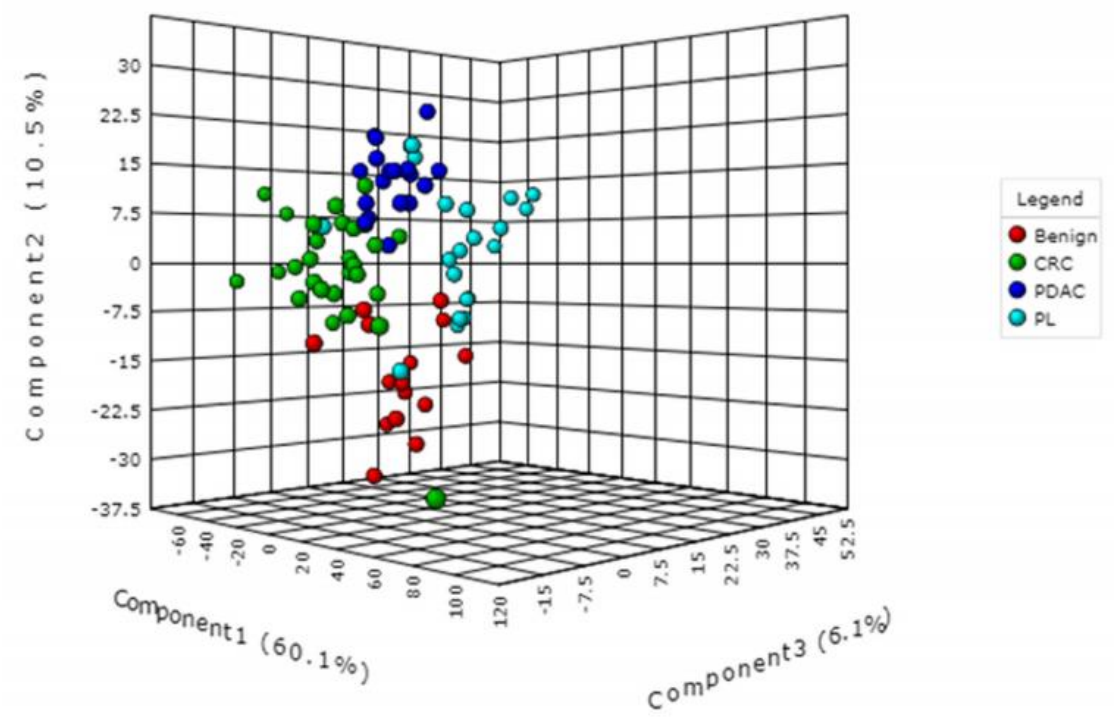

Figure 6: Partial least squares discriminant analysis (PLS-DA) plot showing interclass separation between the different diagnostic groups (pancreatic disease (benign), colorectal cancer (CRC), pancreatic lesions (PL), and pancreatic ductal adenocarcinoma (PDAC), based on overall tissue metabolite profile (Unger et al., 2018).

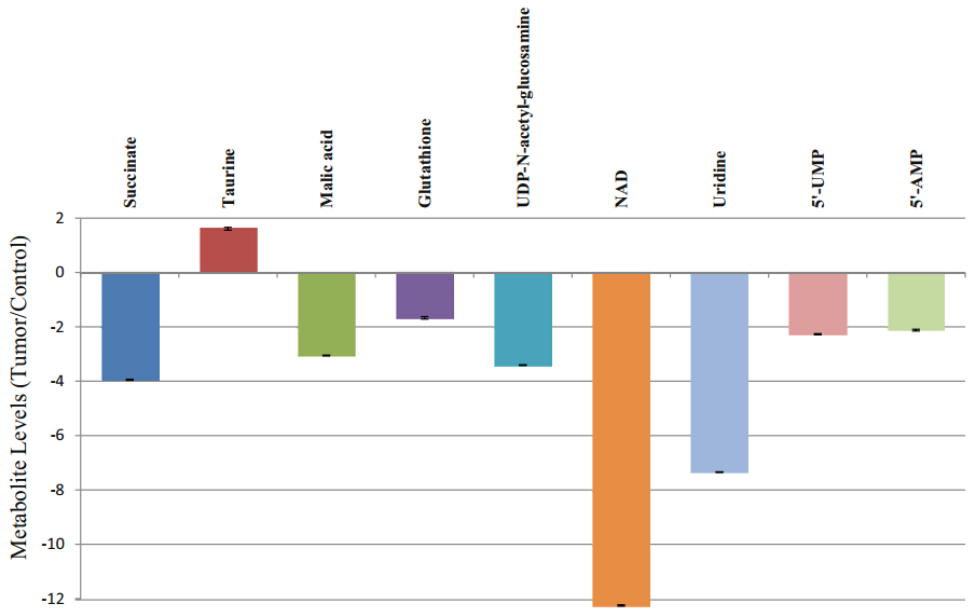

Figure 7: Determination of relative quantitation of metabolites (Kaur et al., 2012).

Metabolomics analyses were also used to differentiate PDAC from Chronic pancreatitis (Mayerle et al., 2018) and to demonstrate that PDAC cells rely on a non-canonical Glutamine pathway to support anabolic process that fuel proliferation. Whereas most cells use glutamate dehydrogenase (GLUD1) to convert glutamine-derived glutamate into α-ketoglutarate in the mitochondria to fuel the tricarboxylic acid cycle, PDAC relies on a distinct pathway in which glutamine derived aspartate is transported into the cytoplasm where it can be converted into oxaloacetate by aspartate transaminase (GOT1) (Figure 8). Subsequently, this oxaloacetate is converted into malate and then pyruvate, ostensibly increasing the NADPH/NADP1ratio which can potentially maintain the cellular redox state (Son et al., 2013). Furthermore, in most cancer cells glutamine flux into mitochondria contributes to proliferation but in PDAC enhanced glutamine anaplerosis results in a pronounced suppression of tumor growth. A cell membrane permeable α-ketoglutarate analog or overexpression of glutamate dehydrogenase lead to decreased proliferation and increased apoptotic cell death in PDAC cells (Jeong et al., 2016).

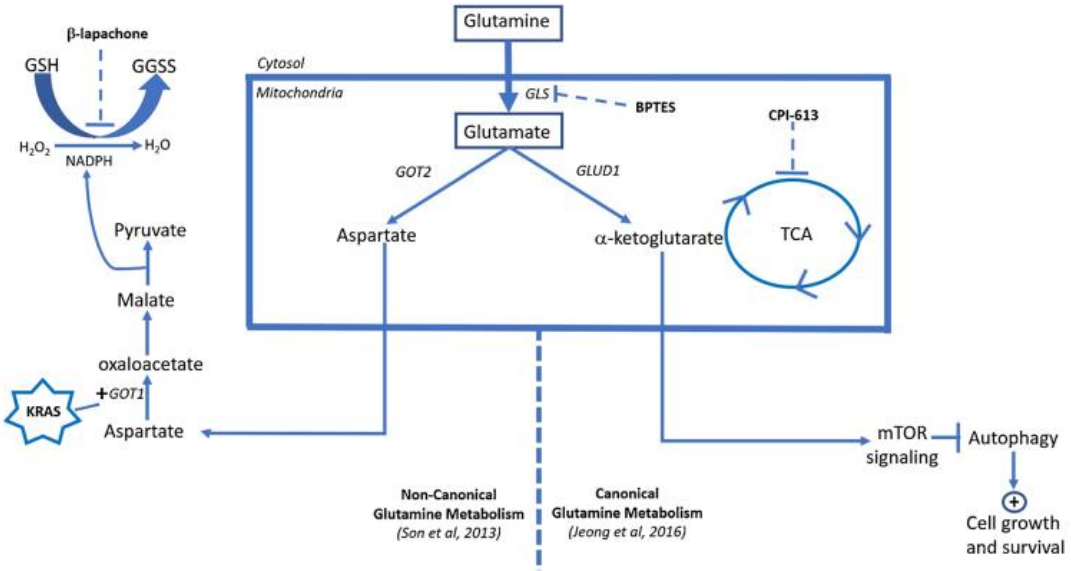

Figure 8: Glutamine pathways in PDAC

In summary, mass spectrometry-based metabolomics may be used as a technology platform for the analysis of metabolites alteration with the aim of developing metabolic biomarkers for early pathology diagnostics, therapy response prediction, and new prognostic markers of Pancreatic Ductal Adenocarcinoma.

3.4 Lipidomics of PDAC

Several studies demonstrated that an elevated body mass index and an excessive body weight (BW) are significant risk factors for PDAC. This is a great concern, as obesity rates are rising worldwide. The number of obese individuals in the U.S. alone has doubled to 59 million over the past two decades. One of the key causes of this surge in obesity is consumption of a high-fat diet (HFD). Therefore, determining the mechanistic effect of such diet on PDAC development at the molecular level is critical (Philip et al., 2013). While proteomic and metabolomic analyses have been utilized to probe and characterize pancreatic tumors, lipidomic has not been rigorously applied to identify perturbations in pancreatic cancer patient samples (Jiang et al., 2013). Lipidomic analyses represent a further contribution to finding new potential diagnostic, prognostic and predictive biomarkers (Perrotti et al., 2016). Lipidomics has been widely used in many non-cancer areas, and in some cancers, such as in pancreatic adenocarcinoma, thyroid cancer, colon cancer, hepatocellular carcinoma, glioblastoma, prostate cancer (Zhou, 2014) and pancreatic cancer.

Lipids play many essential roles in cellular functions, such as survival, proliferation and death, since they are involved in chemical-energy storage, cellular signaling, cell membranes, and cell–cell interactions in tissues. These cellular processes are strongly related to carcinogenesis pathways, particularly to transformation, progression, and metastasis (Perrotti et al., 2016). Metabolic reprogramming is now firmly recognized as a hallmark of cancer. In addition to genetic and epigenetic alterations, development of PC involves significant alterations of cellular metabolism, supporting rapid proliferation of cancer cells (Swierczynski et al., 2014). The lipids formed in cancer cells play two important roles. Firstly, they are building blocks for cell membrane formation during cell proliferation (mainly cholesterol, phosphatidylcholine, phsphatidylserine, phosphatidylethanolamine). Secondly, they play an important role as signaling molecules (phosphatidylinositol, phosphatidic acid, diacylglycerol), or substrates for post-translational protein modification, including palmitoylation and prenylation. In addition, it has been suggested that the growth-promoting effect of lipids on pancreatic cancer cells

occurs at multiple levels: transduction of signals induced by hormones, structural role on cell membranes, and as energy supply (Urayama et al., 2010).

Lipids can sufficiently stimulate proliferation of pancreatic cancer cells lines and in fact high fat diet (HFD) in mice can act as the external stimulus to induce inflammation that then promotes Ras activation (Philip et al., 2013); however a wide variety of tumors have activated de novo synthesis of fatty acids (FAs) irrespective of the levels of circulating lipids. Lipogenic enzymes are frequently overexpressed in many cancer types, including pancreatic cancer. By means of reactions catalyzed by citrate synthase (CS), present in mitochondria, and ATP citrate lyase (ACLY), present in cytosol, cytosolic acetyl-CoA, a key substrate for lipid biosynthesis is formed (Figure 9). In the first-step of FA synthesis, cytoplasmic Acetyl-CoA is generated from citrate by the enzyme called ATP-citrate lyase (ACLY) and then converted to malonyl-CoA by Acetyl-CoA carboxylase (ACC). Acetyl-CoA and malonyl-CoA are coupled to the Acyl-carrier protein (ACP) domain of the multi-enzyme protein called fatty acid synthase (FASN), and via several reactions of acetyl-group condensation by the FASN in NADPH-dependent manner, a basic 16-carbon saturated FA palmitic acid is generated (Figure 9). The data suggest a direct link between lipogenic enzyme activity (FASN and ACLY) and tumor progression to a metastatic phenotype; in fact, overexpression of FASN gene is associated with poor prognosis in PC patients (Swierczynski et al., 2014).

Mammalian cancer cells rely mostly on saturated (SFAs) or monounsaturated FAs (MUFAs). In mammalian cells, three types of fatty acid desaturases introduce carbon double bond, in the endoplasmic reticulum (ER) membranes, at D5 (D5-eicosatrienoyl-CoA), D6 (D6-oleoyl(linolenoyl)-CoA) or D9 (D9-stearoyl-CoA) (“Dx” indicates carbon double-bond position counting from thecarboxylic acid end). Stearoyl-CoA desaturase (SCD) SCD is the rate-limiting enzyme catalyzing the synthesis of 16-carbon palmitoleate and oleate from palmitoyl-CoA and stearoyl-CoA. MUFAs are less susceptible to peroxidation, thus increasing the resistance of cancer cells to oxidative stress (Rysman et al., 2010).

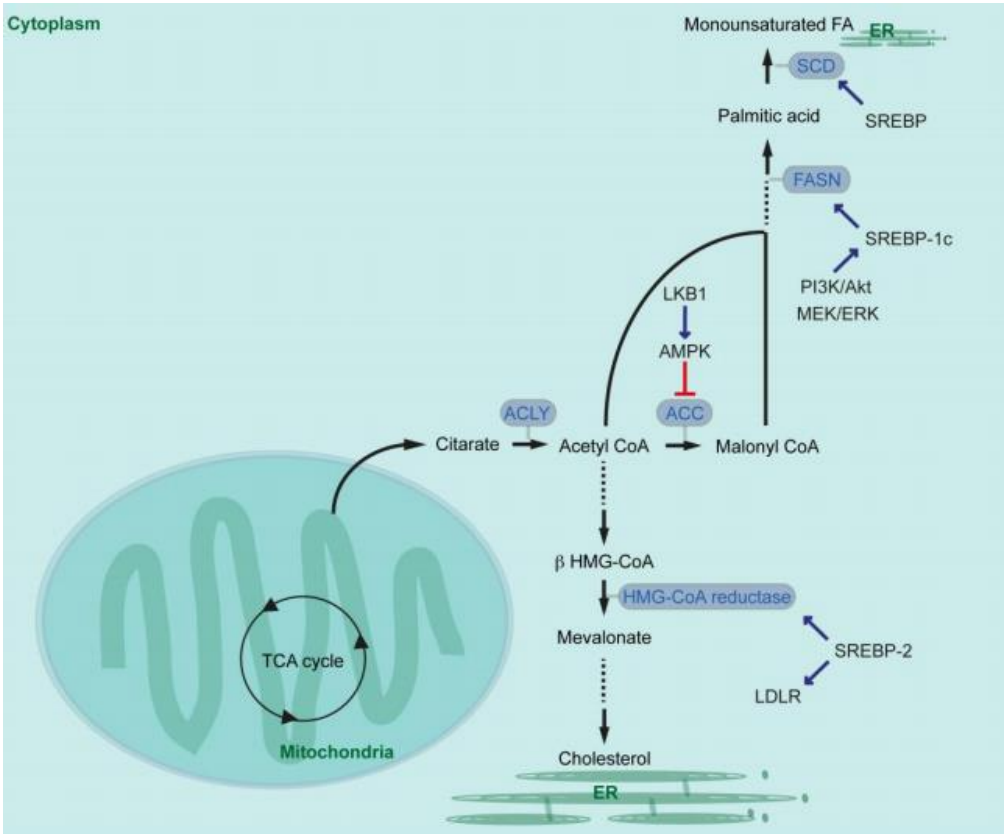

Figure 9: Central pathway for fatty acid and cholesterol synthesis (ACC: Acetyl-CoA carboxylase; ACLY: ATP-citrate lyase; AMPK: AMP-activated protein kinase; ER: endoplasmic reticulum; FA: fattyacid; FASN: fatty acid synthase; HMG: 3-hydroxy-3-methylglutaryl-coenzyme A; LKB1: liver kinase B1;LDLR: low-density lipoprotein receptor; SCD: D9-stearoyl-CoA desaturase; SREBP: sterol regulatoryelement-binding protein; TCA cycle: tricarboxylic acid cycle)

On the contrary, greater intake of omega-3 (ω-3 or n-3, containING double bond at the third carbon atom from the end of chain) polyunsaturated fatty acids (n-3 PUFAs), such as 18-carbon linolenic acid (ALA), 20-carbon eicosapentaenoic acid (EPA), and 22-carbon docosahexaenoic acid (DHA) reduces pancreatic cancer risk (Sunami et al., 2018). Elevated level of MUFAs is maintained mostly by stearoyl-CoA desaturase 1 (SCD1). Increased SCD1 expression is observed in pancreatic cancer cells and in pancreatic cancer patients. Inhibition of SCD1 activity in some tumors (e.g. in prostate cancer) leads to inhibition of cancer cell growth (Swierczynski et al., 2014). High concentration of omega-6 fatty acids (e.g. arachidonic acid) was detected in the plasma of PDAC patients. Omega-6 fatty acids increase the production of pro-inflammatory enzymes and cytokines including COX-2, tumor necrosis factor (TNF-a), and interleukin (IL)-1beta.

Furthermore, TNF-a is a potent activator of nuclear transcription factor NF-kB. Consistent with this, TNF-a, IL-1, and NF-kB are over-expressed and activated in PDAC. NF-kB controls expression of numerous genes involved in inflammation and immune response processes including proliferation, invasion and adhesion, angiogenesis, and apoptosis (Urayama et al., 2010).

Zhang et al (Zhang et al., 2012) reported that PC can be diagnosed by means of 1H nuclear magnetic resonance (NMR)-based metabolomic profiles. These authors showed that numerous plasma metabolites, including lipids, are either elevated (e.g., VLDL) or decreased (e.g., HDL, LDL and 3-hydroxybutyrate) in patients with this malignancy. Yabushita et al (Yabushita et al., 2013) revealed that serum chenodeoxycholic acid, a major constituent of bile acids (which play a key role in lipid digestion in the alimentary tract), is elevated in the experimental model of PDAC. Also Urayama et al (Urayama et al., 2010) claimed an elevated serum levels of some bile acids (taurocholic acid and tauroursodeoxycholic acid) in PC patients.

Other significant lipid alterations observed in pancreatic cancers were the increased of the phosphorylated sphingolipids, sphingosine-1-phosphate (S1P) and sphinganine-1-phosphate (dhS1P). It has been recognized and accepted by most researchers that sphingosine kinase acts like an oncogene and is upregulated in many human cancers. Mechanistically, S1P and dhS1P are typically considered pro-inflammatory, pro-mitogenic, and/or chemotaxic lipids that may serve to facilitate the progression of pancreatic cancer (Jiang et al., 2013).

Lipids can also be tumor-stroma communication mediators for cancer and stroma cells. High fat diet-fed mice with oncogenic KRAS and p53 mutation-induced pancreatic tumors (KPC mice) show larger primary PDACs and higher rates of metastasis than mice fed with standard diet. Fatty acids presumably generated by adipose tissue are incorporated into pancreatic cancer cells, and increase LD formation and tumor cell migration (Sunami et al., 2018). Hence, both understanding the tumor microenvironment and stroma and characterization of factors of intercellular communication are necessary for developing novel strategies for the future therapy of pancreatic cancer.

In conclusion, lipidomics provides a unique opportunity to detect, both quantitatively and qualitatively, numerous individual lipid species in parallel, which informs us about which individual lipid species contribute to an overall increase of total cholesterol, phospholipids, TAG, or ω-3/6 fatty acids, etc. Lipid profiles provide useful information to determine the metabolic pathways of altered lipids in pancreatic cancer.

4. Pancreatic Cancer Stem Cells (CSC)

Pancreatic ductal adenocarcinoma (PDAC) is the most common malignant neoplasm of the pancreas and presents poor prognosis. One of the most virulent aspects of this cancer is the ability to resist chemotherapy and early metastases, leaving few effective options for curative treatment. Treatment resistance is due to the plasticity of tumor cells within pancreatic tumors, and in particular from pancreatic cancer stem cells (CSC). (Ilmer and Horst, 2015). Indeed, it is now universally accepted that metastasis, chemi-resistance and PDAC disease relapse are driven by a subpopulation of highly plastic "stem cells" within the tumor known as cancer stem cells (CSCs). CSCs are small subpopulations of quiescient cells (0.001-0.1%) of cancer cells that are found in the tumor (Yi et al., 2018). Their phenotype is generally associated with epithelial-to-mesenchymal transition (EMT) in which epithelial cells lose their characteristics, acquiring stem cell-like features (Dalla Pozza et al., 2015). During malignant progression, cells undergo an epithelial-to-mesenchymal transition (EMT), in which they lose epithelial characteristics and acquire invasive properties and stem cell-like features (Rhim et al., 2012). CSCs have the ability to renew themselves indefinitely via asymmetric and symmetric division. Asymmetric (differentiation) division gives rise to a CSC and a differentiated tumor cell, while symmetric (self-renewal) division gives rise to two identical CSCs. In both cases, the self-renewal capacity remains intact, which ensures the pool of CSCs and supports the hierarchical model of tumor cell heterogeneity, with the CSC being the cell solely responsible for the formation of tumors, while non-CSC cells lack this capacity (Valle et al., 2018). In addition, based on their distinct characteristics, CSCs are divided into different subsets including quiescent CSCs and invasive CSCs. Invasive CSC is a major motivation to cancer metastasis. Additionally, quiescent CSCs may differentiate into invasive CSCs in specific microenvironments, proliferating to fulfill specific needs (i.e. replacing dying cells after cytotoxic therapies) and thereby promoting distant tumor metastasis (Jiang et al., 2017). Quiescence, self-renewal, and differentiation imply an elevated degree of metabolic plasticity that represent the hallmark of CSCs and is often responsible for disease relapse or tumor free survival (Mancini et al., 2018).

CSCs vary their metabolism according to different microenvironment by acquiring different phenotypes as hypoxic or normoxic or quiescent with respect to the proliferant (Peiris-Pagès et al., 2016). However, the metabolic characteristics of the plastic nature of CSCs, which are able to reside in a dormant state and can rapidly proliferate when the need to repopulate the tumor mass is not fully understood (Peiris-Pagès et al., 2016).

While in normal cells mitochondria represent the main source of energy production through the tricarboxylic acid (TCA) cycle coupled to oxidative phosphorylation (OXPHOS), cancer cells can produce ATP via glycolysis even under normoxic conditions (Warburg effect) (Mancini et al., 2018). Collected glucose is converted to pyruvate and then metabolized to lactate, which is secreted by tumor cells in order to boost the local spread of the tumor (Dando et al., 2015). Under these circumstances, glucose is also metabolised through the pentose phosphate pathway (PPP) which produce large quantities of reduced NADPH and other macromolecules to generate the necessary building blocks required for sustaining high rates of cellular division. At variance with what has been observed for the majority of the differentiated tumor cells, CSCs in other cancer types have demonstrated OXPHOS as the preferred energy production process (Sancho et al., 2016). Moreover CSCs are extremely reliant on the activity of enzymes involved in lipid metabolism, such as stearoyl-CoA desaturase 1 (SCD1) and 3-hydroxy-3-methylglutharyl-coenzyme A reductase (HMG-CoAR) (Mancini et al., 2018). Lipids are essential components of cell and organelle membranes, and fatty acids are required for proliferation of the bulk tumor mass and also for CSCs maintenance. The glycolytic intermediates could be used by CSCs for de novo lipogenesis to increase self-renewal growth suggesting that different metabolic pathway could be well coordinated in CSCs to maximize the benefits. Both lipid catabolism and anabolism alterations are associated with acquisition of stemness during cancer development (Yi et al., 2018). Remarkably, a common point of view is that CSCs possess special metabolic properties that distinguish them from the bulk of the tumor, and that such biochemical properties may constitute a basis for the development of new therapeutic strategies to eliminate CSCs (Dando et al., 2015). Given that CSCs are considered to be the source from which cancer cells arise, are therapy resistant and are responsible for metastatic dissemination, eliminating them could potentially achieve a permanent cure for the patient.

In addition, if conventional therapy fails to kill CSCs, acting only against differentiated cancer cells, the tumor can eventually relapse. The specific elimination of CSCs may thus represent one of the most important challenges of current cancer research (Peiris-Pagès et al., 2016). So in order to definitively eliminate CSCs in a tumor without harming normal cells, it will be necessary to thoroughly study their biology and to elucidate their weaknesses and features. CSCs and tumor cells may adapt their metabolic profile based on nutrients availability, so there is the necessity to clarify the link between metabolic plasticity and the transition among the various states characterizing CSCs (quiescence, self-renewal, differentiation) in order to develop a therapy to synergistically target multiple metabolic pathways in CSCs. However the high heterogeneity of CSCs, which originates from genotypic and phenotypic plasticity, and their low presence in cancer sample tissues make their isolation and correct identification extremely difficult, strongly limiting the realization of biochemical studies. In order to obtain valid and reproducible results, the biochemical approach to CSC pathophysiology can take advantage of the observation that CSCs can be isolated and enriched from several human cancer cell lines (Brandi et al., 2016). Recently, Pozza et al (Dalla Pozza et al., 2015) have been able to isolate cancer stem-like cells from five out of nine PDAC cell lines showing that Panc-1 cancer stem like cells (Panc1 CSCs) isolated from parental cell line by using the CSC selective medium, represent a model of great importance to deepen the understanding of the biology of pancreatic adenocarcinoma. Panc-1 CSCs showed the highest tumorsphere-forming ability, were more resistant to the action of the anticancer drugs, had typical surface stem cell markers, and when subcutaneously injected into nude female mice were more tumorigenic than parental cells.

My thesis deals with omics science applied to analyze the variation of PANC CSC cellular metabolism. Firstly, through proteomics and metabolomics, we compered control cells and PANC CSC for identifying the altered metabolic pathways of pancreatic cancer cells. Subsequently, we performed a time course analysis that confirmed for the first time that these cells rely on specific pathways and that they have a marked metabolic plasticity typical of CSC. Finally, in order to develop CSC-targeted therapies, new liposomal diethyldithiocarbamate/copper ($Cu(DDC)_2$) formulations were investigated demonstrating their high capacity to inhibit the proliferation and the sphere forming capability of CSCs.

5. *Proteomic analysis of pancreatic cancer stem cells: Functional role of fatty acid synthesis and mevalonate pathways*

5.1 Introduction

Pancreatic ductal adenocarcinoma (PDAC) is one of the most aggressive solid tumours with a mortality projected to surpass that of breast and colorectal cancer by 2030 in the United States (Rahib et al., 2014). More than 85% of patients who undergo surgical resection of small pancreatic tumours with clear surgical margins and no evidence of metastasis, die from metastasis within 5 years (Neoptolemos et al., 2004, Abbruzzese et al., 2014), a finding that is consistent with early spread. Standard chemo- and radiation therapies, as well as new treatments targeting known oncogenes or growth factors, do not offer significant improvement of survival (Rhim et al., 2012).

In line with these clinical observations, in a mouse model of PDAC, cellular dissemination leading to liver metastasis has been demonstrated to occur prior to the formation of an identifiable primary tumour. In addition, these circulating pancreatic cells have been shown to exhibit a mesenchymal phenotype and the expression of typical markers of cancer stem cells (CSCs). The CSC theory of cancer development is nowgenerally accepted to explain the cellular heterogeneity observed within a tumour. Following this paradigm, only small subpopulations of the tumour cells, the CSCs, are capable to self-renew, to give rise to a tumour and to recapitulate its heterogeneity by residing at the top of the cellular hierarchy. CSCs potentially explain several phenomena of cancer such as minimal residual disease, resistance to chemo- and radiation therapies, cancer recurrence and metastases (Islam et al., 2013). Stem cells from several cancers, both liquid and solid, including PDAC, have been identified and shown to be particularly resistant to a broad spectrum of anticancer drugs (Abdullah et al., 2013). The existence of CSCs has attractive prospective for identification of CSC-targeted therapies through the determination of the crucial molecules regulating the unique CSC properties. However, despite the enormous potential of CSCs as a new diagnostic and therapeutic target for human cancers, the specific molecular features of these cells are still far to be clarified mainly because of the difficulty to isolate sufficient amount of CSCs from tissue samples.

Recently, cancer cell lines have been shown to be an alternative source for CSC research. Along these lines, our group has been able to isolate cancer stem-like cells from five out of nine PDAC cell lines (Dalla Pozza et al., 2015) and has demonstrated that Panc1 CSCs showed the highest tumoursphere-forming ability and were the most resistant to the action of various anticancer drugs. In order to deepen the knowledge of the specific molecular features of these cells, a proteomic approach has then been chosen (Cecconi and Zamo, 2011). In particular, the secretome analysis of Panc1 CSCs has identified a total of 43 proteins secreted at higher level by pancreatic CSCs compared to the parental cell line (Tang et al., 2008). These data, together with ELISA assays performed on sera of PDAC patients, has suggested that at least one of the highly secreted proteins by CSCs, i.e. ceruloplasmin, is a promising marker for patients negative for CA19–9 (Brandi et al., 2016). Here, we report the proteomic analysis of the intracellular proteins of Panc1 CSCs and parental (P) cells. We show that in Panc1 CSCs 115 proteins were up-regulated and 115 down-regulated as compared to parental cells. In silico functional pathway analysis and network reconstruction based on signalling reactions reported in literature demonstrates a predominant association of the up-regulated proteins with glycolysis/gluconeogenesis, pentose phosphate pathway (PPP), pyruvate-malate cycle, and lipid metabolism and of down-regulated proteins with Krebs cycle, spliceosome and non-homologous end joining. A metabolomic analysis on glycolysis, Krebs cycle and PPP confirmed the modulation of these pathways. Among the identified proteins, fatty acid synthase (FASN) and acetoacetyl-CoA transferase (ACAT2) were among the most highly up-regulated and were chosen for further analysis. Our data indicate that treatment of cells with cerulenin, a specific FASN inhibitor, orwith atorvastatin, a specific inhibitor of the 3-hydroxy-3-methyl-glutaryl-coenzyme A reductase (HMGCR), an enzyme located downstream to ACAT2 in the metabolic pathway that produces isoprenoids and cholesterol, preferentially decrease cell viability of Panc1 CSCs compared to parental cells. All our findings constitute a significant advance in the comprehension of PDAC CSC biology and provide interesting potential targets for the therapeutic approaches to PDAC designed to specifically eliminate the CSC cellular component of the tumour.

5.2 Materials and methods

5.2.1. Cell culture

The human PDAC cell line Panc1, called here Panc1 parental cells, was grown in RPMI 1640 supplemented with 10% FBS, 2mMglutamine, and 50 μg/mL gentamicin sulfate (Gibco, Life Technologies). Adherent cells were maintained in standard conditions for a few passages at 37 °C with 5% CO2. Panc1 CSCs were obtained as previously described (Dalla Pozza et al., 2015). Briefly, adherent cells were cultured in CSC medium (i.e. DMEM/F-12, B27, fungizone, penicillin/streptomycin, heparin, epidermal growth factor and fibroblast growth factor) for at least 1–3 weeks or until the appearance of tumourspheres, which were then cultured in CSC medium for at least three passages before initiating the experiments.

5.2.2. Sample preparation

Samples were prepared as previously described (Brandi et al., 2016) . Briefly, Panc1 cells and Panc1 CSCs cell pellet was collected, lysed in 0.5 M TEAB (Sigma) and 0.1% SDS supplemented with protease inhibitor cocktail 1× (Roche), sonicated 3 times for 10 s, stored at −80 °C for 30 min and then sonicated again 3 times for 10 s. Samples were then centrifuged at 14,000 ×g for 10 min at 4 °C to remove debris, and the supernatants were collected and stored
and −80 °C. Protein concentration was determined using BCA protein assay.

5.2.3. Protein digestion and iTRAQ labeling

For this experiment, iTRAQ 8-plex reagents (Sciex, Framingham, USA) were used for the simultaneous analysis of the conditioned media and whole cell lysates of Panc1 cells and Panc1 CSCs. The samples labeled with 114, 116, 117, and 121 iTRAQ tags were used for the secretome analysis of and the data have already been published. In the present work were instead analyzed the samples labeled with 113, 115, 117, and 119 tags. In particular, one biological replica of Panc1 cell line and of Panc1 CSC whole cell lysates were labeled with iTRAQ reagent 113 and 115, respectively, and a second biological replicate

(froma different cell culture passage) was labeled in the same order with iTRAQ reagents 117 and 119. Protein digestion, iTRAQ labeling, and peptide fractionation and desalting were carried out as already described (Brandi et al., 2016).

5.2.4. LC-MS/MS analysis and data processing

Desalted fractions were reconstituted in 40 μL 0.1% formic acid and 5 μL aliquots were delivered into a Triple TOF 5600 (Sciex) via an Eksigent Nano Ultra cHiPLC System (Sciex) mounted with amicrofluidic trap (200 μm×500μm Chrom XP C18-CL 3 μm300 Å) and analytical column (15 cm × 75 μm) packed with Chrom XP C18–CL 3 μm. A Nano Spray III source was fitted with a 10 μm inner diameter Silica Tip emitter (New Objective, Woburn, USA). The trap column was washed with 2% ACN/0.1% formic acid for 10 min at 2 μL/min. A gradient of 2–50% ACN/0.1% formic acid (v/v) over 90 min was applied at a flow rate of 300 nL/min. Spectra were acquired automatically in positive ion mode using information-dependent acquisition powered by Analyst TF 1.5.1 software (Sciex). Up to 25MS/MS spectra were acquired per cycle (approximately 10 Hz) using a threshold of 100 counts per s and with dynamic exclusion for 12 s. The rolling collision energy was increased automatically by selecting the iTRAQ check box in Analyst, and manually by increasing the collision energy intercepts by 5. TOF-MS spectra were acquired for 250 ms (mass range 400–1650 Da) and MS/MS spectra for 100 ms each (mass range 100–1400 Da). Mass spectrometer recalibration was performed at the start of every fifth sample using a β-galactosidase digest standard. Data analysis was performed using Protein Pilot software (Version 4.2, revision 1340, Sciex) using default settings and with bias and background correction applied. The data were searched against UniProt/SwissProt database (2013_2, total 30,309,316 entries, 40,464 human entries searched) using the Paragon algorithm (4.2.0.0, version 1304, Sciex). The mass tolerance for both precursor and fragment ions was 10 ppm (Shilov et al., 2007). The variable modifications selected for the search were ‘biological modifications’ (probability-based modification search of 461 biological, chemical and artefactual modifications), while the fixed modifications were carbamidomethylation of cysteines, and iTRAQ modification of

C-terminal lysine residues and peptide N-termini. A global FDR value of 1% was used based on the number of proteins identified before 1% of the identifications were derived from a match to the reverse database (Tang et al., 2008) (equating to an unused score of 1.09 and a confidence of 91.9%). Similarly, a global FDR cut-off of 1% was used as the criterion for acceptance of individual MS/MS spectra and in this case corresponded to a confidence of 93.8%. Ratios were calculated from the areas under the curve for each iTRAQ reporter ion selecting different denominators depending on the comparisons to be made. Mean ratios were calculated based on all occurrences (up to 7) of all peptides for which there was a peptide confidence of N15% and where the protein was confidently identified through other evidence. Where a single peptide was used for quantification, the peptide confidence cut-off was 95%. Where a single peptide was used for identification, the cut-off was 99%. The Paragon algorithm performs a Student t-test on the unweighted log ratios (for background corrected data) and reports the p-value: for a final error rate of 5% and with 1157 proteins quantified, the Bonferroni correction suggests a significant p-value at 0.0043.

5.2.5. Bioinformatics analysis of identified proteins

Known and predicted protein associations were analyzed and visualized with STRING version 10 software (http://stringdb.org/). We retrieved interactions that were of at least high confidence (score 0.7), based exclusively on experimental and database knowledge, while excluding all other prediction methods implemented in STRING (such as text-mining and co-expression). Additional white nodes and network depth were kept to the minimum value (1), in order to exclude as many false positive interactions as possible.

Moreover, Ingenuity Pathway Analysis (IPA, Ingenuity Systems, Redwood City, CA) was used to perform a comprehensive analysis of modulated proteins that characterized Panc1 CSCs. The IPA Core Analysis allowed to identifying the most significant networks, biological functions, perturbed canonical pathways as well as potential upstream regulators associated with this signature. The settings were as follows: i) Reference set: Ingenuity Knowledge Base; ii) Relationship to include: Direct and Indirect; iii) Filter Summary: Consider only molecules and/or relationships where (species = Human) AND (confidence = Experimentally Observed). The most important networks were calculated on the basis of the IPA score (N40) which take into account the number

of focus proteins and the size of the network to approximate the relevance of the network to the original list of proteins. Proteins associated with canonical pathways were estimated as significant using Fisher's exact test (p-value ≤0.01) to determine the probability that the association between identified proteins and a canonical pathway could be explained by chance alone. We also performed the IPA Upstream Regulator analysis to identify a putative cascade of upstream transcriptional regulators that can further explain the observed expression changes in Panc1 CSCs. The upstream regulators were assumed as valid effectors of gene/protein expression if the corresponding p-value obtained by Fisher's exact test was ≤0.01. Activation z-score algorithm was used to allow for prediction whether an upstream regulator is activated ($z \geq 2$) or inactivated ($z \leq -2$) based on the direction of expressional change of the associated genes.

5.2.6. Western blot analysis

Western Blot analysis was performed on two independent biological replicates of Panc1 and Panc1 CSCs to validate quantitative data obtained by MS, and on a biological replicate of Panc1 CSCs to verify the level of expression of FASN and of ACAT2 after inhibition of fatty acid synthesis and mevalonate pathways. Protein samples were diluted 1:1 with Laemmli's sample buffer (62.5 mM Tris-HCl, pH 6.8, 25% glycerol, 2% SDS, 0.01% Bromophenol Blue), heated for 5 min at 95 °C and separated by SDS/polyacrylamide gel electrophoresis (PAGE) on 10-20% T acrylamide gels in Tris/glycine/SDS buffer. Proteins were then electroblotted onto polyvinilydene fluoride membranes (Bio-Rad, Hercules, CA) at 80 V for 1 h and 30 min at 4 °C. Amido Black staining was used to confirm equal protein loading in different lanes. Non-specific sites were blocked by incubating the membranes with 5% non-fat dried milk and 0.05% Tween-20 (Sigma-Adrich) in Tris-buffered saline for 1 h at room temperature.

Membranes were incubated with the primary antibodies at the appropriate dilutions in 1% non-fat dried milk, 0.05% Tween-20 in Tris-buffered saline for 3 h at room temperature. Blots were then incubated 1 h at room temperature with the appropriate horseradish peroxidase (HRP)-conjugated secondary antibody (see the Supplemental Table 1).

The immunocomplexes were visualized by chemiluminescence using the ChemidocMP imaging system (Bio-Rad Laboratories) and the intensity of the chemiluminescence response was measured by processing the image with Image Lab software (Bio-Rad).

5.2.7. Metabolite extraction

Metabolomic analyses on Panc1 cells and Panc1 CSCs were performed as previously reported. Cells were prepared following the protocol published by Sana et al. (Sana et al., 2008), with minor modifications as previously reported (D'Alessandro et al., 2001). The sample was resuspended by adding 0.15 mL of ice-cold ultra-pure water (18MΩ) to lyse cells. The tubes were plunged into dry ice or a circulating bath at −25 °C for 0.5 min and then into a water bath at 37 °C for 0.5 min. To each tube was added 0.6 mL of −20 °C methanol and then 0.45 mL of −20 °C chloroform. The tubes were mixed every 5 min for 30 min. Subsequently, 0.15 mL of ice-cold pH-adjusted ultra-pure water was added to each tube and these were centrifuged at 1000 ×g for 1 min at 4 °C, before being transferred to−20 °C for 2–8 h. After thawing, liquid phases were recovered and an equivalent volume of acetonitrile was added to precipitate any residual protein. The tubes were then transferred to a refrigerator (4 °C) for 20 min, centrifuged at 10,000 ×g for 10 min at 4 °C and the collected supernatants were dried to obtain visible pellets. Finally, the dried samples were re-suspended in 0.1 mL of water, 5% formic acid and transferred to glass autosampler vials for LC/MS analysis.

5.2.8. Rapid-resolution reverse-phase HPLC for metabolite separation

An Ultimate 3000 Rapid Resolution HPLC system (DIONEX, Sunnyvale, USA) was used to perform metabolite separation. The system featured a binary pump and vacuum degasser, well-plate autosampler with a six-portmicro-switching valve, and a thermostated columncompartment. A Phenomenex Luna 3 μm HILIC 200 A (150 × 2.0 mm), protected by a guard column HILIC 4 × 2.0 mm ID (Phenomenex), was used to perform metabolite separation over a phase B to phase A gradient lasting 35 min. For the HILIC separation, a solution of 50mM ammonium acetate was prepared by dissolving ammonium acetate in deionized water. Aqueous ammoniumacetate was mixed with acetonitrile (95:5, v/v). This was used for the mobile phase 'A'. The eluent 'B' was composed of a mixture of 50 mM aqueous ammonium acetate: water plus acetonitrile (95:5), v/v). Acetonitrile, formic acid, and HPLC-grade water and metabolite standards (≥98% chemical purity) were purchased from Sigma Aldrich.

5.2.9. Mass spectrometry: Q-TOF settings

Due to the use of linear ion counting for direct comparisons against naturally expected isotopic ratios, time-of-flight instruments are most often, being the best choice for molecular formula determination. Thus mass spectrometry analysis was carried out on an electrospray hybrid quadrupole time-of-flight instrument MicroTOF-Q (Bruker-Daltonik, Bremen, Germany) equipped with an ESI-ion source. Mass spectra for metabolite-extracted samples were acquired in negative ion modes. ESI capillary voltage was set at 4500 V (−) ion mode. The liquid nebulizer was set at 27 psi and the nitrogen drying gas was set to a flow rate of 6 L/min. Dry gas temperature was maintained at 200 °C. Data were stored in a centroid mode. Data were acquired with a stored mass range of 50–1200 m/z. Because calibration of the mass analyzer is essential in order to maintain a high level of mass accuracy, instrument calibration was performed externally every day with a sodium formate solution consisting of 10 mM sodium hydroxide in 50% isopropanol: water, 0.1% formic acid. Automated internal mass scale calibration was performed through direct automated injection of the calibration solution at the beginning and at the end of each run by a 6-port divert-valve.

5.2.10. Metabolite data elaboration

Replicates were exported as mzXML files and processed through MAVEN.52; mass spectrometry chromatograms were elaborated for peak alignment, matching and comparison of parent and fragment ions, and tentative metabolite identification (within a 10 ppm mass-deviation range between observed and expected results against the imported KEGG database). MAVEN is an open-source software that could be freely downloaded from the official project websites (http://genomics-pubs.princeton.edu/mzroll/index.php?show=download). Results were graphed with Graphpad Prism 5.01 (Graphpad Software Inc). Statistical analyses were performed with the same software, as a result of paired t-test or two-way ANOVA among the results obtained from Panc1 and Panc1 CSCs.

5.2.11. Cerulenin and atorvastatin treatments, cell proliferation assay and morphologic changes

Cerulenin and atorvastain were obtained from Sigma-Aldrich St. Louis, MO. Cerulenin was dissolved in ethanol at a final concentration of 20 mg/mL and stored at −20 °C. Atorvastatin was dissolved in dimethyl sulfoxide (DMSO, Sigma-Aldrich) at a final concentration of 10 mg/mL and stored at room temperature. Panc1 and Panc1 CSCs (5 × 103 cell/well) were cultured in 96-well plates and incubated at 37 °C with 5% CO2. Twenty-four hours later, cells were treated with a serial concentration of cerulenin (0, 5, 10, 25, 50, 100, 250, and 500 μM) or of atorvastatin (0, 2.5, 5, 10, 25, 50, 100, and 250 μM). Three independent experiments were performed. After 48 h of each treatment, resazurin dye solution was added in an amount equal to 10% of the culture medium volume and plates were incubated for 1 h at 37 °C with 5% CO2. Metabolic activity of living cells was measured fluorometrically by monitoring the increase in fluorescence at a wavelength of 590 nm, using an excitation wavelength of 535 nm on an automatic microplate reader. The effect of inhibitors on cellular morphology was assessed by collecting phase-contrast microscopy images of Panc1 and Panc1 CSCs cells after 48 h.

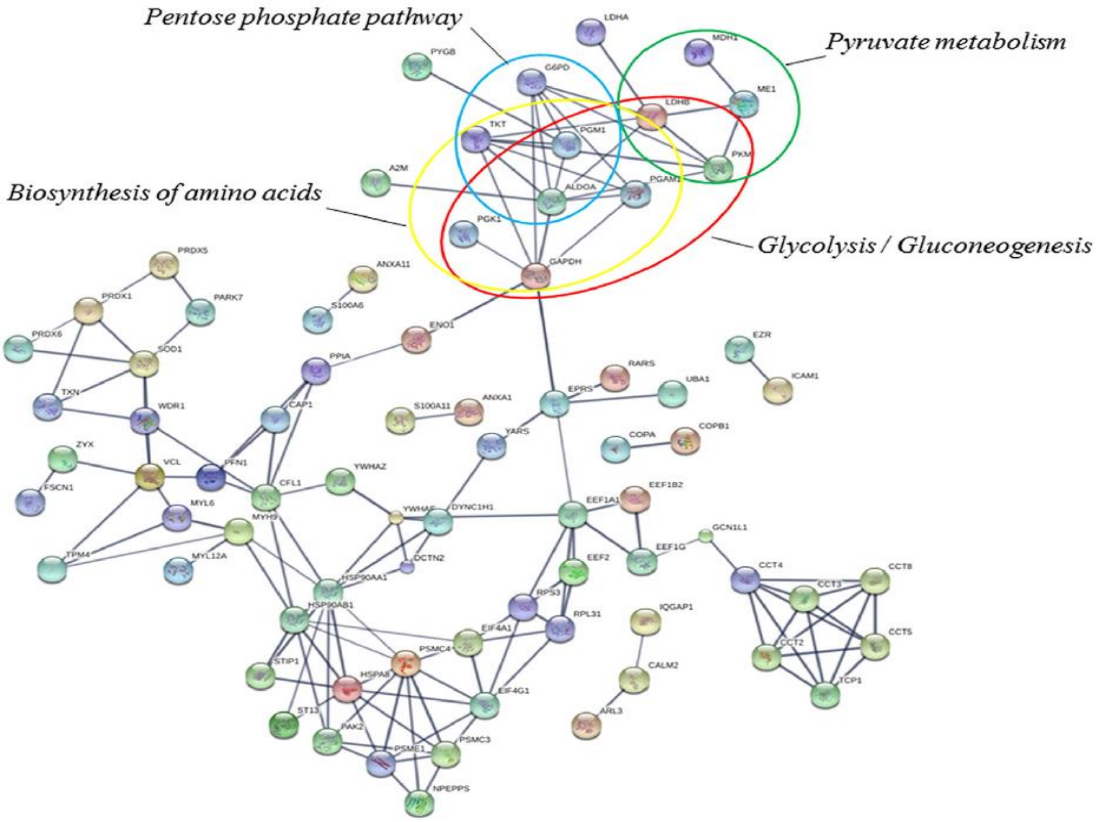

Figure 5.1: Protein network of up-regulated proteins of Panc1 CSCs. Schematic viewof knownand predicted protein interactions according to the STRING database (v. 10). Each node represents a protein, and each edge represents an interaction. Only interactions with the highest confidence score (0.700) are shown. Interactions include physical and functional associations, showing the evidence view. Thicker edges represent stronger associations

5.2.12. Statistical analysis

The data for inhibitors-treated cells and non-treated controls were compared using two-way analysis of variance (ANOVA) and Student's t-test. P-values b0.05 were regarded statistically significant. All data were processed using GraphPad Prism Software Version 6.0 (La Jolla, CA, USA).

5.3 Results

5.3.1. Differential profile of the whole cell proteome in Panc1 CSCs respect to Panc1 cells

Protein expression profiles of Panc1 cells and Panc1 CSCs were investigated using the iTRAQ approach. A total of 2045 proteins with at least 93.8% confidence and an Unused ProteinPilot scores N1.09 (equating to a global FDR of 1%) were identified and among them 1157 proteins were quantified (Supplemental Table 2). Of these, 608 were identified via a single peptide with a confidence of 99% (Supplemental Table 3). Differential protein expression was considered to be significant when the expression increased or decreased with a fold change of 1.5 and a p-value smaller than 0.05 in both biological replicates. A total of 230 proteins were found differentially expressed (Supplemental Table 4) and among them115 proteins were up-regulated and 115 down-regulated in Panc1 CSCs as compared to Panc1 parental cells.

5.3.2. Interaction networks, pathway analyses, and upstream regulators of Panc1 CSC proteins

STRING analysis emphasized that the majority of the differentially expressed Panc1 CSC proteins interact within established complexes or have functional relationships.
The most striking pathways involving the proteins up-regulated in Panc1 CSCs compared to parental cells belong to carbon metabolism and are, in particular, glycolysis/gluconeogenesis, pyruvate metabolism, biosynthesis of amino acids, and pentose phosphate pathway (Figure 5.1). On the contrary, the down-regulated proteins are mainly involved in the interactions with molecular components of the spliceosome and non-homologous end joining (Figure 5.2).

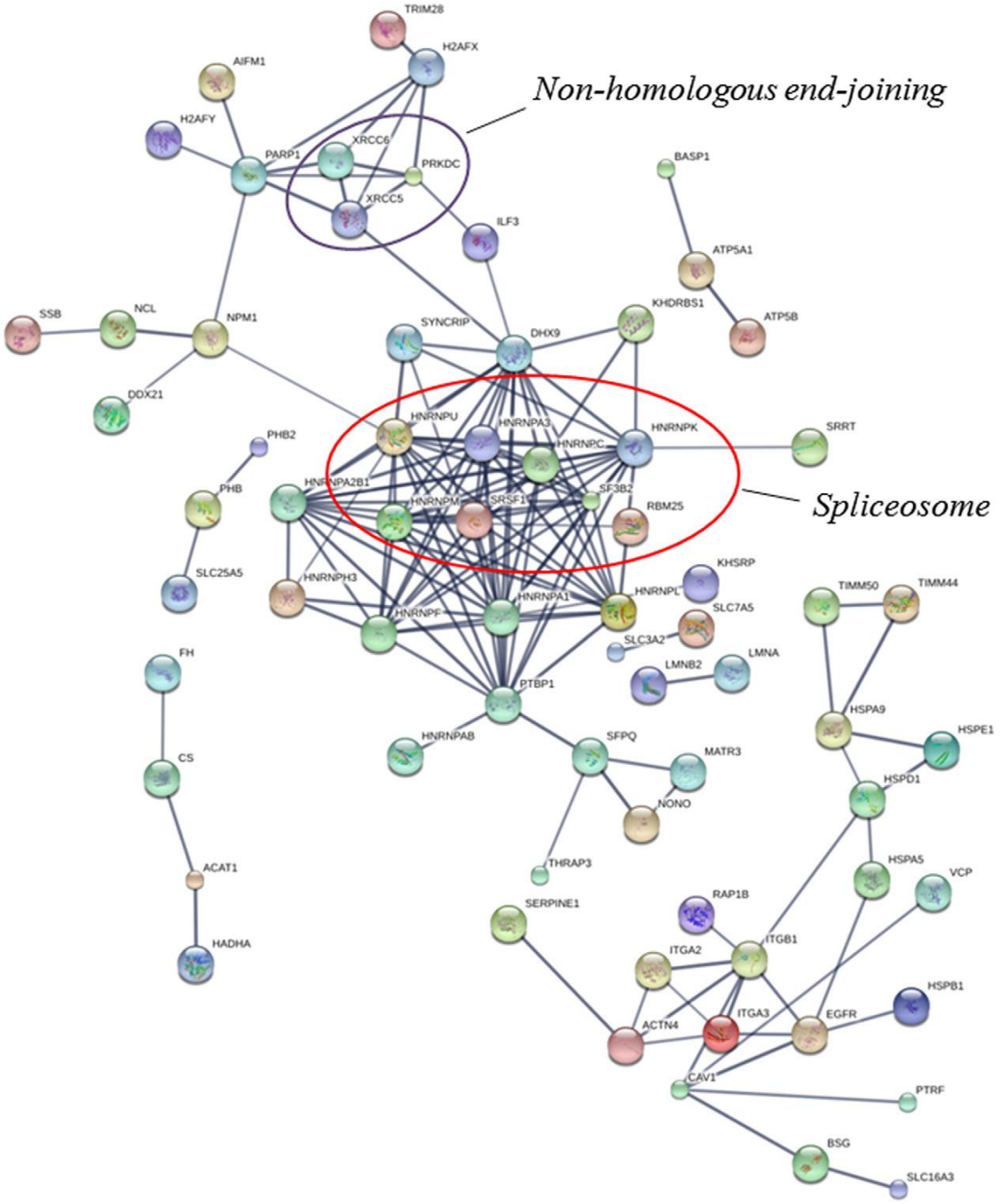

Figure 5.2: Protein network of down-regulated proteins of Panc1 CSCs. Schematic view of known and predicted protein interactions according to the STRING database (v. 10). Each node represents a protein, and each edge represents an interaction. Only interactions with the highest confidence score (0.700) are shown. Interactions include physical and functional associations, showing the evidence view. Thicker edges represent stronger associations

To reveal significant networks and biological functions relevant to Panc1 CSCs, we also performed an IPA. The up-regulated proteins show the highest-score for networks including cell death and survival, cellular assembly and organization, cell-to-cell signalling

and interaction, cellular development, growth and proliferation, and carbohydrate metabolism, while the down-regulated proteins are involved in cell death and survival, cellular growth and proliferation, and RNA posttranscriptional modification (Supplemental Figure 1). Next, we systematically evaluated the biological functions of the identified proteins. Most of the regulated Panc1 CSC proteins appear to be involved in cancer, cellular growth and proliferation (Table 5.1). In particular, the up-regulated proteins are specifically involved in cellular movement and free radical scavenging, while the down-regulated proteins are specifically connected to the post-transcriptional modification of RNA and to cellular response to therapeutics. Overall, IPA software revealed that the Panc1CSC modulated proteins show a significant link with 21 or 19 different pathways for up- or down-regulated proteins, respectively (Supplemental Table 5). The ten top canonical pathways (p-value ≤0.001) are shown in Figure 5.3. Among the most statistically significant canonical pathways, glycolysis (p-value: 7.94 E-11) and gluconeogenesis (p-value: 1.12 E-10) are included for the up-regulated proteins and DNA double-strand break repair by non-homologous end joining (p-value: 1.23 E-06) and telomere extension by telomerase (p-value: 1.66 E-06) for the down-regulated proteins. Finally, the IPA software allowed us to examine also the potential upstream regulators associated with the above-described proteomic profiles. In particular, the upstream regulators predicted to be significantly activated include the transcription factors HIF1A (p= 1.29E-09, z=2.228) and SMARCA4 (p=5.36E-06, z=2.219), as well as the estrogen-related receptor gamma ESRRG (p = 4.24E-07, z = 2.180), while the transcription factor NR1H4 (p = 2.08E-05, z = −2.236) is predicted to be inhibited in Panc1 CSCs. A complete list of transcriptional upstream regulators with significant p-values ($p \leq 0.01$) can be found in Supplemental Table 6.

Table 1
IPA-predicted top biological functions for up-regulated and down-regulated proteins of Panc1 CSCs.

Top biological functions (Panc1 CSCs up-regulated proteins)	P values[a] (ranging from)	No. of molecules[b]
Diseases and disorders		
Dermatological diseases and conditions	1.21E-02–1.05E-10	34
Neurological disease	1.21E-02–9.23E-09	49
Skeletal and muscular disorders	1.16E-02–9.23E-09	50
Psychological disorders	1.21E-02–9.54E-09	34
Cancer	1.25E-02–3.13E-08	102
Molecular and cellular functions		
Cellular growth and proliferation	1.21E-02–1.17E-15	58
Cell death and survival	1.21E-02–1.80E-11	52
Cellular development	1.21E-02–8.62E-08	34
Cellular movement	1.24E-02–1.22E-06	30
Free radical scavenging	1.08E-02–1.50E-06	12
Physiological system development and function		
Cell-mediated immune response	1.21E-02–3.47E-05	4
Hematological system development and function	1.21E-02–3.47E-05	14
Immune cell trafficking	1.21E-02–3.47E-05	10
Endocrine system development and function	1.21E-02–5.40E-04	4
Organismal survival	7.10E-04–7.10E-04	9
Top biological functions (Panc1 CSCs down-regulated proteins)	**P values[a] (ranging from)**	**No. of molecules[b]**
Diseases and disorders		
Infectious diseases	6.07E-03–2.85E-08	33
Dermatological diseases and conditions	6.07E-03–1.14E-07	22
Cancer	6.07E-03–2.15E-07	105
Organismal injury and abnormalities	6.07E-03–2.15E-07	105
Neurological disease	6.07E-03–6.74E-07	42
Molecular and cellular functions		
Cellular growth and proliferation	6.07E-03–1.56E-18	64
RNA post-transcriptional modification	6.07E-03–2.22E-17	23
Cell death and survival	6.07E-03–2.24E-15	54
Cellular development	6.07E-03–8.12E-10	55
Cellular response to therapeutics	1.00E-03–1.48E-09	7
Physiological system development and function		
Skeletal and muscular system development and function	1.09E-04–8.12E-10	12
Tissue development	6.07E-03–8.12E-10	30
Cardiovascular system development and function	6.07E-03–3.70E-07	18
Organismal development	6.07E-03–3.70E-07	21
Hair and Skin development and function	6.07E-03–2.03E-05	11

[a] Fisher's exact test was used to calculate a p value for each protein of the dataset identified in the biological function studied, indicating the probability that each biological function assigned to the data set is assigned by chance; then we have a range of p values corresponding to all p values calculated for all proteins of the dataset in the biological function.
[b] The number of molecules of the differentially expressed protein dataset is shown.

5.3.3. Western blot analyses of selected proteins identified by iTRAQ

Seventeen differentially expressed proteins (ten up-regulated and seven down-regulated in Panc1 CSCs), for which commercial antibodies were available, were selected for validation using Western blot analyses. The expression level of proteins in Panc1 cells and Panc1 CSCs were compared on two biological replicates. As shown in Figure 5.4, Western blot results are consistent with the MS quantification data. Notably, in Panc1 CSCs relative to parental cells, MARCKS is up-regulated at intracellular level only as intact (~80 kDa), but not as cleaved (~40 kDa) form and more isoforms of Integrin beta-1 (ITGB1) and hnRNP A2/B1(HNRNPA2B1) are immune detected and all appear to be down-regulated.

5.3.4. Metabolomic analysis of Panc1 CSCs

Since the proteomic analysis revealed that carbon metabolism (mainly glycolysis and pyruvate metabolism) is the pathway that characterizes the proteins induced in Panc1 CSCs (Figure 5.1), we determined fold-change variations of the concentration levels of several key metabolites of glycolysis, Krebs cycle, and the energetic metabolism.

Figure 5.1 A shows that the glycolytic intermediates are mainly present at higher level in Panc1 CSCs in comparison to Panc1 parental cells. In particular, Panc1 CSCs show a significant increase in glucose-6 phosphate, fructose-1,6 bisphosphate, glyceraldehyde-3 phosphate, and lactate, while pyruvate decreases. We next investigated whether the accumulation of glycolytic intermediates was associated to an increase in refueling of pentose phosphate pathway (PPP). Interestingly, Panc1 CSCs reveal the accumulation of PPP intermediates, both of the oxidative phase (D-gluconic acid and D-ribose 5-phosphate) and non-oxidative phase (sedoheptulose 7-phosphate and Dxylulose phosphate) (Figure 5.1B).

In line with the increased level of glycolysis metabolites, Krebs cycle intermediates including succinate, fumarate, and malate are decreased and two Krebs cycle-related metabolites, glutamine and glutamate, are decreased and increased, respectively, in Panc1 CSCs compared to Panc1 P cells (Figure 5.1C).

5.3.5. Decreased cell viability of Panc1 CSCs in response to inhibition of fatty acid synthesis and mevalonate pathways

The observation that FASN was expressed at 18 fold higher level in Panc1 CSCs compared to Panc1 cells led us to investigate the role of fatty acid synthesis in Panc1 CSC viability. For this purpose, we tested the effect of cerulenin, a specific FASN inhibitor, on the proliferative activity of Panc1 cells and Panc1 CSCs. The cell viability assay was performed 24 (data not shown) or 48 h after the beginning of the treatment with cerulenin at concentrations ranging from 0 to 500 μM.

As shown in Figure 5.6A, cerulenin is able to decrease cell viability at a significantly higher level in Panc1 CSCs compared to Panc1 cells with IC50 values of 15.6 μM ± 1.3 and 24.2 μM ± 1.7, respectively. This result strongly suggests an increased cell viability role of fatty acid synthesis in CSCs compared to parental cells. In a parallel experiment, conceived on the observation that ACAT2 was expressed at 21 fold higher level in Panc1 CSCs compared to Panc1 cells, we examined the role of isoprenoids/cholesterol synthesis in Panc1 CSC viability. For this purpose, we used the drug atorvastatin, which is known to specifically inhibit HMG-CoA reductase, an enzyme located downstream to ACAT2 in the metabolic pathway that produces isoprenoids and cholesterol.

We cultured both Panc1 cells and Panc1 CSCs for 24 (data not shown) and for 48 h with atorvastatin at concentrations ranging from 0 to 250 μM. As shown in Figure 5.6B, atorvastatin strongly inhibits the viability of Panc1 CSCs, while only slightly reduces that of Panc1 cells, with IC50 values of 43 μM ± 24.8 and N250 μM, respectively.

This result strongly suggests an increased cell viability role of isoprenoids/cholesterol synthesis in CSCs compared to parental cells. To verify whether treatments with cerulenin and atorvastatin had an effect on the expression level of FASN and ACAT2 and to ascertain that the up-regulation of FASN observed in Panc1 CSCs was not a consequence of the presence of growth factors in the culture medium, a western blot analysis was performed. As shown in Figure 5.7, FASN level is independent of the presence of EGF and FGF in the culture medium and is not modulated by the treatment with the specific inhibitor cerulenin, which is a covalent inactivator of the β-ketoacyl synthase reaction

on FAS. On the contrary, the expression level of ACAT2 in Panc1 CSCs appears to be increased after the inhibition of the mevalonate pathway by atorvastatin.

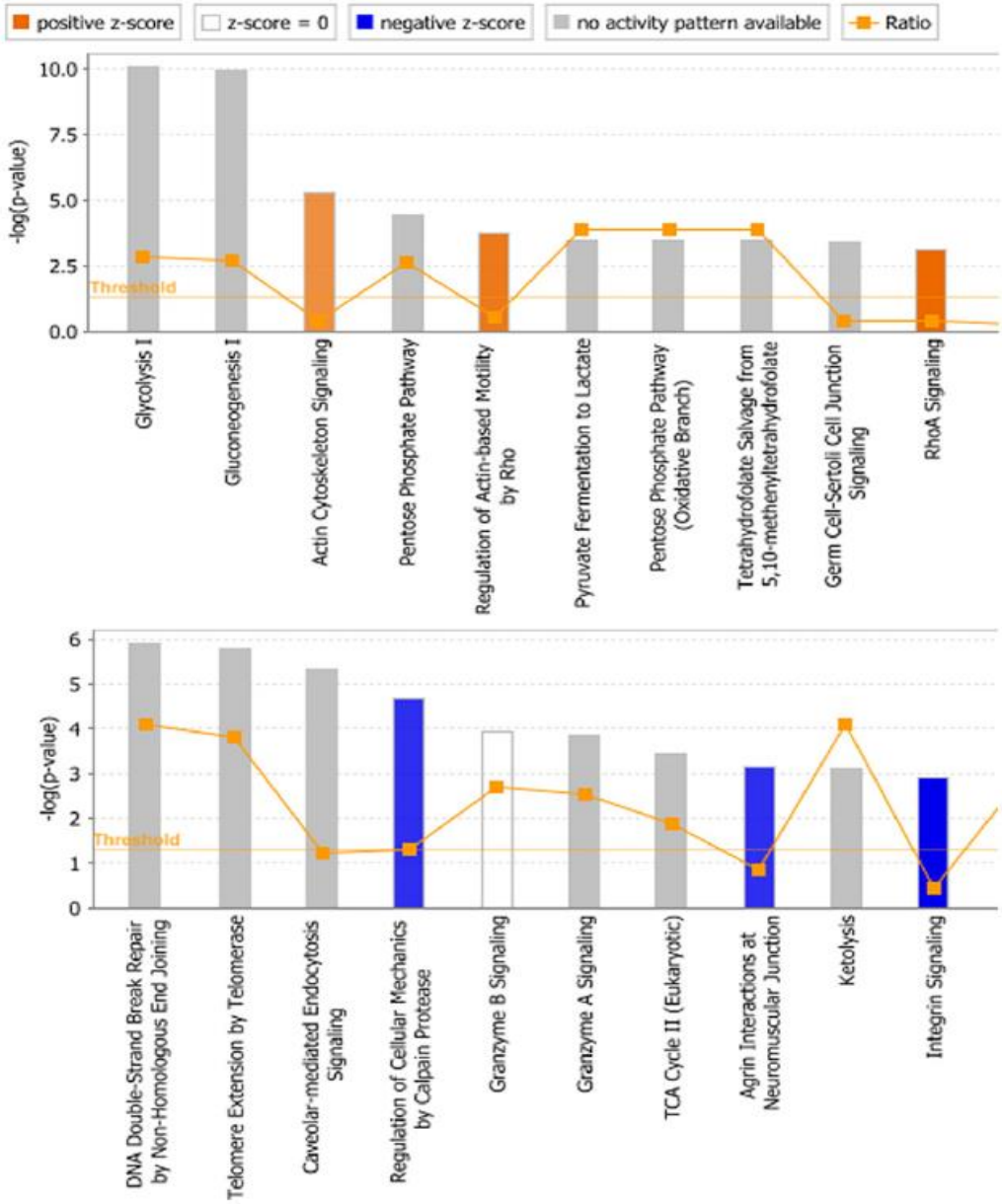

Figure 5.3: IPA Canonical Pathways analysis. The top 10 significantly altered canonical pathways associated with up-regulated (upper panel) and down-regulated (lower panel) proteins of Panc1 CSCs. The y-axis indicates the statistical significance calculated using the right-tailed Fisher exact test and the p value indicates the probability of association of proteins with the canonical pathway by random chance alone. Thus, taller bars equate to increased significance. The threshold line represents the default significance cut-off at p = 0.05. The ratio is calculated as follows: the number of molecules found in a given pathway divided by total number of molecules that constitute that specific canonical pathway. The orange and blue coloured bars indicate predicted pathway activation, or predicted inhibition, respectively (z-score). White bars are those with a z-score at or very close to 0. Gray bars indicate pathways where no prediction can currently be made.

5.3.6. Morphologic changes of Panc1 cells and Panc1 CSCs in response to the inhibition of fatty acid synthesis and mevalonate pathways

To evaluate if the inhibition of fatty acid synthesis had an effect on cellular morphology, we examined cells by a phase-contrast microscope at 48 h after treatment with 0, 25, 100 or 250 μMcerulenin. Before treatment, Panc1 cells exhibited a typical epithelial morphology with intact cell-to-cell contacts, while Panc1 CSCs exhibited a mesenchymal morphology with cell aggregates (or spheroids) and a more dispersed colony appearance suggesting an epithelial mesenchymal transition (EMT) phenotype. Interestingly, after cerulenin treatment, Panc1 cells exhibited only a decreased cell-to-cell contact, while Panc1 CSCs showed drastic changes in cell morphology, with reduction of spheroids suggesting cytoskeletal reorganization (Figure 5.8A).

The analysis also indicated that the anti-proliferative/viability effect was due, at least in part, to the decrease in cell number after cerulenin treatment. We also evaluated the effect of atorvastatin on the morphology of Panc1 cells and Panc1 CSCs. As shown in Figure 5.8B, the effect on cell morphology of this inhibitor was similar to that of cerulenin.

Phase-contrast microscopy images show in fact that after atorvastatin treatment Panc1 CSCs were characterized by a reduction of spheroids suggesting cytoskeletal reorganization, while Panc1 cells exhibited a decrease in cell-to-cell contacts. In addition, Panc1 CSCs were rounded and detached after atorvastatin treatment.

5.4 Discussion

5.4.1. Activated metabolic pathways in Panc1 CSCs

Our previous study (Brandi et al., 2016) showed higher secretion level of different proteins in Panc1 CSCs compared with the parental cells, and hence suggested possible involvement of these proteins in the processes of pancreatic cancer differentiation, invasion, and metastasis.

In the present study, with the aim of further deepening the understanding of pancreatic CSC biology, we carried out a proteomic analysis of Panc1 and Panc1 CSC whole-cell extracts to investigate the intracellular molecular mechanisms characterizing pancreatic CSCs. The data obtained revealed the regulation of some key metabolic pathways in
Panc1 CSCs (Figure 5.9).

Our proteomic results indicate that glycolysis and gluconeogenesis (Figure 5.1 and Figure 5.3), previously reported to be involved in the secretome of both Panc1 cells and Panc1 CSCs (Brandi et al., 2016), are also strongly represented by intracellular up-regulated proteins in Panc1 CSCs. In particular, data show that fructose-bisphosphate aldolase A (ALDOA, +15.31), triosephosphate isomerase (TPI1, +13.25), glyceraldehyde-3-phosphate dehydrogenase (GAPDH, +9.21), phosphoglycerate kinase 1 (PGK1, +2.37), phosphoglucomutase-1 (PGM1, +18.29), phosphoglycerate mutase 1 (PGAM1, +12.26), alpha-enolase (ENOA, +13.48), and pyruvate kinase isozymes M1/M2 (PKM, +18.76) are all more highly expressed in Panc1 CSCs than in the parental cells. Furthermore, Panc1 CSCs also express an increased level of both L-lactate dehydrogenase A and B chains (LDHA, +10.12, LDHB, +15.13), which indicates an accentuation of the Warburg effect. According to these data, the upstream regulator analysis performed in silico by IPA has identified, among other activated regulators, the transcription factor HIF1A.

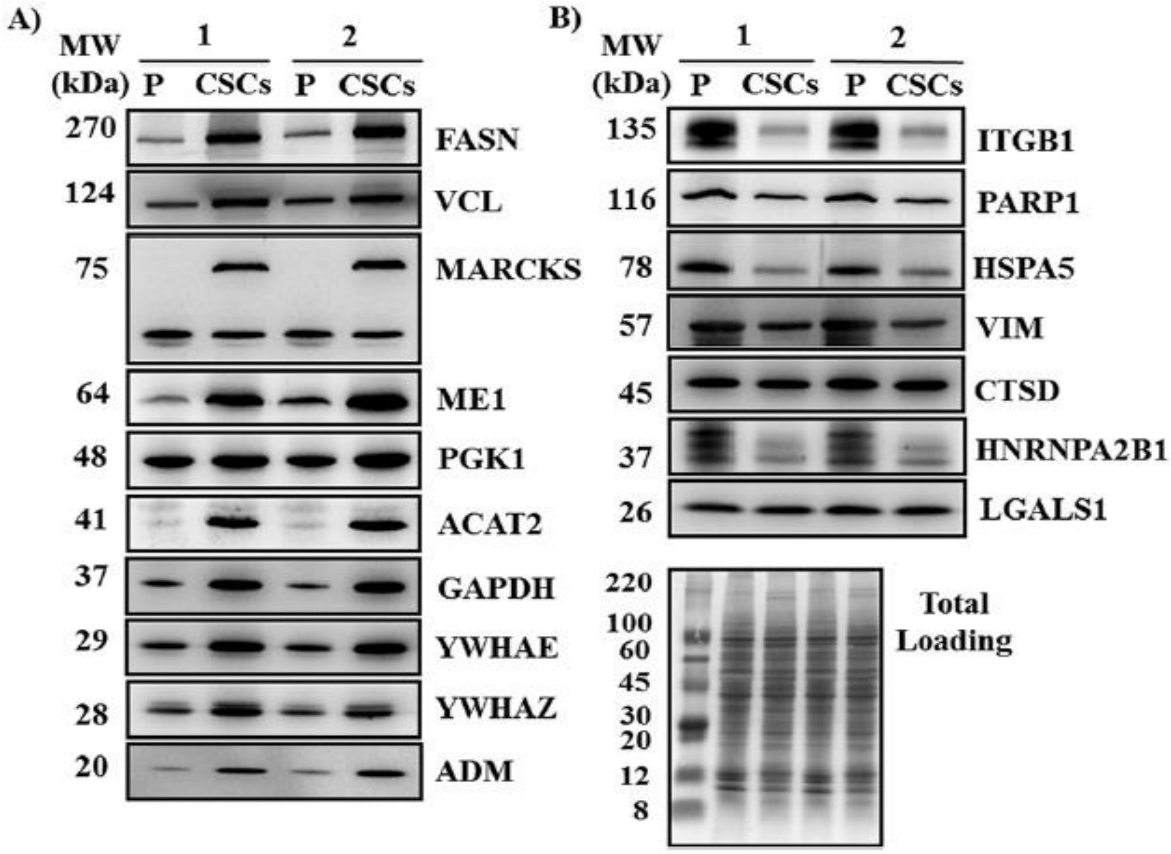

Figure 5.4: Western Blotting validation. Differential expression of Panc1 CSC up-regulated (A) and down-regulated (B) proteinswas verified in two biological replicates (1 and 2). Proteinswere resolved in 10–20% SDS-PAGE gels, transferred onto PVDF membranes, and probed with specific antibodies against the indicated targets. Amido Black staining was used as total loading control.

Indeed, HIF1α, which is typically up-regulated even in solid malignancies in normoxia, modulates stem cell fate reprogramming through glycolytic shift and upregulation of PKM2 (Prigione et al., 2014, Cheng et al., 2013). Notably, it has also been demonstrated that HIF1A promotes pancreatic ductal adenocarcinoma invasion and metastasis by activating transcription of the actin-bundling protein fascin (Zhao et al., 2014). In line with this finding, we found that fascin is up-regulated 7.06 fold in Panc1 CSCs as compared to parental cell line (see Suppl. Table 4). In agreement with the increased expression of glycolytic enzymes, our metabolomic data show that in CSCs the level of glucose-6 phosphate is enhanced, suggesting an increased activity of exokinase in CSCs, despite its expression not differing between cell lines, as shown by the proteomic data.

The other glycolytic intermediates that were analyzed were present at higher levels in CSC compared to parental cells, though the 2-phopshoglycerate level was not significantly different, confirming a more glycolytic metabolism for CSCs. In line with this observation and with the proteomic data, the level of lactate is also significantly higher in CSCs than in parental cells. The recent literature describes CSCs as being primarily glycolytic or preferentially relying on oxidative phosphorylation depending on tumour-type and microenvironment (Sancho et al., 2016). However, it has been shown that in glucose rich environments, proliferating CSCs primarily utilize aerobic glycolysis for their bioenergetic needs, while in glucose (and oxygen) deprived conditions, CSCs shift to a quiescent, slow cycling state relying on mitochondrial oxidative metabolism (Luo and Wincha, 2015). In particular, the activation of the glycolytic programme favours stemness via various mechanisms (Dong et al., 2013, Shen et al., 2015) including enhanced antioxidative capacity, with pentose phosphate pathway (PPP) being the most relevant. Our results indicate that several up-regulated proteins of Panc1 CSCs belong to "free radical scavenging" among top biological functions (Table 1) and to PPP as a statically significant perturbed pathway (Figure 5.1 and Figure 5.3). Among PPP enzymes, Panc1 CSCs show over-expression of glucose-6-phosphate 1-dehydrogenase (G6PD, +5.61), 6-phosphogluconate dehydrogenase (PGD, +11.67), and trans ketolase (TKT, +5.66). These results are also confirmed by the metabolomic analysis which highlights the increase of PPP intermediates (Figure 5.9). The PPP is a major glucose metabolic pathway required for cellular demands of anabolism and antioxidant defense. Indeed, the main purpose of PPP is to regenerate NADPH from NADP+ through an oxidation/reduction reaction. This reaction is coupled to the formation of ribose 5-phosphate from glucose 6-phosphate, thus making PPP among the major metabolic pathways involved in malignancies (D'Alessandro et al., 2014). Our data show increase of metabolic intermediates and byproducts especially of the oxidative phase of PPP (D-gluconic acid and D-ribose 5-phosphate). The increase of oxidative phase intermediates might be explained through diversion to purine salvage pathway (PSP), as observed in red blood cell (Gevi et al., 2012). Purine nucleotides may be synthesized in cells de novo or reconstructed from already existing free purine bases through the salvage reactions (reutilization) (Gevi et al., 2012).

In Panc1 CSCs, in line with the up-regulation of enzymes involved in glycolysis and PPP, we also observed an induction of enzymes involved in the pyruvate-malate cycle (citrate-pyruvate cycle) (Figure 5.1 and Figure 5.3), i.e. the cytosolic ATP-citrate synthase (ACLY, +2.77), cytoplasmic malate dehydrogenase (MDH1, +10.17) and cytosolic NADP-dependent malic enzyme (ME1, +12.19).

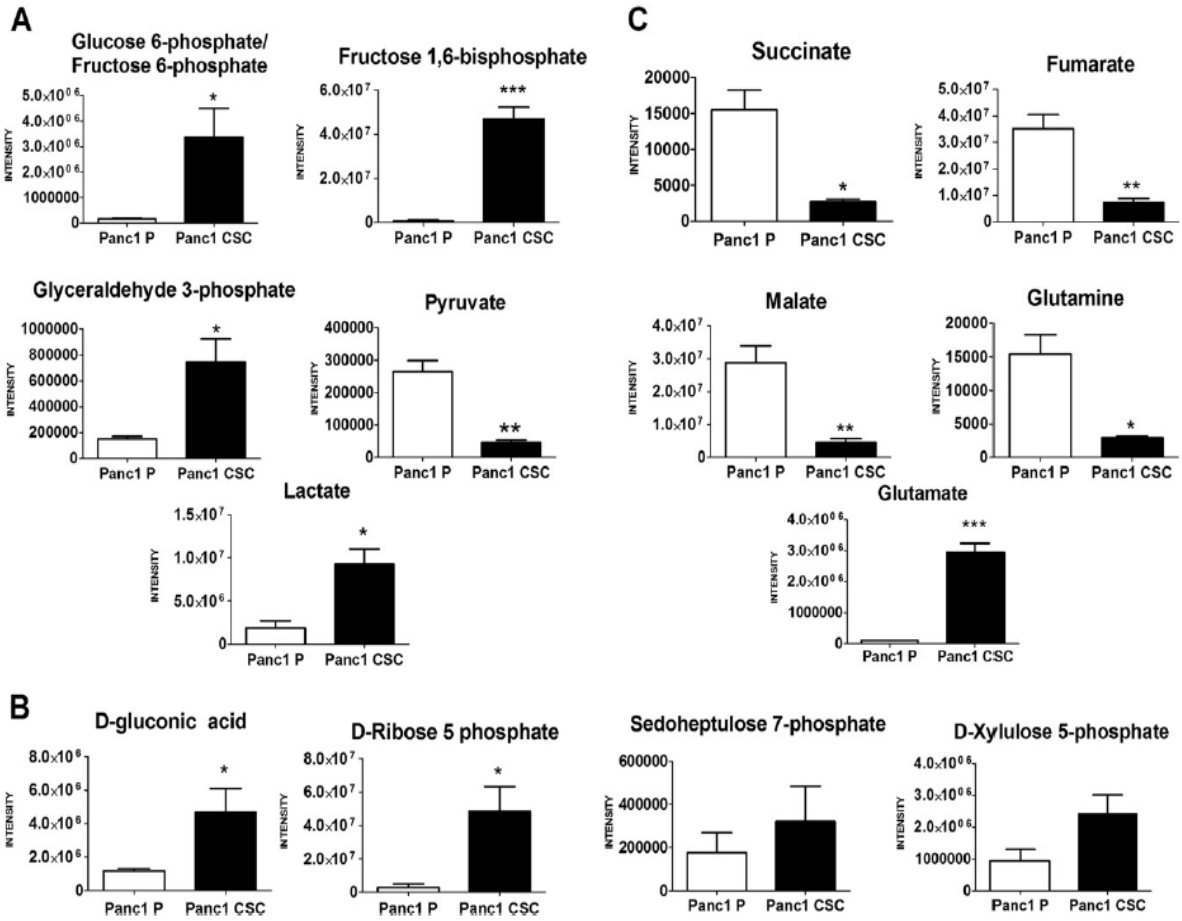

Figure 5.5: Metabolites analysis. Absolute metabolomics quantification (arbitrary ion counts) of metabolites from glycolysis (A) Pentose phosphate pathway (B) and Krebs cycle (C) in Panc1 parental cells (P; white histogram) and Panc1 CSCs (black histogram). Values are presented as mean ± SD. The data were analyzed using Student's t-test: *$p < 0.05$, **$p < 0.01$, and ***$p < 0.001$ in Panc1 CSCs versus Panc1 P cells.

This pathway is responsible for citrate transport out of the mitochondria into the cytosol where it is cleaved by ACLY to oxaloacetate and acetyl-CoA, which is available for fatty acid synthesis.

On the other hand, cytosolic oxaloacetate is hydrogenated by MDH1 to give NAD+ and malate, which is then oxidized by ME1 to pyruvate in a reaction which also provides NADPH mainly for fatty acid synthesis. Thus, NADH generated in glycolysis is converted to NADPH for fatty acids synthesis, while simultaneously regenerating the NAD+ needed to continue glycolysis (Schulze and Harris, 2012). Recently, it has been reported that PDAC cells rely on the pyruvate-malate cycle to increase the NADPH/NADP (+) ratio, and that xaloacetate is produced by a metabolic reprogramming mediated by the KRAS oncogene (Son et al., 2013). Accordingly, we demonstrate that Panc1 cells, which are known to possess a KRAS mutation (Moore et al., 2001) express enzymes of the pyruvate-malate cycle and that these enzymes are even more expressed in Panc1 CSCs. Consistently with the up-regulation of enzymes involved in glycolysis, PPP, and pyruvate-malate cycle, we also found that Panc1 CSCs have a strong induction of two cytosolic enzymes involved in lipid metabolism, the cytosolic acetylCoA acetyl transferase (ACAT2, +21.19 fold), which synthesize acetoacetylCoA in the mevalonate pathway leading to cholesterol, and the fatty acid synthase (FASN, +18.36 fold), which synthesize fatty acids. Recently, in proliferating cells, it has been demonstrated that NADPH production, beyond the important contribution of PPP and the malic enzyme (ME1), originates from the serine-driven one-carbon metabolism, in which oxidation of methylene tetrahydrofolate to 10-formyl-tetrahydrofolate is catalysed by themethylene tetrahydrofolate dehydrogenase (MTHFD) with the reduction of NADP to NADPH (Fan J et al., 2014). Our data demonstrate for the first time that Panc1 CSCs are characterized by increased levels of the cytosolic MTHFD1 (+3.19) compared to parental cells suggesting that stemness requires a higher contribution of the folate pathway for NADPH homeostasis.

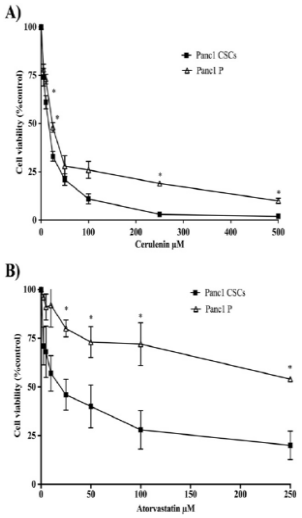

Figure 5.6: Anticancer effects of fatty acid andmevalonate pathways inhibition. Cerulenin and atorvastatin effectively inhibited Panc1 CSCs viability. (A) Comparison of cerulenin effects on Panc1 and Panc1 CSC cells viability. Cells were treated for 48 h at doses ranging from 0 to 500 µM. (B) Evaluation of atorvastatin effects on Panc1 and Panc1 CSC cells viability. Cells were treated for 48 h at doses ranging from 0 to 250 µM. The data were analyzed using Student's t-test. *p<0.05.

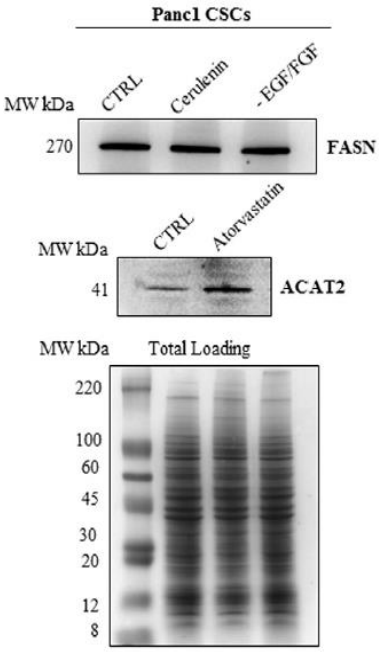

Figure 5.7:Western Blotting analysis of Panc1 CSCs. (A) FASN protein levels in Panc1 CSCs control (CTRL) and treated with cerulenin, and grown without EGF and FGF (-EGF/FGF). (B) ACAT2 protein levels in Panc1 CSCs control (CTRL) and treated atorvastatin. Proteins were resolved in 10–20% SDS-PAGE gels, transferred onto PVDF membranes, and probed with specific antibodies against the indicated targets. Amido Black staining was used as total loading control.

5.4.2. Repressed pathways in Panc1 CSCs

As a further confirmation of a switch to a glycolytic metabolism at the expense of the mitochondrial oxidative metabolism, Panc1 CSCs also show a down-regulation of some key enzymes of the Krebs cycle (Supplemental Table 4).

In support of these results, the metabolomic data show that the level of three Krebs cycle intermediates, i.e. succinate, fumarate, and malate, is significantly decreased in CSCs in comparison to parental cells (Figure 5.5B). Furthermore, glutamine level is decreased in CSCs compared to parental cells, suggesting either a less active glutamine-transport inside the cell or a greater conversion of glutamine to glutamate. Indeed, glutamate level is enhanced in CSCs compared to parental cells, suggesting a minor incorporation of glutamate in the mitochondrion and, together with the other results, a less active Krebs cycle in CSCs in comparison to parental cells. In Panc1 CSCs, proteins involved in spliceosome formation and non homologous end joining pathway appear to be down-regulated compared to Panc1 cells (Figure 5.2 and Figure 5.3), in particular, several hnRNPs (A1, A3, A/B, A2/B1, C1/C2, H3, K, L, M, U, Q), two splicing factors (3B subunit 2, 1 serine/arginine-rich), and the RNA-binding protein 25. The down-regulation of multiple types of hnRNPs may represent a strategy of stem cells to keep their undifferentiated state. Indeed, it has been demonstrated that hnRNPs play a key role in the stem cell differentiation process, as for example in the case of embryonic stem cells differentiated into smooth muscle cell, or of multipotent hematopoietic stem cells differentiated into the different types of blood cell, or of neural stem cell differentiated into neuronal cells (Chen et al., 2013). The non-homologous end-joining (NHEJ) pathway is one of the main mechanisms for repairing breaks in double-stranded DNA.

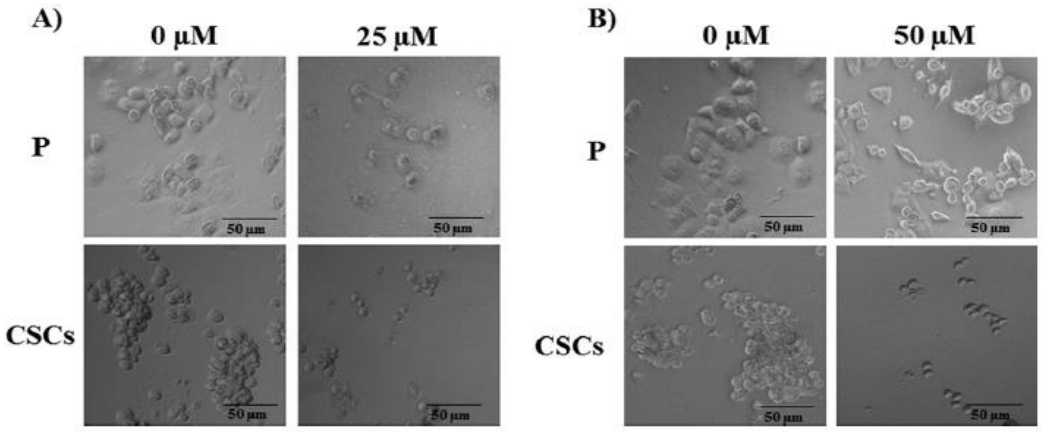

Figure 5.8: Cellular morphology after inhibition of fatty acid synthesis and mevalonate pathways. Phase-contrast microscopy images of Panc1 and Panc1 CSCs after 48 h of cerulenin (A) and atorvastatin (B) treatments.

In Panc1 CSCs, representative proteins of this pathway (Figure 5.2 and Figure 5.3), i.e. poly [ADP-ribose] polymerase 1 (PARP1, −1.96), DNA-dependent protein kinase catalytic subunit (PRKDC, −2.27), and X-ray repair cross-complementing proteins 5 and 6 (XRCC5 −1.89, XRCC6 −1.92), are down-regulated. Interestingly, PARP1 is a pro-apoptotic enzyme (Hassa, 2009), the expression of which has been shown to be specifically reduced in stem cells with spherical morphology as compared tomonolayer cells (Lee et al., 2016). Furthermore, XRCC5 and XRCC6 encode for Ku80 and Ku70 proteins, which form the Ku heterodimer that is involved in repairing double-strand breaks in DNA for maintaining the integrity of genome function. Either Ku70 or Ku80 themselves have also unique functions that are independent of the other Ku subunit (Kim, 2008), as for instance the tumour suppressor activity of Ku70(Puebla-Osorio et al., 2014). In particular, it has been reported that colonic epithelial cells of mice with Ku70 deficiency and p53R172P mutation (Ku70−/−PP) show higher rates of proliferation and induction of β-catenin/Wnt pathway, which is important in promoting EMT. Notably, our previous data demonstrated that Panc1 CSCs express higher levels of typical EMT markers compared to parental cells (Dalla Pozza et al., 2015).

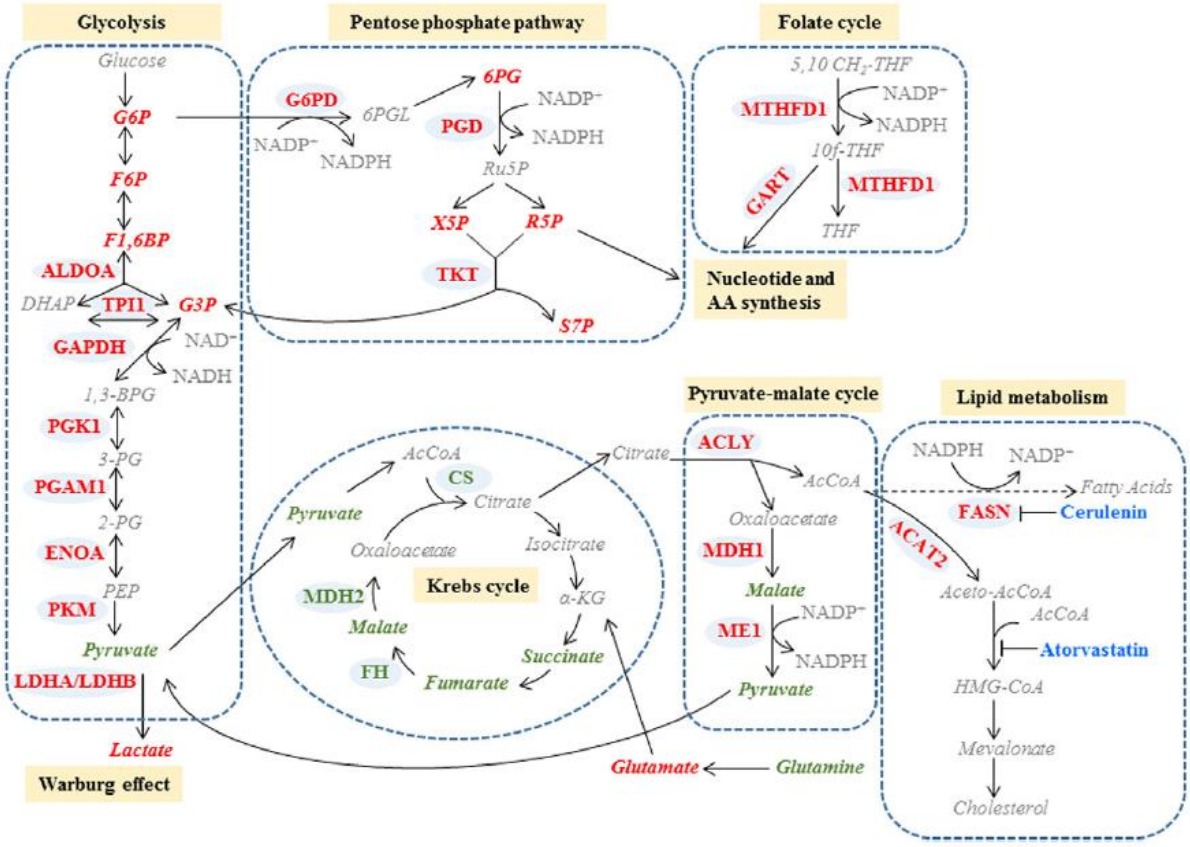

Figure 5.9: Overview of key metabolic pathways in Panc1 CSCs. The up- and down-regulated proteins (enzymes) and metabolites identified in Panc1 CSCs compared to Panc1 P and mentioned into the discussion are shown in bold red and green, respectively. Proteins and metabolites that were not identified in this work are shown in gray. The inhibitors are shown in light blue.

5.4.3. Functional role of fatty acid synthesis and mevalonate pathways in Panc1 CSC viability

Among the most strongly induced proteins of Panc1 CSCs, we found of particular interest FASN and ACAT2 that, as mentioned above, are involved in lipid metabolic pathways. Notably, high expression level of FASN has been linked to a significantly poor prognosis of PDAC patients and it has been shown to depend upon the induction of EGFR/ERK signaling (Bian et al., 2015). Furthermore, FASN has been shown to promote EMT in many cancers, including ovarian (Jinag et al., 2014), breast (Li et al., 2014) and colorectal (Zaytseva et al., 2012) cancer. Our results demonstrate that the overexpression of FASN in Panc1 CSCs is independent of the presence of EGF and FGF in the medium, suggesting a constitutive activation of the EGFR/ERK pathway.

Inhibition of FASN is known to selectively target cancer cells for apoptosis, mainly by interfering with membrane function, inhibiting DNA replication and anti-apoptotic proteins, and accumulating the malonyl-Co-A substrate (Mullen et al., 2015). Cerulenin is a natural FASN inhibitor that binds specifically and irreversibly to the β-ketoacyl synthase domain of FASN, thus preventing the condensation reaction between the elongating fatty acid and successive malonyl residues. Interestingly, our results show that cerulenin inhibits Panc1 and Panc1 CSC proliferation, with a greater anticancer activity on stem cells (Figure 5.6A). This is a new observation that could open novel lines of investigation for the development of PDAC CSC target specific therapeutic strategies. The other metabolic pathway that caught our attention was the mevalonate pathway, which is involved in cholesterol production, because of the strong up-regulation in Panc1 CSCs of ACAT2, one of its key enzymes. The mevalonate pathway affects cancer metastasis in several ways by influencing EMT, cytoskeleton remodelling, as well as cell motility and polarity (non-canonical Wnt/planar pathway). Statins are competitive inhibitors of this pathway by acting on the enzyme the 3-hydroxy-3-methyl-glutaryl-coenzyme A reductase (HMGCR) and blocking the conversion of HMG-CoA to mevalonate.

The statins occupy the catalytic site of HMGCR at the level of the binding site for HMG-CoA, thus blocking the access of this substrate to the active site. In the last two decades, the successful and widespread uses of statin drugs for hypercholesterolaemia have revealed their potential anticancer effects demonstrating that the use of statins is associated with reduced cancer-related mortality (Jiang et al., 2014). Inhibition of mevalonate pathway by statins has shown to have an antitumour effect against certain CSCs, but their effects have never been investigated on pancreatic CSCs (Warita et al., 2014).

Our data demonstrate that atorvastatin, a synthetic statin, inhibits cell growth of both Panc1 cells and Panc1 CSCs and that CSCs are considerably more sensitive than parental cells (Figure 5.6B), suggesting ACAT2 as a potential target for PDAC CSC specific therapy. In conclusion, the different cytotoxic effects by inhibiting fatty acid synthesis and mevalonate pathways on Panc1 and Panc1 CSCs suggest that the acute reduction of fatty acids or cholesterol production per se are not the major source of cell injury, but could target specific stemness characteristics.

CONCLUSIONS

In summary, the proteomic and metabolomic analysis on Panc1 cells and Panc1 CSCs highlighted the main metabolic routes used by pancreatic cancer stem cells to survive,

proliferate and disseminate in distinct healthy tissues. In particular, these data indicate that the maintenance of high fatty acid synthesis and mevalonate pathway levels could make critical contribution to survival of pancreatic cancer stemcells. Although targeting tumour metabolismis still in the early days of translation to patients, the improvement on knowledge of deranged metabolic pathways, in particular in cancer stem cells, will accelerate the development of novel therapeutic strategies.

Supplementary data to this article can be found online at doi:10.1016/j.jprot.2016.10.002.

Acknowledgments

This work was supported by AIRC 5 per mille grant n. 12182, Italy, the NIHR Liverpool Pancreas Biomedical Research Unit, and the Consorzio Interuniversitario Biotecnologie (CIB), Italy. I. Dando is a fellow of Fondazione Umberto Veronesi, Italy. E. Dalla Pozza is a fellow of ARC-Net (Applied Research on Cancer Network), University of Verona, Italy.

6. Time course analyses of pancreatic cancer stem cells

6.1 Introduction

Pancreatic cancer is a highly lethal disease characterized by its dismal prognosis and resistance against conventional therapies such as chemotherapy or radiotherapy. Only ~20% of pancreatic cancer patients are eligible for surgical resection, which is the only curative therapy, though the 5-year survival in these patients is less than 25% (Bartholin et al., 2012). Its poor prognosis of pancreatic cancer is mainly attributed to the malignant behavior of pancreatic cancer. Indeed, extensive local invasion and early systemic dissemination are hallmarks of pancreatic cancer (Yin et al., 2011). This behaviour is also associated with epithelialto-mesenchymal transition (EMT) and with the establishment of circulating pancreatic cells which maintain a mesenchymal phenotype and express typical markers of cancer stem cells (CSCs) (Lee et al., 2008). Cancer stem cells (CSCs) are undifferentiated quiescent cells characterized by their ability to self-renew coupled with unique plasticity and metabolism. In PDAC, CSCs are a small subpopulation within the tumor and are reported to be responsible for driving tumorigenesis and progression of disease (Perusina Lanfranca et al., 2018). Isolation and subsequent studies of CSCs from different types of tumors pointed to these cells as major components of conventional treatment failure. As a consequence, targeting CSCs is a promising perspective for the development of novel more effective anticancer therapeutic protocols (Chen et al., 2016). Recently, Brandi et al have been able to isolate cancer stem-like cells from five out of nine PDAC cell lines. In particular, they have demonstrated that Panc-1 cancer stem like cells (Panc1 CSCs) isolated from parental cell line by using the CSC selective medium, represent a model of great importance to deepen the understanding of the biology of pancreatic adenocarcinoma (Brandi et al., 2016).

In a previous study, starting from this Panc1 CSCs, we found that a subpopulation of Panc1 CSCs are characterized by an up-regulation of glycolysis, pentose phosphate pathway, pyruvate-malate cycle, and lipid metabolism and by a down-regulation of Krebs

cycle. Moreover, fatty acid synthesis and mevalonate pathways are shown to play a critical contribution to the survival of pancreatic cancer stem cells. On this basis, in order to deepen the knowledge of these cells, we went through metabolomic changes of this cells over time. We performed a time course analysis at different time-points (2, 4, 8 weeks) and we highlighted changes both at a phenotypic and at a metabolic level. CSCs showed, over time, a tumorsphere – forming ability associated with high expression of stamness markers and acquisition of the characteristic quiescent state at 8 weeks. These results confirm the high metabolic plasticity of CSCs that change their metabolism depending on the external conditions. Moreover, our in vitro model closely mimes in vivo stem cells.

6.2 Materials and Methods

6.2.1 Cell culture

The human PDAC cell line Panc1, called here Panc1 parental cells, was grown in RPMI 1640 supplemented with 10% FBS, 2mMglutamine, and 50 μg/mL gentamicin sulfate (Gibco, Life Technologies). Adherent cells were maintained in standard conditions for a few passages at 37 °C with 5% CO2. Panc1 CSCs were obtained as previously described (Dalla Pozza et al., 2015). Briefly, adherent cells were cultured in CSC DMEM/F-12 medium for 2, 4, and 8 weeks. Photos of the cells were acquired with 5X and 10X objectives after having plated cells in a 24-wells plate.

6.2.2 RNA extraction and real-time PCR

Total RNA was extracted using TRIzol Reagent (Life Technologies) and 1 microgram of RNA was reverse transcribed using first-strand cDNA synthesis. Real-time quantification was performed in triplicate samples by SYBR Green detection chemistry with Power SYBR Green PCR Master Mix (Applied Biosystems) on a 7900HT Fast Real-Time System (Thermo Fisher) and normalized on RPLP0.

The primers used were:

CDH1 forward, 5-GAC ACC AAC GAT AAT CCT CCGA-3

CDH1 reverse, 5-GGC ACC TGA CCC TTGTACGT-3

CD44v6 forward, 5-AGG AAC AGT GGT T TGGCA AC-3

CD44v6 reverse, 5-CGA ATG GGA GTC TTC TCT GG-3

ribosomal protein large P0 (RPLP0) forward, 5-ACA TGTTGC TGG CCA ATA AGG T-3

RPLP0 reverse, 5-CCT AAAGCC TGG AAA AAG GAG G-3

Oct3/4 forward, 5-GAC AGG GGG AGG GGA GGA GCT AGG

Oct3/4 reverse, 5-CTT CCC TCC AAC CAG TTG CCC CAA AC-3

c-Myc forward, 5-CGT CTC CAC ACA TCA GCA CAA-3

c-Myc reverse, 5-CAC TGT CCA ACT TGA CCC TCT TG-3

NANOG forward, 5-AGT CCC AAA GGC AAA CAA CCC ACT TC-3

NANOG reverse, 5-TGC TGG AGG CTG AGG TAT TTC TGT CTC-3

Sox-2 forward, 5-GGG AAA TGG GAG GGG TGC AAA AGA GG-3

Sox-2 reverse, 5-TTG CGT GAG TGT GGA TGG GAT TGG TG-3

Zeb-1 forward, 5-GTT ACC AGG GAG GAG CAG TGA AA-3

Zeb-1 reverse, 5-GAC AGC AGT GTC TTG TTG TTG TAG AAA-3

The following cycling conditions were used: 95° C for 10 min, 40 cycles at 95° C for 15 s, 60° C for 1 min, and 72° C for 30 s. The average of cycle threshold of each triplicate was analyzed according to the 2 (-DDCt) method.

6.2.3 Clonogenicity assay

Cells were sorted and one cell per well was plated in three 96-wells plates for each condition. After 15 days, the number of wells with more than three live cells was counted. After 30 days, the diameter of each sphere was measured.

6.2.4 Metabolite extraction

Panc1 cells and Panc CSCs were prepared following the protocol published by Sana et al. (Sana et al., 2008) with minor modifications and metabolomics analyses were performed out. The sample was resuspended by adding 0.15 mL of ice-cold ultra-pure water (18MΩ) to lyse cells. The tubes were plunged into dry ice or a circulating bath at −25 °C for 0.5 min and then into a water bath at 37 °C for 0.5 min. To each tube 0.6 mL of −20 °C methanol and then 0.45 mL of −20 °C chloroform were added. The tubes were mixed every 5 min for 30 min. Subsequently, 0.15 mL of ice-cold pH-adjusted ultra-pure water was added to each tube and these were centrifuged at 1000 ×g for 1 min at 4 °C, before being transferred to−20 °C for 2–8 h. After thawing, liquid phases were recovered and an equivalent volume of acetonitrile was added to precipitate any residual protein. The tubes were then transferred to a refrigerator (4 °C) for 20 min, centrifuged at 10,000 ×g for 10 min at 4 °C and the collected supernatants were dried to obtain visible pellets. Finally, the dried samples were re-suspended in 0.1 mL of water, 5% formic acid and transferred to glass autosampler vials for LC/MS analysis.

6.2.5 Lipid extraction LC-MS analysis

Lipids were extracted with Chloroform:methanol (2:1, v/v), according to the original Folch procedure. Briefly, ice-cold methanol and chloroform were added directly to the cell pellet. The suspension was vortexed and incubated on ice for 20 min. After the addition of water, used to separate the aqueous and organic layer, the suspension was incubated on ice for an additional 10 minutes.

Samples were centrifuged and then the lower phase (organic) layer was transferred to a new tube. The aqueous layer was re-extracted with 2:1 chloroform/methanol. The chloroform layers were combined for the analysis. Finally samples were dried dry in a rotational vacuum concentrator, and reconstituted in 50 µL of isopropanol (IPA) and then transferred to an LC vial with glass insert.

6.2.6 UHPLC-MS/MS

For metabolomics approach twenty microliters of samples (3 biological replicates × 3 technical replicates × 2 conditions × 2 cultivars) were injected into an Ultra High-Performance Liquid Cromatography (UHPLC) system (Ultimate 3000, Thermo) and run in positive ion mode. A Reprosil C18 column (2.0 mm × 150 mm, 2.5 µm - Dr Maisch, Germany) was used for metabolite separation. Chromatographic separations were achieved at a column temperature of 30 °C and flow rate of 0.2 mL/min. A 0–100% linear gradient of solvent A (ddH2O, 0.1% formic acid) to B (acetonitrile, 0.1% formic acid) was employed over 20 min, returning to 100% A in 2 min and a 6-min post-time solvent A hold. The UHPLC system was coupled online with a mass spectrometer Q-Exactive (Thermo) scanning in full MS mode (2 µscans) at 70,000 resolution in the 67 to 1000 m/z range, target of 1 × 106 ions and a maximum ion injection time (IT) of 35 ms. Source ionization parameters were: spray voltage, 3.8 kV; capillary temperature, 300 °C; sheath gas, 40; auxiliary gas, 25; S-Lens level, 45. Calibration was performed before each analysis against positive ion mode calibration mixes (Piercenet, Thermo Fisher, Rockford, IL) to ensure sub ppm error of the intact mass.

For lipidomics approach an Ultra High Performance Liquid Chromatography (UHPLC) system (Ultimate 3000, Thermo) was used to perform lipid separation. Samples were loaded onto a Reprosil C18 column (2.0 mm × 150 mm, 2.5 µm — Dr Maisch, Germany) for lipid separation.Chromatographic separations were achieved at a column temperature of 30 °C and a flow rate of 0.2 ml/min. Mobile phase were A (60:40 acetonitrile/ water) and B (90:10 isopropanol/acetonitrile), each containing 0.1% formic acid. The gradient program included 32% B at 0 min, 40% B at 1 min, a hold at 40% B until 15 min, 45% B at 4 min, 50% B at 5 min, 60% B at 8 min, 70% B at 11 min, and 80% B at 14 min. The total run time was 21 min, including a 3-min equilibration step. The UHPLC system was

coupled online with a Q Exactive mass spectrometer (Thermo). The instrument operated in positive ionization mode with full scan (FS) and data dependent acquisition (DDA). The settings for FS were as follows: resolution, 70,000; automatic gain control (AGC) target, 3e6; maximum injection time (IT), 100 ms; scan range, *m*/*z* 150-2000. Settings for DDA mode were as follows: resolution, 35.000; AGC target, 1e5; maximum IT, 75 ms; isolation window, *m*/*z* 1.7, HCD with stepped normalized collision energy (NCE), 30. Each sample was analyzed with 3 technical (independent analysis of the same extract) replicates.

6.2.7 Metabolomic- lipidomics data processing and statistical analysis

Raw files of replicates were exported, converted into mzXML format through MassMatrix (Cleveland, OH), and then processed by MAVEN software (http://maven.princeton.edu/). Mass spectrometry chromatograms were elaborated for peak alignment, matching and comparison of parent and fragment ions, and tentative metabolite identification (within a 2 ppm mass-deviation range between observed and expected results against the imported KEGG database). To further explore the metabolic differences between Panc1 cells and CSCs at several time pointes, multivariate statistical analyses were employed using the MetaboAnalyst 3.0 software. Before the analysis, raw data were normalized by median and auto-scaling to increase the importance of low-abundance ions without significant amplification of noise. The web- based tool MetPA (Metabolomic Pathway Analysis), which is incorporated into the MetaboAnalyst platform, was used to perform pathway analyses. Data for metabolites detected in all samples were submitted into MetPA with annotation based on common chemical names. Accepted metabolites were verified manually using HMDB, KEGG, and PubChem DBs. A Homo sapiens pathway library was used for pathway analysis.Global test was the selected pathway enrichment analysis method, whereas the node importance measure for topological analysis was the relative betweenness centrality. Metabolites subject to major changes were graphed with Graphpad Prism 5.01 (Graphpad SoftwareInc). Statistical analyses were performed with the same software. Data are means of three replicates ± SD. The different letters indicate significant difference ($p \leq 0.05$ ANOVA) by Bonferroni's

Multiple Comparison Test. For lipidomic analysis raw files of replicates were exported and then processed by Lipid Search software.

6.2.8 Cell proliferation rate

Cell proliferation rate was performed plating 30,000 cells/well in a 24-wells plate for CSCs and in a 6-wells plate for Parental; the analysis times chosen for the experiment were at 2, 4, 7 and 10 days after the plating. At each timing cells were collected and counted with the Trypan blue assay. Three independent experiments were performed.

6.2.9 Cell cycle analysis

Cell cycle distribution was analyzed by staining 3x105 cells with PI. Then, cells were washed with PBS, incubated with 0.1% sodium citrate dihydrate, 0.1% Triton X-100, 200 mg/ml RNase A, 50 mg/ml PI (Roche Diagnostics, Milan, Italy), and analyzed using a flow cytometer (FACScalibur, Becton Dickinson). The percentage of cells in the various stages of the cell cycle was determined using the ModFitLT software (Verity Software House, Topsham, ME, USA). Three independent experiments were performed for each assay condition.

6.2.10 Cell senescence assay through beta-galactosidase

Cell senescence assay was performed with Senescence beta-galactosidase staining kit. The cells were plated in 6-wells plate and following day without reaching the confluence, the cells were centrifugated, washed with PBS and fixed 30 min with Fixative Solution. After the cells were washed with PBS and stained with Beta-galactosidase Staining Solution overnight at 37°C. Photos of the cells were acquired with 5X and 10X objectives.

6.2.11 OCR (oxygen consuption rate)

The assay was pefromed with a kit “MitoXpress Xtra Oxygen Consumption Assay” (Agilent). The easy-to-use MitoXpress Xtra assay allows measurement of extracellular oxygen consumption rates (OCR) with whole cell populations. Rates of oxygen consumption are calculated from the changes in fluorescence signal over time. The reaction is non-destructive and fully reversible so this is useful to measurement of time courses analysis.

6.3 Results

6.3.1 Morphologic changes of Panc1 cells and Panc1 CSCs

In this study we examined changes in cellular morphology of Panc CSCs cultivated for several weeks. Our results showed that Panc1 cells exhibited a typical epithelial morphology with intact cell-to-cell contacts, while Panc CSCs at 2 weeks exhibited cell aggregates and a more dispersed colony. At increased days of cultures (4 weeks), of appearance small spheres are outlined with cellular ramifications that become clearly visible at 8 weeks with well-rounded shape. These results underline morphology changes over time starting from aggregates to spheres formation, typically in CSCs, at 8 weeks (Figure 6.1A).

In order to compare gene expression of stem cell marker in CSC and confirm the acquisition of epithelial mesenchymal transition (EMT) phenotype, Real Time PCR analyses were carried out. The results showed high expression, over time, of several CSC markers (OCT3/4, C-MYC, NANOG, SOX2, ZEB-1 CD44-46) in comparison with Panc1 cells. Additionally CDH1, a major marker of epithelial cell states, was significantly reduced at 8 weeks confirming an acquisition of EMT phenotype (Figure 6.1B).

To evaluate the capability of a single cell to grow into a large colony through clonal expansion we conducted a clonogenic assay. Clonogenic activity is a sensitive indicator of undifferentiated cancer stem cells because CSC is able to proliferate on its own while a differentiated cell needs to cell-cell contact and hardly replicates at the conditions of the assay. So, for each condition (control, 2 weeks, 4 weeks and 8 weeks) we plotted a single cell for plate and we evaluated their proliferation ability (Figure 6.1C).

After 15 days, plates with more than 3 cells were counted indicating starting of proliferation and so they were stamness (Figure 6.1C left side).

At day-30 the diameter of colonies was measured (Figure 6.1C right side). Results show that all plates with more than 3 cells (CSCs) formed spheres with the same diameter regardless of the incubation period, so that CSCs were less present at 2 weeks there were less CSCs showed the same ability to form spheres as 8-weeks grown CSCs.

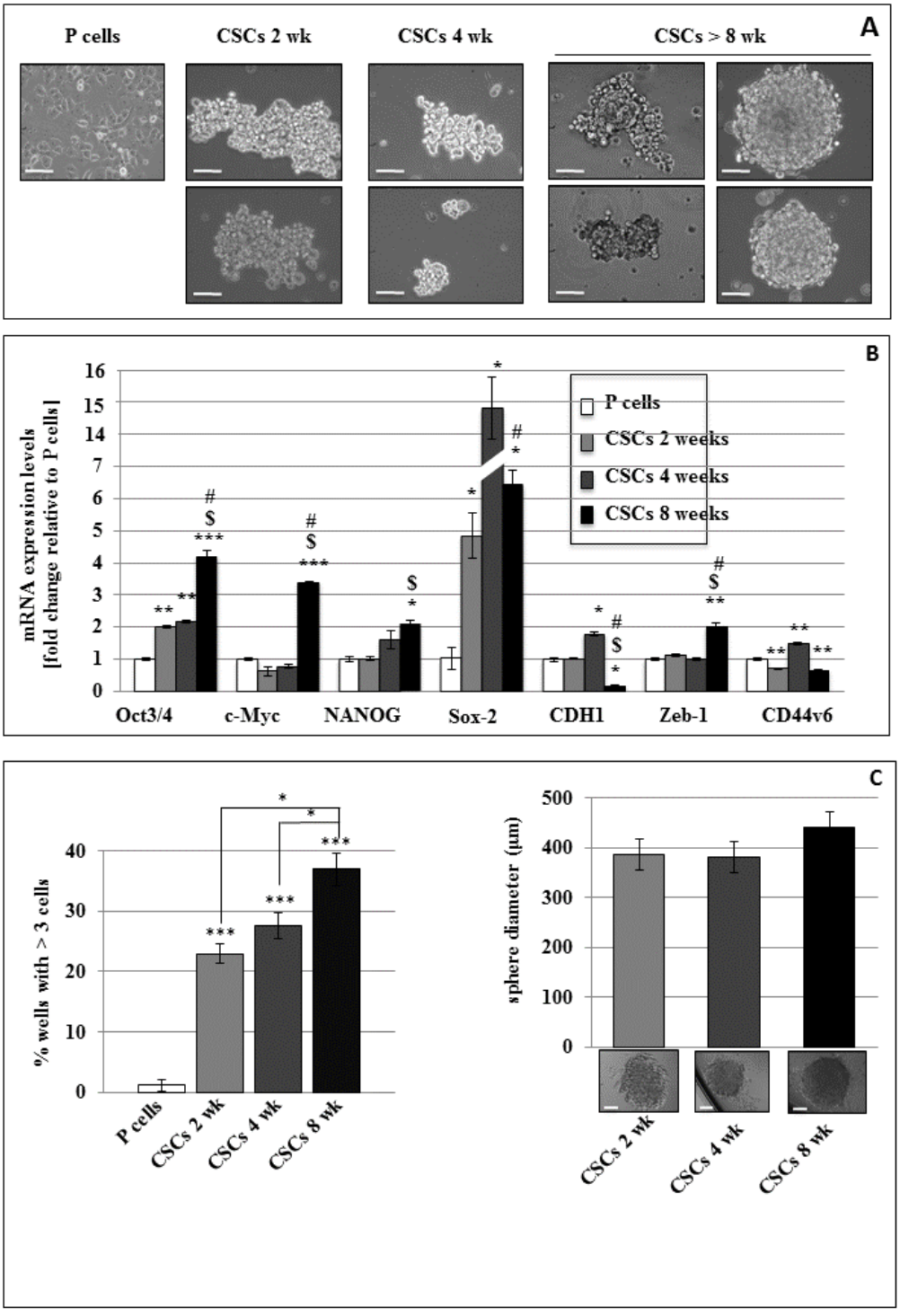

Figure 6.1: morphological analyses of Panc CSCs and CSCs at 2, 4, 8 weeks. Panel A: morphology changes of CSCs over time starting from aggregates at 2 weeks, to spheres formation at 2 weeks at 8 weeks. Panel B RT-PCR of stamness marrkers Oct3/4, C-Myc, Nanog, Sox2, Zeb-1 Cd44-46 and CDH1 that confirm the acquisition of epithelial mesenchymal transition (EMT) phenotype. Panel C: clonogenic assay. At 15 days, plates with more than 3 cells was misured (Figure 6.1C left side). At 30 days the sphere diameter don't change between 2 weeks and 4 weeks. These CSCs show the ability to form spheres as 8-weeks grown CSCs (Figure 6.1C right side).

6.3.2 Time-course metabolomic and lipidomic analyses

Based on our earlier results, we decided to investigate metabolic variation of PDAC CSCs at different time of growth. To this end we used LC-resolution mass spectrometry platforms to performed untargeted metabolomics and lipidomics analyses. To identified the most relevant pathways altered during time we used the bioinformatics Metabolomics Pathway Analysis (MetPA) by MetaboAnalyst 3.0 which combines results from the pathway enrichment analysis with the pathway topology analysis. Results demonstrated that CSCs undergoes several metabolic switches during time. The majority of metabolic pathways that are significantly altered over time are relative to amino acids and carbon metabolism (Figure 6.2). Moreover, finding showed more significant alterations between control and CSCs than in CSCs at several time points. Since the identified metabolites into meaningful metabolic pathways, do not provide information about the direction (up-regulation or down-regulation) of the enrichment, to complement this analysis, bar graph models were constructed for the peak areas of each identified metabolites, by also considering their pathways belongings (Figure 6.3). The variations of the concentration levels over time were analyzed for metabolites of glycolysis, pentose phosphate, amino acids and the energetic metabolisms.

Figure 6.3 clearly shows that, in the first 2 weeks of growth CSCs take advantage of glycolytic metabolism (Figure 6.3A). In fact, both the first glycolytic phosphate precursors and the intermediate of pentose phosphate pathway were up-regulated (Figure 6.3B). Moreover these cells produce high amounts of lactate indicating an accentuation of the Warburg effect. Conversely, during the following two weeks, CSCs efficiently switch their metabolism towards mitochondrial oxidative phosphorylation (OXPHOS), which generates more adenosine triphosphate (ATP) than glycolysis. After 4 weeks of growth the last metabolites of glycolysis become upregulated showing that a rebalance of oxidative pathways occurs. In addition, also citrate is more produced at this time. Besides fueling the oxidative mode of the TCA, citrate can also be converted into acetyl-CoA to be employed for fatty acid and cholesterol synthesis to support the membrane need associated with intense proliferation (Figure 6.4A).

From the energy point of view, the restoration of oxidative metabolism has been confirmed both by increased oxygen consumption rates at 4 weeks as measured by OCR (Figure 6.4B), and by down-regulation of AMP and GMP intermediates (Figure 6.4C).

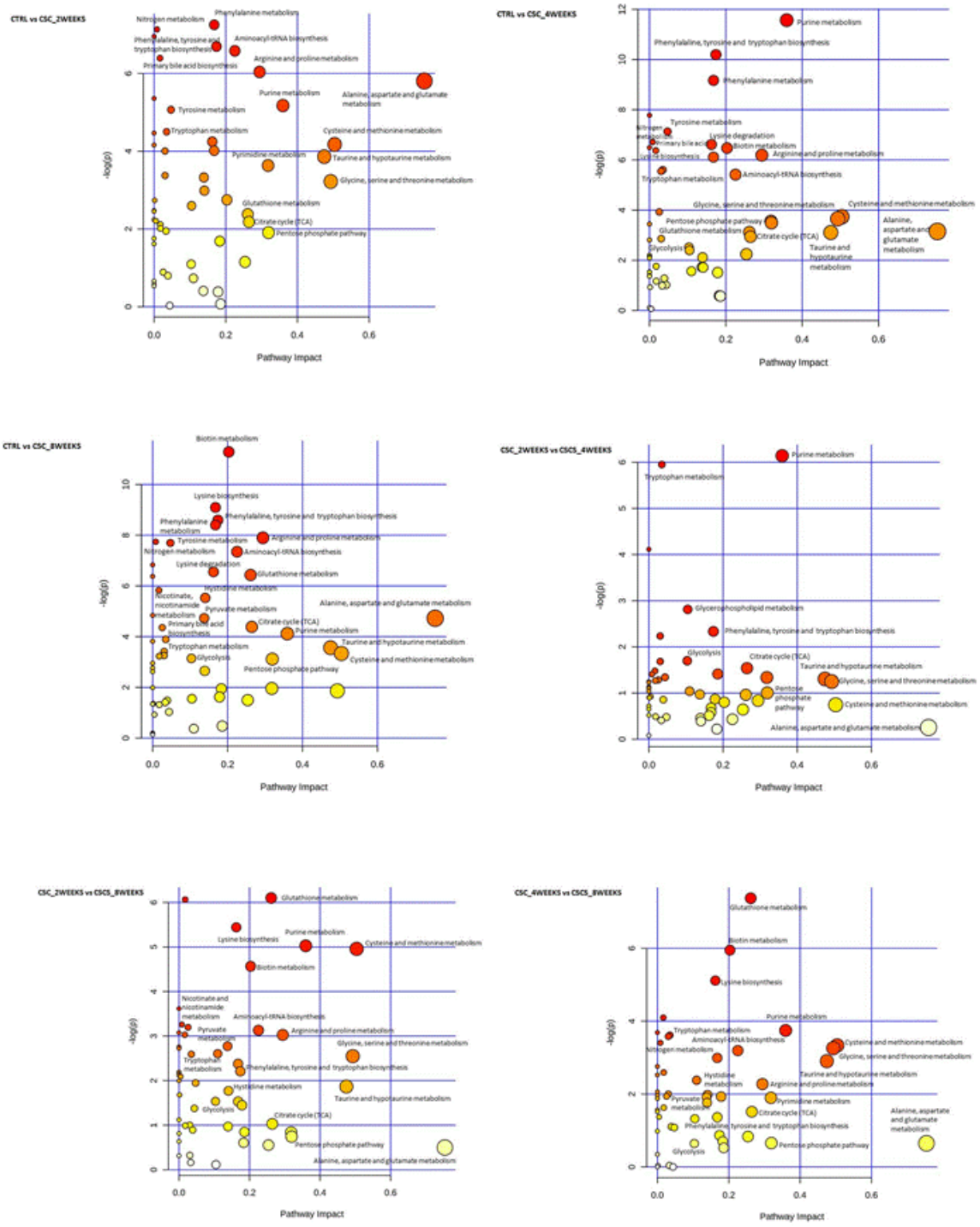

Figure 6.2: Metabolomic Pathway Analysis (MetPA) as generated by MetaboAnalyst software package. All the matched pathways are displayed as circles. The color of each circle is based on p-values (darker colors indicate more significant changes of metabolites in the

corresponding pathway), whereas the size of the circle corresponds to the pathway impact score. Select pathways with high pathway impact and/or high p-value are labeled.

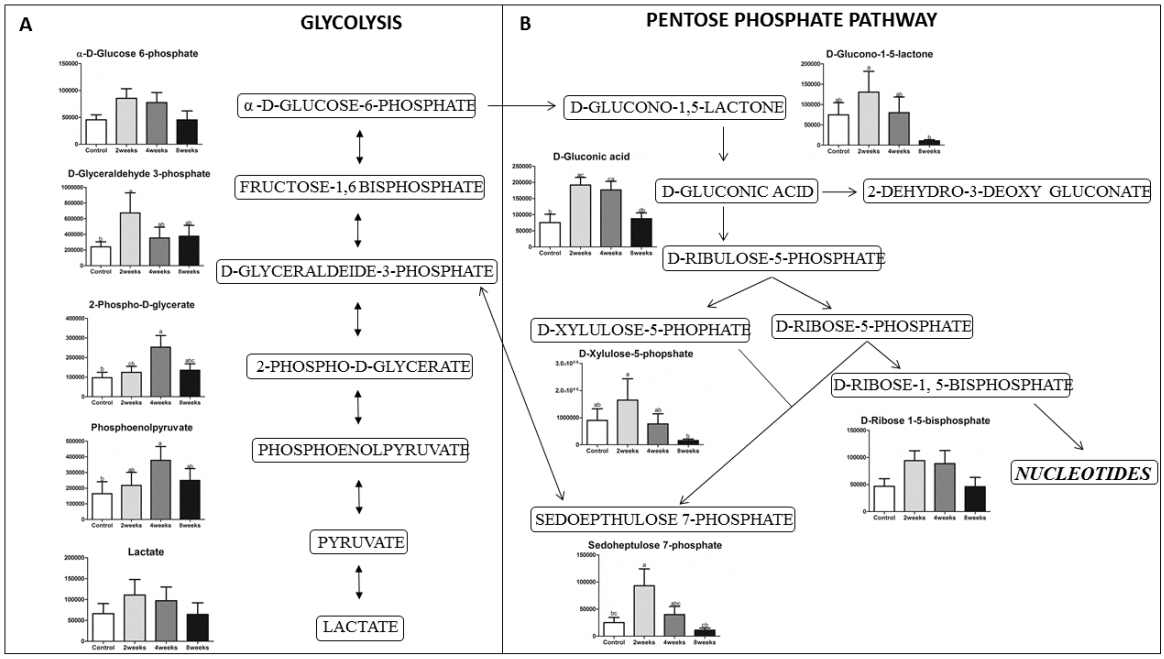

Figure 6.3 Alterated metabolomic pathways in PDAC cells. Panel A: Time course metabolomics analysis of Glycolysis. Panel B:Time course metabolomics analysis of Pentose Phosphate Pathway.Data are means of three replicates ± SD. The different letters indicate significant difference ($p \leq 0.05$ ANOVA) by Bonferroni's Multiple Comparison Test.

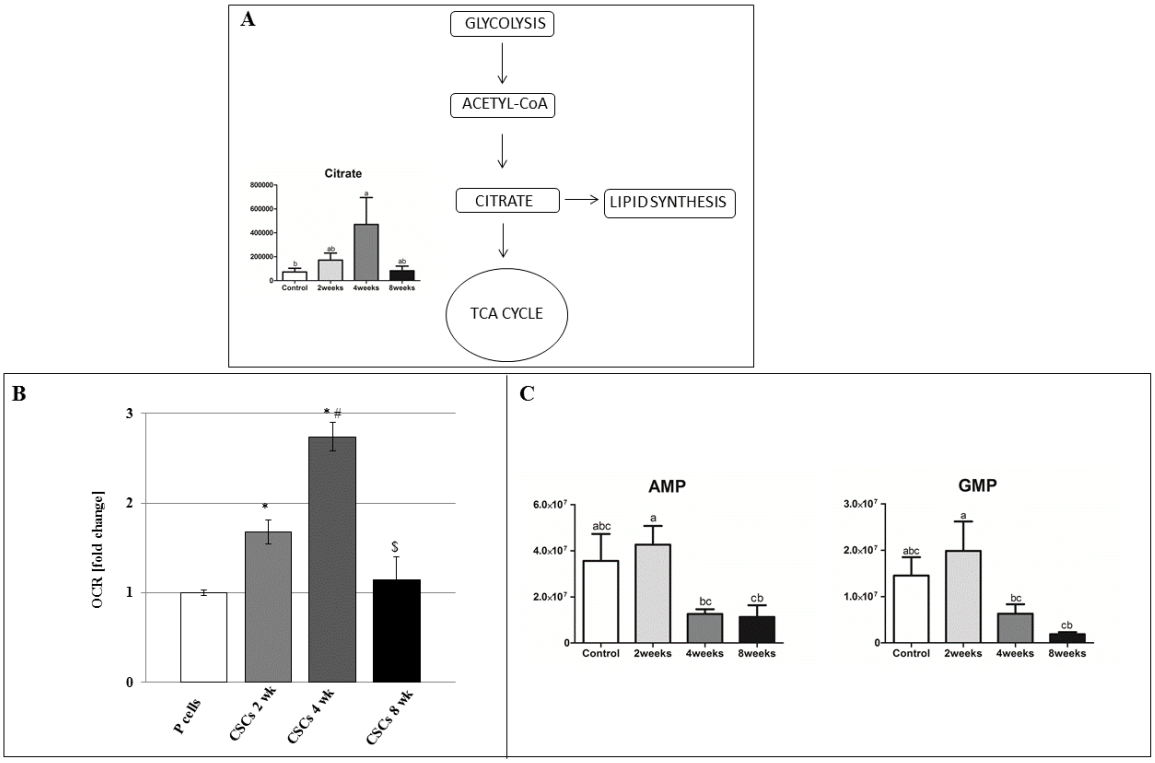

Figure 6.4 metabolic switch of CSCs at 4 weeks. Panel A level of citrate metabolites at 4 weeks. It's used to lipid synthesis. Panel B Increase of oxygen consumption rate in CSCs at 4 weeks. Panel C decrease levels of AMP and GMP in CSCs at 4 weeks.

One of the most interesting results of the analysis was the evidence that glucose uptake, glycolysis and flux through central carbon metabolism were reduced at 8 weeks. As shown in Figure 6.5 all intermediates of metabolism were strongly down-regulated. This low metabolic state in CSCs is known as quiescence and is characterized by a decreasing growth rate.

The lipidomics analysis detected a total of 6 classes of lipids: ceramides (CER), diacylglycerol (DAG), Phosphatidylcholine (PC), phosphatidylethanolamine (PE), sphingomyelin (SM) and tryglicerides (TG). AS shown in Figure 6.5, PC, PE, SM, the main membrane phospholipids, were up-regulated just at 2 weeks to ensure proliferation of these cells. Moreover, at 8 weeks also all lipid classes were down regulated. These results are in agreement with those obtained by metabolomics, confirming a decrease of proliferation (Figure 6.5).

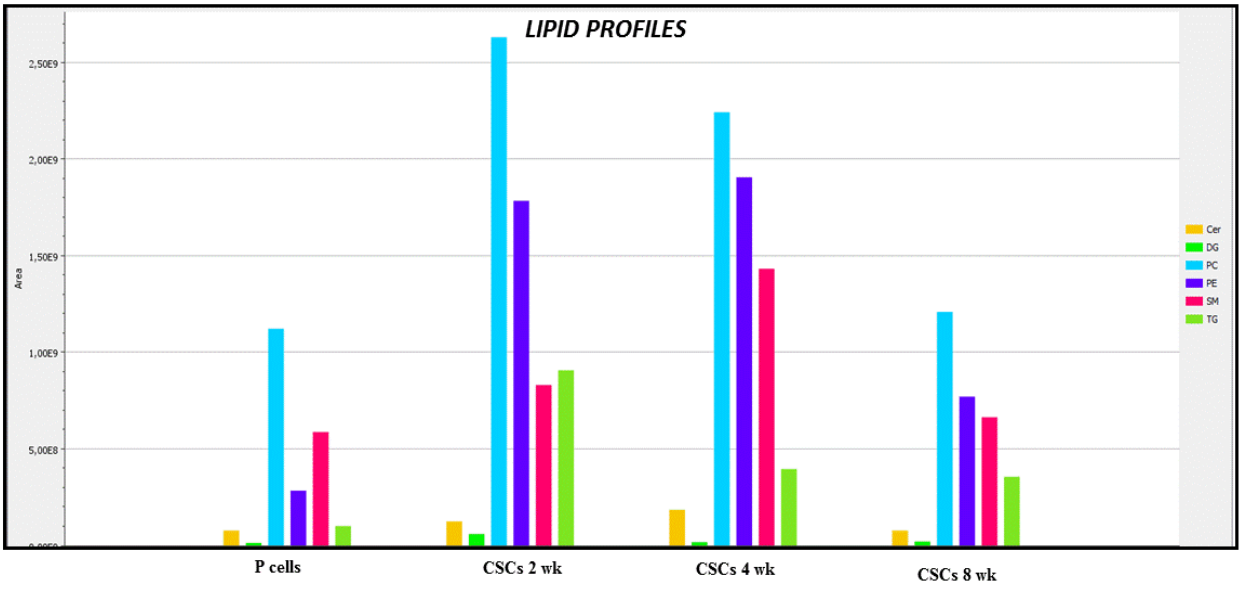

Figure 6.5: Time course analyses of Lipid. Data showed a decrease level of lipid profile at 8 weeks. Ceramides (CER), diacylglycerol (DAG), Phosphatidylcholine (PC), phosphatidylethanolamine (PE), sphingomyelin (SM) and tryglicerides (TG).

6.2.4 Decreased cell proliferation of Panc1 CSCs over time

The observation that, over time, there are metabolic changes metabolism that proceed to a cell quiescence state, lead us to analyze the cell proliferation rate of these cells at different time points (Figure 6.6A). The cell proliferation rate assay, that monitors the number of cells within 10 days, showed a more reduced of proliferation of 8-week CSCs than Panc cells. Similarly also 2 and 4 weeks CSCSs reached a plateau state after 10 days.

This finding was further validated with cell cycle analyses (Figure 6.6B). The cell cycle distributions were investigated by flow cytometry, demonstrating that the ratio of cells in G0/G1-phase was higher than one of other stages. Indeed the ratio of S- and, in particular, G2/M-phase cells significantly decreased at 8 weeks.

However, as G0/G1 phase represents a large temporal fraction of the cell cycle, it is possible that also senescent subpopulations are present therein. Thus, to explore the presence of senescent CSCs, cultures were stained for senescence-associated β-galactosidase activity at 2, 4 and 8 weeks. As shown in Figure 6.6C no differences between 4 and 8 week grown CSCs were detected, confirming that 8-week CSCs enter the quiescent state.

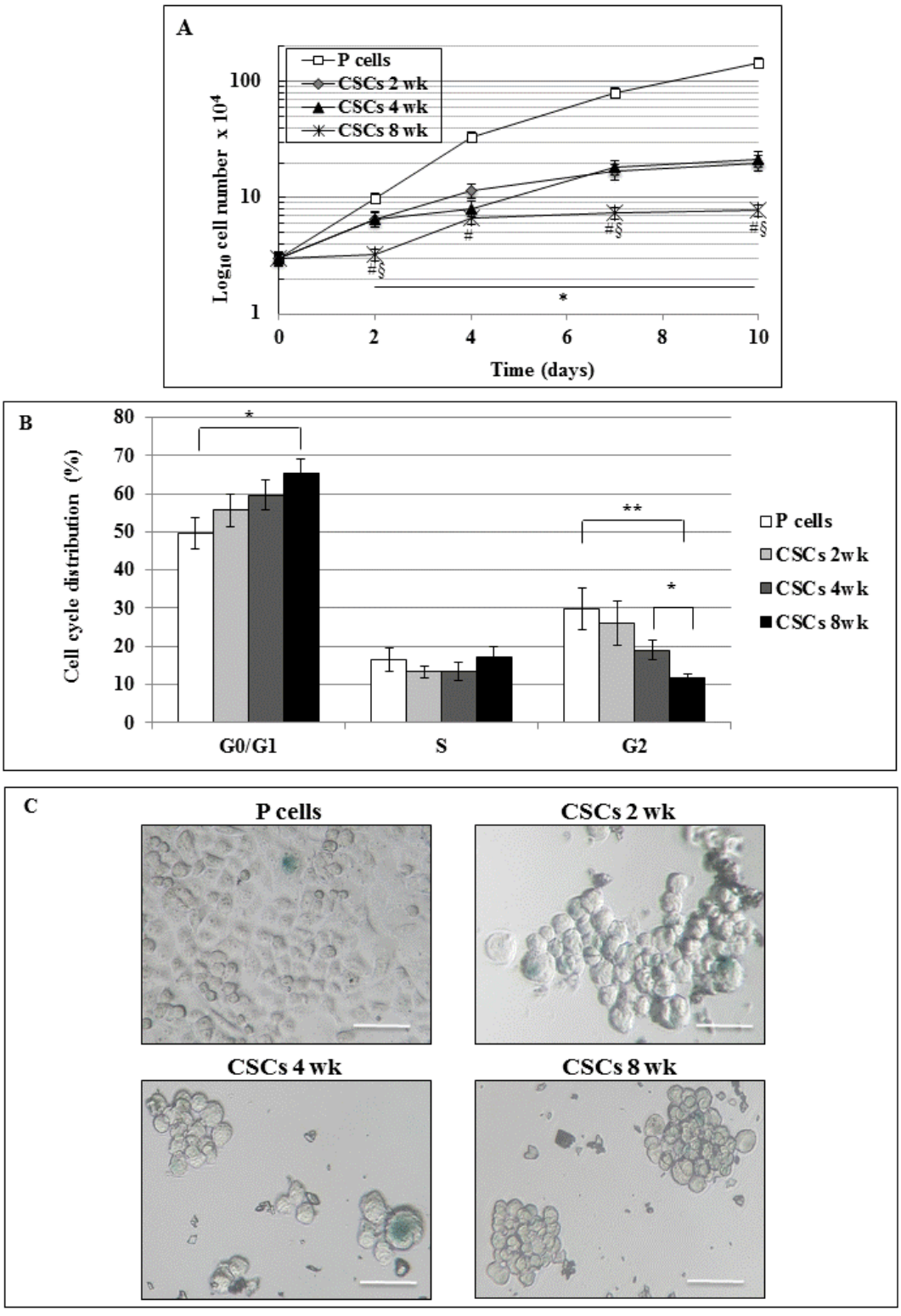

Figure 6. 6. Assays of cell proliferation of Panc1 CSCs. Panel A: cell proliferation rate assay of P cells, 2-weeks CSCs 4-weeks CSCs and 8-weeks CSC within 10 days. Panel B: The cell cycle distributions in different phases G0/G1, S, G2. Data show a significant increase of 8-weeks CSCs in G0/G1 phase.

6.4 Discussion

Pancreatic Cancer Stem Cells (CSCs) account for less than 1% of all pancreatic cancer cells (Bao et al., 2013). They have the capacity of self-renewal, differentiation, resistance to therapy (Yu et al., 2012) and they are able to survive in hostile environments through acquisition of a quiescence state (Delphin et al., 2012). CSC can change from a less differentiated stem-like phenotype to highly active differentiated cells that constitute the bulk of the tumor (Perusina Lanfranca et al., 2018). Due to the high plasticity, a better understanding phenotypic characteristics of this cellular subpopulation and of metabolic changes required for CSC self-renewal, cell division, and quiescence may improve existing therapies and deepen insight into the role of CSCs in pancreatic cancer progression (Rao and Mohammed, 2015). For this reason, for the first time, we analyzed a time course of Panc CSCs to investigate the existence of was an effectives plasticity which leads metabolic switch over time.

6.4.1 Changes in morphology

During time CSCs acquired a cancer stem cell phenotype with characteristic spheroid-formation. Spheroids are characterized by their well-rounded shape, presence of cancer cells, and their capacity to promote in vitro expansion of CSCs if compared to the bulk of tumors (Weiswald et al., 2015). The capability to form spheroids is now considered a characteristic of CSCs due to the propensity of stem cells to propagate as spheroid bodies (Pastrana et al., 2011). Thus, tumor-derived spheroid cultures have been closely tied to in vitro studies of cancer stemness (Ishiguro et al., 2017). This phenotypic variation is also recorded with the stamness marker analysis. Unfortunately no universal cell markers of PDAC CSCs have been unequivocally identified to date (Perusina Lanfranca et al., 2018). However, accumulating data reveal abnormal elevated expression levels of key stemness factors, like Nanog, Oct4, and Sox2, in several types of cancer stem cells (Amini et al., 2014) (Wang et al., 2013). In the present study, we observed an increase of Nanog, Oct4, and Sox2 thus confirming an acquisition of stamness over time. Similarly, also detected an increase of CD44-46.

This results was in agreement with Hong and colleagues who demonstrated showing that CSCs in pancreatic tumor tissues are associated to drug resistance and metastatic potential, with pancreatic tumor cells having a CD44 positive CSC phenotype, which correlates with tumor histological grade and poor clinical outcomes (Hong et al., 2009). Interestingly *CDH1* gene coding E-cadherin, highly expressed in epithelial cells, undergo a significant decrease over time. E-cadherin modulates epithelial structure remodeling and the maintenance of epithelial stemness, moreover its loss of E-cadherin during tumor progression may result in epithelium to mesenchyme transition (EMT) (Spaderna et al., 2007). CSCs often exhibit EMT properties. This reciprocal relationship between EMT and CSCs might have many implications in tumor progression (Liu and Fan, 2015). In cancers, EMT is implicated in the progression of tumors towards a metastatic phenotype and is marked by a loss of epithelial features and an upregulation of mesenchymal properties (Delphine et al., 2012). Remarkably these results show, for the first time, the high plasticity level of CSCs that over time change their phenotype. 8-week CSCS can be considered as the best in vitro model with highly level of stamness and epithelial mesenchymal transition (EMT) phenotype. Basically they very closely mimic characteristics of stem cells in patients affected by PDAC.

Metabolic changes in PDAC CSCs

The discovery of an elevate plasticity of CSC lead us to explore if to a phenotypic variation also corresponds a change in metabolism over time. By applying high resolution mass spectrometry, we showed that the most significant metabolic changes were relative to energy metabolism, in fact over time CSCs shift from glycolysis to OXPHOS. Glycolytic flux is elevated at 2 weeks to provide ATP and intermediate metabolites through the pentose phosphate pathway for nucleotide biosynthesis. This unusual utilization of glucose results in the production of lactate in the presence of oxygen sufficiency (aerobic glycolysis) and is known as the Warburg effect (Upadhyay et al., 2013). So, at this state, CSCs increased the Warburg effect for rapid proliferation, with the pentose phosphate pathway generating ribose-5-phosphate for nucleotides biosynthesis (Figure 6.3B). It has been well verified that pluripotent stem cells mainly utilize glycolysis for energy production, cell growth and proliferation.

Moreover, the lactate production acidifies the surrounding environment of cancer cells, inhibits the activation of Natural Killer and Cytotoxic T cells, and plays an important role in the growth of cancer (Hirschhaeuser et al., 2011).

Over time, energy production of CSCs shifts to the mitochondrion, a double-membrane organelle that regulates cellular levels of ATP. It well known that some mitochondrial circuitries can adapt to serve bioenergetic or anabolic functions, hence endowing malignant cells with considerable metabolic plasticity (Fendt et al., 2013). The reversibility of many reactions of the tricarboxylic acid (TCA) cycle ensures metabolic adaptation (Pietrocola et al., 2015). One key TCA intermediate is citrate that has a crucial roles in intersection between catabolic and anabolic metabolism, and hence operates as a major node of flexibility of CSCs (Rohrig and Schulze, 2016). Indeed besides entering in TCA, citrate can also be converted into acetyl-CoA and employed for fatty acid and cholesterol synthesis to support the membrane need associated with intense proliferation (Porporato et al., 2018). Lipids are essential components of cell and organelle membranes, and fatty acids are required for proliferation of the bulk tumor mass and also for CSC maintenance (Wang et al., 2018). Hence, in addition to lipids introduced with the diet, de novo CSC lipogenesis become necessary to increase self-renewal growth (Kinlaw et al., 2016). Together with their roles as biomass components, phospholipids and cholesterol play regulatory roles as signaling molecules that engage specific receptors and transcription factors (Wang et al, 2018). So it is not surprising that phospholipid level increased over time.

The most remarkable finding reported in our study is that after 8 weeks CSCs acquire a quiescent phenotype. This result pointed out not only by lipidomic and metabolomic analysis, but also confirmed with morphology and cells proliferation assays. When conditions are unfavorable for proliferation, many cells have the capacity to enter a non-dividing state, sometimes for years, while retaining their ability to reenter the proliferative cell cycle (Valcourt et al., 2012). This quiescence state is common in stem cells that remain in the G0 phase and accordingly reduce their metabolism and proliferation rate.

Quiescent CSCs have vastly lower needs for energy and material to generate biomass if compared rapidly with proliferating cells (Perusina Lanfranca et al., 2018), so they are less glycolytic, consume less glucose, and produce less lactate (Chae and Kim, 2018). CSCs in a dormant state are almost impossible to eliminate by general anti-cancer drugs, which usually target proliferating cancer cells, and targeted therapies for CSCs are therefore needed (Chae and Kim, 2018). Our results underline the interplay between metabolism and proliferation as a strategy to respond to changes in the local environment.

6.5 Conclusions

Over the past years, the importance of pancreatic CSCs for tumor progression and metastasis has been established, so it became clear the necessity to understand PDAC CSCs biology and their distinct molecular features. CSCs have high plasticity that ensures their survival and renders them a primary source for tumor recurrences after or even during treatment. To improve the understanding of their metabolomic characteristics we have carried out a comprehensive time course analysis of Panc CSCs. We demonstrated the ability of these cells to change their metabolism and phenotype over time. CSCs reach a quiescent phase after 8 weeks of growth to survie and respond to changes in the local environment. For the first time, we showed an in vitro model which is very close to the characteristics of stem cells in patients with PDAC. Panc1 CSCs cultivated for many weeks increase over time the expression of markers of stamness with some metabolites that play a key role in the regulation of energy metabolism. The evidence of a quiescent state acquisition is useful to improve the research of novel therapeutic agents that specifically target on dormant CSCs.

7. Pancreatic cancer stem cell proliferation is strongly inhibited by diethyldithiocarbamate-copper complex loaded into hyaluronic acid decorated liposomes

7.1 Introduction

Pancreatic ductal adenocarcinoma (PDAC) is a highly lethal disease that is frequently diagnosed at a late stage and represents the fourth leading cause of cancer-related deaths in the modern world with a five- year survival rate around 5–7% (Siegel et al., 2016, Eskander et al., 2016). In the clinic, the present therapies rarely reduce tumor size and counteract tumor reappearance, thus rendering the identification of new therapeutic strategies necessary. A growing body of evidence suggests that PDAC initiation, growth, metastasis and resistance to therapy are driven by a small population of cells, called cancer stem cells (CSCs) or tumor initiating cells (Li C et al., 2007, Hermann PC et al., 2007, Rasheed et al., 2010). Pancreatic CSCs were identified in 2007 by Li et al. (Li et al., 2007), who showed that pancreatic cancer cells with the CD44+/CD24+/ESA+ phenotype (0.2–0.8% of all pancreatic cancer cells) possessed a 100-fold increased tumorigenic potential compared with marker negative cancer cells and just a small fraction of CD44+/CD24+/ESA+ cells was sufficient to give rise to tumors histologically indistinguishable from the primary human tumor. After this discovery, great efforts have been made to understand the CSC biology in terms of origin and propagation, and their role in cancer progression and metastasis promotion. CSC population shows specific features, including the ability to self-renew, to produce a more differentiated progeny, to grow in independent anchorage conditions, and to resist to standard chemotherapy engendering disease relapse following treatment (Hermann et al., 2007, Visvader Lindeman et al., 2012). In the context of chemo resistance and recurrence, a major impact on tumor progression can derive from the use of treatments directed against not only differentiated cells, that re-present the bulk of the tumor, but also CSCs (Lonardo et al., 2011). Thus, in order to develop CSC-targeted therapies, it is important to take advantage of CSC specific features, that in part have already been identified, and of *in vitro* cell

cultures and patient-derived xenograft models (Dalla Pozza et al., 2015, Jimeno et al., 2009) that re-present the tumor heterogeneity of PDAC. For instance, a frequent strategy used in this field has been the targeting of CD44-expressing CSCs with its specific ligand, hyaluronic acid (HA) (Wang et al., 2015, Muntimadugu et al., 2016). The anti-alcoholism drug disulfiram (DSF, Antabuse®) has been shown to act as antitumoral drug (Cen et al., 2002, Lovborg et al., 2006, Cho et al., 2007) and represents a possible candidate as an anti-CSC agent in breast cancer and glioblastoma (Kim et al., 2016, Liu et al., 2012). The anticancer activity of DSF has not yet been fully elucidated. Indeed, several mechanisms have been proposed, such as the inhibition of aldehyde dehydrogenase, proteasome, NF-κB, DNA methyltransferase, and multidrug resistance p-glycoprotein activities (Lovborg et al., 2006, Liu et al., 2012, Han et al., 2013, Paranjpe et al., 2014). Furthermore, when used in combination with copper, DSF becomes a strong inducer of radical oxygen species (ROS) (Allensworth et al., 2015). Despite its powerful anticancer activity, the development of DSF-based cancer therapy has been hampered by its poor solubility in biological fluid and instability in gastric juice and bloodstream (Johansson, 1992). To overcome these limitations, the development of drug delivery systems is crucial in order to protect DSF from degradation and increase drug concentration in tumor site (Peer et al., 2007). Moreover, the encapsulation of DSF into nanoparticles renders it suitable for intravenous administration. One of the most known drug delivery system is liposomes, which, because of their structure, can encapsulate a wide range of molecules with hydrophilic, amphiphilic, or lipophilic characteristics. In addition, the phospholipidic framework ensures complete biocompatibility (Akbarzadeh et al., 2013). Along the years, the research in liposome field has been gradually oriented to- wards the development of systems capable of specifically recognizing the target cells (Deshpande et al., 2013). This strategy, known as active targeting, involves the use of a targeting agent able to “drive” the nanosystem directly on the target cells by recognition of specific molecules overexpressed on cell surface. According to this strategy, different liposomes decorated with antibodies, peptides, small molecules, or aptamers have been developed and have shown a significant improvement in tumor drug ac- cumulation (Torchilin, 2008). In this work, we designed liposomes containing DSF or diethyl- dithiocarbamate copper complex Cu (DDC)2 in order to obtain a nanotechnology platform able to selectively target and destroy pancreatic CSCs.

This study is basically divided in two parts. The first concerns the preparation and characterization of liposomal formulations containing DSF and Cu (DDC)2 either plain or targeted, thus selective for pancreatic CSCs. For the active targeting strategy, HA was chosen as targeting agent because pancreatic cancer cell lines, such as Panc1 cells, and CSCs have been shown to display an over-expression of its receptor, CD44 (Li et al., 2015). Moreover, HA is a biodegradable, non immunogenic and non toxic polymer, features that make it a good candidate as a targeting agent (Mattheolabakis et al., 2015, Misra S et al., 2011). In order to obtain liposomes decorated with HA, conjugates between the phospholipid 1,2-dipalmitoyl-*sn*-glycero-3- phosphoethanolamine (DPPE) and HA were synthesized and incorporated in the liposomal preparations. HA of low molecular weight (MW) (4800 and 17000 Da) were chosen as targeting agents on the basis of our previous work that demonstrated a strong affinity of the oligomers towards CD44 positive pancreatic tumor cells (Arpicco et al., 2013, Dalla Pozza et al., 2013). The second part of the study concerns the *in vitro* evaluation of the effect of DSF and Cu (DDC)2 liposome formulations on proliferation of CSCs derived from PDAC cell lines or patients and the analysis of ROS to define the differential activity of the formulations on parental cells and CSCs.

7.2 Materials and methods

7.2.1. Materials and instruments

Sodium hyaluronate of MW 4800 (HA4800) and 17000 (HA17000) Da were purchased from Lifecore Biomedical (Chaska, MN). All the phospholipids were provided by Avanti Polar-Lipids distributed by Spectra 2000 (Rome, Italy). Solvents, *N*-acetyl-L-cysteine (NAC), diacetylated 2′,7′-dichlorofluorescein (DCF-DA) probe and all the other chemicals were obtained from Sigma-Aldrich (Milan, Italy). HPLC analyses were carried out using a Merck Hitachi HPLC System (Milan, Italy). The analytical column was a Symmetry C18 column, 5 μm (Merck) equipped with a C18 column guard (Merck Hitachi HPLC) system. Spectrophotometric analyses were performed using Beckman Coulter DU 730 UV–vis spectrophotometer. Mass spectrometry analyses (MS) were carried out using

electrospray ionization (ESI) or by atmospheric pressure chemical ionization (APCI), in positive ion mode, on a Micromass ZQ spectrometer (Waters). The 1H nuclear magnetic resonance (NMR) spectra were recorded on a Bruker 300 Ultrashield instrument (Karlsruhe, Germany) in a mixture of D2O, CD3OD, CF3CO2D in a volume ratio of 6:3:1 at room temperature, with Me4Si (TMS) as internal standard. Differential scanning calorimetry (DSC) was performed using a DSC Q1000 (TA Instruments). CryoTEM was performed at I2BC (Gif-sur-Yvette, France) using a JEOL JEM-1400 operating at 120kV. Images were recorded on a US1000XP camera (Gatan Inc., CA) with a − 4.2 μm defocus. The reactions were monitored by thin-layer chromatography (TLC) on F245 silica gel precoated sheets (Merck).

7.2.2. Synthesis and characterization of hyaluronic acid-phospholipid conjugates

HA-DPPE conjugates were prepared using the method described by Arpicco et al. (Arpicco et al., 2012). A minor modification was introduced in the purification process: to completely eliminate the unreacted phospholipid still present in the conjugate after dialysis, extraction process with di- chloromethane was performed. In this way, the unreacted DPPE was solubilised in the organic phase and thus separated from the conjugate. The aqueous phase was analyzed by TLC (chloroform/methanol 70:30 v/v) to monitor the disappearance of free DPPE from the con- jugate and the extraction with dichloromethane was repeated until complete removal of the free phospholipid. The purified compounds were freeze-dried, and the yield was 30% for HA4800-DPPE conjugate and 60% for HA17000-DPPEconjugate. 1H NMR (D2O, CD3OD, CF3CO2D in a volume ratio of 6:3:1, 300 MHz): d 0.9 (6H, terminal CH3 of DPPE), 1.3 (56H, methylene protons of DPPE), 1.5 (4H, NHCH2CH2), 2.0 (Nac - CH3), 3.3–4.0 (sugar ring protons), 4.4–4.6 (sugar ring protons).

7.2.3. Preparation of DDC/metal complexes

DDC/metal complexes were synthesized by adding dropwise MilliQ® water solution of CuCl2 2H2O (75.53 mg, 0.443 mmol; Cu (DDC)2) or FeCl3 6H2O (119.74 mg, 0.443

mmol; Fe(DDC)2) or ZnSO4 H2O (79.50 mg, 0.443 mmol; Zn(DDC)2) to MilliQ® water solution of DSF active metabolite sodium diethyldithiocarbamate trihydrate (DDC, 100 mg, 0.443 mmol). The reaction was stirred at room temperature for about 10 min until the formation of precipitate, which indicates the occurred complexation. The solution was then filtered and the resulting precipitate was washed three times with MilliQ® water and dried under vacuum. The formation of the DDC/metal complexes was assessed by MS. Cu (DDC)2: (C10H20CuN2S4) calc: 358.98, found: 359.13 [M]+, Fe (DDC)2: (C10H20FeN2S4) calc: 351.99, found: 352.15 [M]+, Zn (DDC)2: (C10H20ZnN2S4) calc: 359.98, found: 360.14 [M]+.

7.2.4. Preparation of liposomes

7.2.4.1. DSF containing liposomes

DSF containing liposomes (LipoDSF-5%PEG) were prepared using the thin lipid film-hydration method mixing together 1,2-distearoil-*sn*- glycero-3-phosphocoline (DSPC), cholesterol (CHOL) and 1,2-dis- tearoyl-*sn*-glycero-3-phosphoethanolamine-N-[amino(polyethylene glycol)-2000] (mPEG2000-DSPE) in 55:40:5 molar ratio. DSF was added to the lipid mixture in 14% ratio (mol drug/mol lipid). The resulting lipid film was hydrated with 900 µl of citric acid buffer (pH 4.8), as DSF is more stable at pH value of 4.5–5 (Chen X et al., 2015). The suspension was vortex mixed for 10 min and bath sonicated. The formulations were extruded (Extruder, Lipex, Vancouver, Canada) at 60 °C under nitrogen through 200nm polycarbonate membrane (Costar, Corning Incorporated, NY) and then purified by gel filtration using Sepharose CL- 4B columns, eluting with HEPES buffer. Liposomes were stored at 4 °C.

7.2.4.2. Cu(DDC)2 containing liposomes

Liposomes (LipoCu (DDC)2–5%PEG) were prepared using a method recently described by Wehbe et al. (Wehbe et al., 2011) with minor modifications. The liposomes were composed of DSPC, CHOL and mPEG2000-DSPE in 55:40:5 molar ratio.

Lipids were dissolved in chloroform and evaporated by rotary evaporator. The resulting lipid film was hydrated with 1ml of CuCl2 solution (300 mM), vortex mixed and incubated for 1h at 60 °C. Liposomes were then extruded as previously reported and purified from unencapsulated CuCl2 through chromatography on Sepharose CL-4B columns, eluting with SHE buffer [sucrose (300 mM), HEPES (20 mM) and EDTA (15 mM)] (pH 7.5). Then, a solution of DDC (0.25 mg/50 µl MilliQ® water) was added to liposomes and incubated for 25 min at room temperature. Finally, liposomal preparations were purified from unencapsulated Cu (DDC)2 through chromatography on Sepharose CL-4B columns, eluting with SH buffer [sucrose (300 mM) and HEPES (20 mM)] (pH 7.5). Liposomes were stored at 4 °C. To prepare HA liposomes (LipoCu (DDC)2–5%HA4800, LipoCu (DDC)2–5%HA17000, LipoCu (DDC)2–2%PEG-3%HA4800, and LipoCu (DDC)2–2%PEG-3%HA17000), the same method was used. Lipid films were made up of DSPC/CHOL/mPEG2000-DSPE (55:40:2 molar ratio) or DSPC/CHOL (55:40 molar ratio) and then hydrated using CuCl2 solution of the different HA-DPPE conjugates (3 or 5 molar ratio).

7.2.5. Liposomes characterization

The mean particle size and polydispersity index (PDI) of the liposomes were determined at 20 °C by dynamic light scattering using a Zetasizer (Nano-ZS, Malvern instruments, UK). Size measurements were performed at a fixed angle of 173° after dilution of the liposome suspensions in MilliQ® water. Each measurement was carried out in triplicate. The surface charge of liposomes was evaluated by zeta potential measurements after dilution of the suspensions in 10mM KCl. Phospholipid phosphorous was assessed in each liposome preparation by phosphate assay after destruction with perchloric acid (Bartlett GR, 1959). The amount of encapsulated DSF was determined by HPLC. Ten µl of liposomal suspension were diluted in 30 µl of methanol, sonicated, vortexed and centrifuged for 5 min at 6000 ×*g*. Then, the clear supernatant was filtered with 0.45 µm PTFE filters and analyzed by HPLC. The column was eluted with methanol/water (80:20 v/v) flow rate 0.8 ml/min. Detection was performed by UV adsorption measurement at 275 nm. Peak heights were recorded and processed on a CBM-10A Shimadzu interface.

The drug concentration was calculated from standard curves. The assay was linear over the tested concentration range (5–50 μg). Each sample was analyzed in triplicate. The amount of Cu (DDC)2 incorporated into liposomes was determined by UV-VIS spectrophotometer: 20 μl of liposomal suspension were diluted in 480 μl of DMSO, sonicated, vortexed and centrifuged for 5 min at 6000 ×*g* and the supernatant was analyzed at 435 nm. Each sample was analyzed in triplicate. Liposomal preparations were analyzed for physical stability in the storage conditions (4 °C) evaluating diameter, zeta potential and drug leakage at different time intervals. Drug leakage was determined by submitting 200μl of liposomes to purification through chromatography on Sepharose CL-4B columns, eluting with HEPES buffer for DSF or SH buffer for Cu (DDC)2 and re- analyzing for drug and phospholipid content as described above. A change in content was interpreted as an indication of liposome instability.

7.2.5.1. Differential scanning calorimetry (DSC)

DSC analysis was performed on hydrated samples. About 20 mg of accurately weighted suspension samples were introduced into a 40 μl aluminum pan and analyzed. DSC runs were conducted from 25 °C to 80 °C at a rate of 10 °C/min under constant nitrogen stream (40 ml/ min). The main transition temperature (Tm) was determined as the onset temperature of the highest peak. Calibration was achieved using indium (Tm = 156.83 °C) and *n*-decane (Tm = −29.6 °C).

7.2.5.2. Cryogenic transmission electron microscopy (cryo-TEM)

Empty and Cu (DDC)2 loaded liposomes (30 mg/ml) were diluted 5× in SH buffer and 5 μl of solution were deposited onto copper grids covered with Lacey carbon film. Excess of solution was blotted off for 5 or 7 s using filter paper and the grids were subsequently frozen in liquid ethane using a Leica EM GP automatic system (Leica, Austria) under 90% humidity atmosphere.

7.2.6. In vitro cell studies

7.2.6.1. Cell lines

The human Panc1 pancreatic adenocarcinoma cell line was grown in RPMI 1640 supplemented with 10% FBS, 2mM glutamine, and 50 μg/ml gentamicin sulfate (Gibco, Thermo Fisher Scientific, Milan, Italy) at 37 °C with 5% CO2. Panc1 CSCs were generated as previously described (Dalla Pozza et al., 2015) and cultured in CSC medium, [DMEM/F-12 (US biological Life Sciences) supplemented with 1 g/l glucose, B27 (Gibco, Thermo Fisher Scientific), 1 μg/ml fungizone (Gibco, Thermo Fisher Scientific), 1% penicillin/streptomycin (Gibco, Thermo Fisher Scientific), 5 μg/ml heparin (Sigma-Aldrich), 20 ng/ml EGF (epidermal growth factor, Peprotech, London, UK), and 20ng/ml FGF (fibroblast growth factor, Peprotech) at 37 °C with 5% CO2.

7.2.6.2. In vitro cytotoxicity assay

Panc1 and Panc1 CSCs were plated in 96-well cell culture plates. Viable cells were counted by Trypan Blue dye exclusion and 7 × 103 cells were seeded in each well. After 24 h both cell lines were treated with a range of concentrations from 0.05 to 100 μM of DSF, Zn(DDC)2, Fe(DDC)2 and Cu(DDC)2 or liposomes (LipoDSF-5%PEG, LipoCu (DDC)2–5%PEG, LipoCu (DDC)2–5%HA4800, LipoCu (DDC)2–5%HA17000, LipoCu (DDC)2–2%PEG-3%HA4800, and LipoCu (DDC)2–2%PEG-3% HA17000). Cell viability was evaluated using resazurin Cell Viability Assay Kit (Immunological Science, Rome, Italy), which is an indicator of cell viability by converting resazurin, a non-fluorescent dye, to resorufin, a highly red fluorescent dye, in response to chemical reduction of growth medium due to cell growth. Sixty μl of resazurin solution (10 μl of resazurin and 50 μl of fresh medium) were added in each well. After 1 h, the fluorescent signal was monitored using 535 nm excitation wavelength and 590 nm emission wavelength. The fluorescent signal generated from the assay is proportional to the number of living cells in the well. Three independent experiments were performed for each condition and cell viability was reported as the percentage relative to control.

7.2.6.3. ROS analyses

The non-fluorescent diacetylated 2,7-dichlorofluorescein (DCF-DA) probe (Sigma-Aldrich), which becomes highly fluorescent upon oxidation, was used to evaluate intracellular ROS production. Briefly, cells were plated in 96-well plates (1 × 104 cells/well) and, the day after, were treated with the various compounds at the indicated concentrations for 24 h. At the end of the various treatments, the cells were incubated in culture medium with 10 μM DCF-DA for 15 min at 37 °C. The cells were washed with PBS and the DCF fluorescence was measured by using a multimode plate reader (Ex485 nm and Em535 nm) (GENios Pro, Tecan). The values were normalized on cell number by using trypan blue solution.

7.2.6.4. Glutathione analyses

Metabolites were extracted as previously reported (Brandi J et al., 2017). Analyses were performed with an Ultimate 3000 Rapid Resolution HPLC system (LC Packings, DIONEX, Sunnyvale, CA) and an electrospray hybrid quadrupole time-of-flight instrument MicroTOF-Q (Bruker-Daltonik, Bremen, Germany) equipped with an ESI-ion source. The procedures and technical settings used were consistent with our previous investigation (Brandi et al., 2017). Because calibration of the mass analyzer is essential in order to maintain a high level of mass accuracy, instrument calibration was performed externally every day with a sodium formate solution consisting of 10mM sodium hydroxide in 50% isopropanol: water, 0.1% formic acid. Automated internal mass scale calibration was performed through direct automated injection of the calibration solution at the beginning and at the end of each run by a 6-port divert-valve. Metabolite data elaboration was performed through MAVEN.52; mass spectrometry chromatograms were elaborated for peak alignment, matching and comparison of parent and fragment ions, and tentative metabolite identification (within a 10 ppm mass-deviation range between observed and expected results against the imported KEGG database).

7.2.6.5. Primary human pancreatic cancer cells

Human PDAC tissues were obtained with written informed consent from all patients. Primary cultures of freshly retrieved cancer cells were obtained from patients with advanced pancreatic cancer (C75, C76, C102) or from *in vivo* patient-derived xenografts (PDX) (A6L, 12556). Tumors were minced, enzymatically digested with collagenase (STE-MCELL Technologies, Vancouver, Canada) and, after centrifugation, cell pellets were resuspended and cultured in RPMI1640 supplemented with 10% FBS and 50U/ml penicillin–streptomycin. PDX-derived tumor cells were cultured until passage 10 (Lonardo et al., 2015). A6L, 12556, C75, C76 and C102 cells were plated in 96-well cell culture plates. Viable cells were counted by Trypan Blue dye exclusion and 3 x 10^3 cells were seeded in each well and cultured as spheres with DMEM:F12 supplemented with B27 and bFGF in anchorage independent suspension conditions for 3 days (first generation spheres). First generation tumor spheres were harvested using a 40μm cell strainer, dissociated into single cells by trypsinization, and then recultured for additional 7 days (second generation spheres). After 3 days, spheres were treated with 0.1 μM of DSF, Cu(DDC)2, LipoCu(DDC)2–5% PEG or LipoCu(DDC)2–2%PEG-3%HA17000 for 24 h. Cell viability was evaluated using resazurin Cell Viability Assay Kit as described in Section 2.6.2. Three independent experiments were performed for each condition and cell viability was reported as the percentage relative to control.

7.2.6.6. Sphere formation assay

Pancreatic cancer spheres of first and second generation were obtained by culturing primary pancreatic cancer cells as described in Section 2.6.5. Ten thousands cells were seeded in each well in 24-well cell culture plate and incubated for 3days. Then, first and second generation spheres were treated with 0.1 μM of DSF, Cu(DDC)2, LipoCu (DDC)2–5%PEG or LipoCu (DDC)2–2%PEG-3%HA17000 for 4 days. After treatment, a CASY Cell Counter (Roche Applied Sciences, Mannheim, Germany) was used to quantify spheres with a diameter > 40 μm. Each condition was performed in triplicate.

7.2.6.7. Statistical analysis

ANOVA (*post hoc* Bonferroni) analysis was performed by GraphPad Prism 5 (GraphPad Software) and used for multiple-group comparison. Student's *t*-test was used for individual group comparison. P-values < 0.05, 0.01, 0.001 were indicated as *, **, ***, respectively.

7.3 Results and discussion

7.3.1. Synthesis and cytotoxic activity of DDC-metal complexes

As widely reported in the literature, DSF and dithiocarbamates are able to form stable complexes with metals such as copper, zinc, gold, and iron (Buac et al., 2012). The resulting complexes show the ability to inhibit proteasome, metalloproteinases and to induce ROS production (Han et al., 2013, Allensworth et al., 2015, Shian et al., 2003). In this work, complexes between DSF active metabolite DDC and zinc, iron and copper were prepared by mixing aqueous solution of the corresponding salts with DDC. The complexation was instantaneous and visible because of the formation of a considerable amount of precipitate. MS analysis confirmed the formation of the complexes revealing that two molecules of DDC were complexed with one atom of metal and indicating that the resulting structure was the same that could be obtained in the reaction between DSF and metals. We decided to use DDC instead of DSF for two reasons. First, because the purification process of the complexes was easier due to the water solubility of both reagents, DDC and metal salts, which were easily separated from the product by water washing. Second, because the method used to prepare liposomes containing Cu (DDC)2 involved the use of DDC to obtain the formation of the complex inside the liposomes (see below). The antitumor activity of DDC/metal complexes was evaluated, at doses ranging from 0 to 100 μM, on Panc1 parental cell line or the derived Panc1 CSCs. Cu (DDC)2 was significantly more efficacious than DSF, Zn (DDC)2 and Fe (DDC)2, inducing a concentration-dependent reduction of growth on both cell lines (Figure 7.1, Table 7.1). Treatments of 72 h with Cu (DDC)2 showed a greater inhibition of cell growth resulting in a total mortality even at low doses both in Panc1 cells and Panc1 CSCs

(Figure 7.1 B and D), with IC50 values of 0.68 ± 0.16 and 0.35 ± 0.03, respectively (Table 7.1). These results demonstrate that Cu (DDC)2 possesses the strongest antitumor activity in our cell models. For this reason and for its well documented anticancer activity (Chen et al., 2006, Guo et al., 2010), Cu (DDC)2 was chosen for the following experiments.

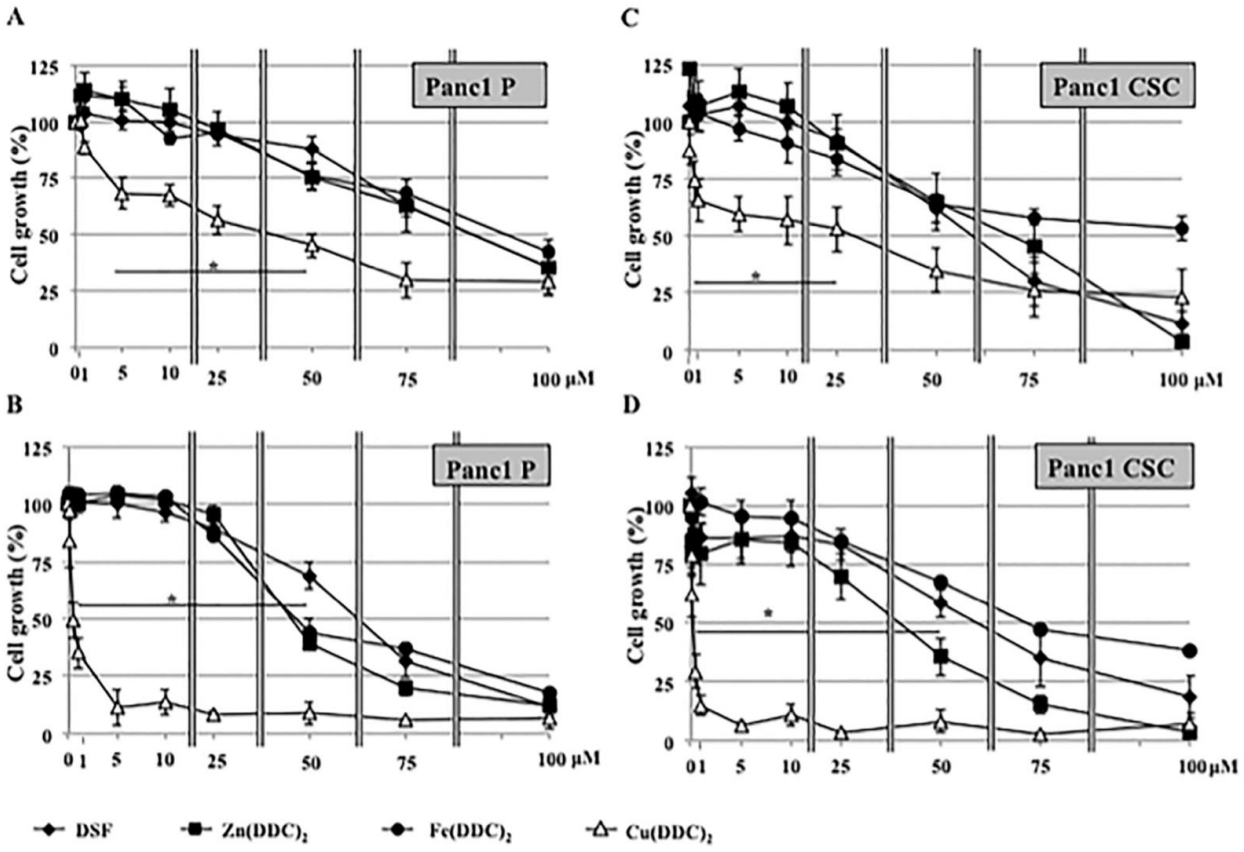

Figure 7.1: Effect of DSF, Zn (DDC)2, Fe(DDC)2, Cu (DDC)2 on Panc1 parental (P) (A and B) and Panc1 CSCs (C and D) cell growth. Cells were seeded in 96-well plates and treated after 24 h with increasing concentrations of DSF formulations for 24 h (A and C) or 72 h (B and D). Cell growth was determined using the resazurin cell viability assay. Values are the means ± SEM of three independent experiments each performed in triplicate. Statistical analysis: DSF or Zn (DDC)2 or Fe (DDC)2*versus* Cu (DDC)2, * $p < 0.05$.

	IC_{50} 24 h (μM)		IC_{50} 72 h (μM)	
	P	CSCs	P	CSCs
DSF	85.5 ± 6.0	60.8 ± 5.9*	65.3 ± 4.2	61.0 ± 10.5
$Zn(DDC)_2$	86.6 ± 2.4	70.3 ± 10.6	45.2 ± 1.2	41.5 ± 7.6
$Fe(DDC)_2$	92.7 ± 2.4	> 100	47.4 ± 3.6	71.6 ± 2.8*
$Cu(DDC)_2$	43.6 ± 10.8$	27.4 ± 7.0$	0.68 ± 0.16$	0.35 ± 0.03$
LipoDSF −5%PEG	73.8 ± 4.2	44.4 ± 0.1*	33.1 ± 0.8#	10.3 ± 1.9#*
LipoCu$(DDC)_2$ −5%PEG	0.46 ± 0.02#	0.68 ± 0.16#	0.28 ± 0.03#	0.08 ± 0.006#*
LipoCu$(DDC)_2$–5%HA4800	0.48 ± 0.001#	0.80 ± 0.31#	0.18 ± 0.003#	0.11 ± 0.08#
LipoCu$(DDC)_2$–5%HA17000	0.34 ± 0.09#	0.97 ± 0.44#	0.18 ± 0.006#	0.04 ± 0.001#*
LipoCu$(DDC)_2$–2%PEG3%HA4800	0.20 ± 0.09#	0.38 ± 0.11#	0.08 ± 0.004#	0.06 ± 0.01#
LipoCu$(DDC)_2$–2%PEG3%HA17000	0.14 ± 0.05#£	0.03 ± 0.004#£	0.20 ± 0.01#	0.02 ± 0.004#*

Table 7.1. IC50 values (expressed as μM) on Panc1 P and Panc1 CSC at 24 h and 72 h after the indicated treatments as determined by resazurin assay, mean ± SEM. P-values < 0.05 were indicated as $ DSF or Zn (DDC)2 or Fe (DDC)2*vs* Cu(DDC) 2; # DSF and DDC metal complex *vs* liposomal complex; £ LipoCu (DDC) 2–5% PEG *vs* LipoCu (DDC) 2−2 % PEG – 3 % HA17000 * P *vs* CSC.

7.3.2. Preparation and characterization of liposomes

7.3.2.1. DSF containing liposomes

This preparation was especially elaborated to find the suitable phospholipidic mixture able to prevent drug leakage. In particular, formulations containing L-α-phosphatidylcholine or 1,2-dipalmitoyl-sn- glycero-3-phosphocholine with different amounts of CHOL (from 10% to 40%) were not stable and after 24 h at 4 °C the total amount of encapsulated DSF was released from liposomes. For this reason, a "rigid" formulation composed of a phospholipid with a high transition temperature (DSPC) and 40% of CHOL was prepared in order to prevent rapid drug leakage. These liposomes displayed a mean size of about 165 nm, low polydispersity index (PDI < 0.1) and negative zeta potential value. Despite favorable characteristics of DSF, *i.e.* low molecular weight and lipophilic structure, its entrapment efficiency (EE) was around 65% (Table 2) corresponding to a final drug loading of 0.8% (mg of drug per mg of phospholipids). However, it is important to note that to obtain a stable liposome formulation, the amount of CHOL was increased to 40% and this probably hampered the complete encapsulation of DSF into the phospholipid bilayer. Liposome stability was evaluated in HEPES buffer at 4°C by measuring, at various times, mean diameter, zeta potential value, drug leakage

and phospholipid content. Liposomes were stable for 35 days maintaining 80% of their initial drug content. Over this period, no appreciable size change (< 10%) and liposome precipitation were observed as well as no change in zeta potential.

7.3.2.2. Cu (DDC)2 containing liposomes

Cu (DDC)2 containing liposomes were prepared by using the method described by Wehbe et al. (Wehbe et al., 2011, Wehbe et al., 2017), which provides the formation of the active Cu (DDC)2 complex inside the preformed liposomes and its con- sequent precipitation within the aqueous core in a single step. The method is based on the different membrane permeability of DDC compared to the complex. Indeed, DDC is water soluble and membrane permeable while the copper complex is water insoluble and membrane impermeable. The lipid film composed of DSPC, CHOL and mPEG-DSPE in 55:40:5 molar ratio was hydrated with a solution of CuCl2 and incubated at 60 °C, then the CuCl2 was eliminated by gel filtration and liposomes containing CuCl2 in the aqueous core were obtained. Then, DDC was added to the liposomes and incubated at room temperature and a drastic color change from light blue to brown was observed indicating the occurred complex formation. Finally, non encapsulated Cu (DDC)2 was removed by gel filtration. In order to prepare hyaluronic acid decorated liposomes, the conjugates HA4800-DPPE or HA17000-DPPE, in molar ratio of 3 or 5%, were added during the hydration phase of lipid film. In this way, the phospholipidic chain was incorporated into the liposome membrane, while the HA was exposed towards the aqueous phase. Liposomes displayed a dimensional range from about 165 nm to 225 nm and the particle size of the HA-liposomes tended to increase with the increase of polymer MW. The PDI was low for all the formulations (< 0.2) and the zeta potential value was negative and lower for HA-liposomes compared to the plain ones, due to the carboxylic negative residues of HA. In particular, the negative charge increased with the increase of HA MW (Table 2). These data confirmed the presence of HA on the surface of the liposomes. The formulations showed a good EE (Table 2), which was similar for plain liposomes and for liposomes decorated with HA4800-DPPE or HA17000-DPPE, indicating that the method of encapsulation ensured high drug loading and that the introduction of the HA-DPPE conjugates did not affect the Cu (DDC)2 encapsulation.

The final drug loading was about 4% for all the liposomal formulations. All formulations were stable at 4 °C for at least 35 days, as shown by the unchanged values of drug leakage, size and zeta potential over this period.

7.3.2.3. Differential scanning calorimetry (DSC)

In order to evaluate the interactions between DSF and the liposome membrane, a DSC analysis was performed (Figure 7.2). The thermogram of pure DSPC presented the main transition, related to the passage from the ripple gel phase (Pβ) to the lamellar liquid–crystalline phase (Lα), at Tonset 54.3 °C. In the presence of mPEG - DSPE, no significant changes in the transition temperature were observed (Tonset 54.0 °C), but a slight enlargement of the peak appeared. When DSF was added, the main transition was shifted to lower temperatures, Tonset 52.8°C, and a substantial broadening of melting temperature peaks was observed, indicating that DSF interacts with the liposome bilayer through hydrophobic interactions by perturbing the phase transition behavior. wavelength and 590 nm emission wavelength. The fluorescent signal generated from the assay is proportional to the number of living cells in the well. Three independent experiments were performed for each condition and cell viability was reported as the percentage relative to control.

Formulation	Size (nm)	PDI	Zeta potential (mV)	EE (%)[a]
LipoDSF-5% PEG	165 ± 5	0.097	−8.9 ± 2.8	64.3 ± 11.1
LipoCu(DDC)$_2$-5%PEG	167 ± 2	0.132	−11.5 ± 0.7	88.8 ± 5.8
LipoCu(DDC)$_2$-2%PEG3%HA4800	176 ± 2	0.105	−19.0 ± 0.9	87.3 ± 3.4
LipoCu(DDC)$_2$-5%HA4800	206 ± 1	0.155	−27.0 ± 1.6	90.0 ± 2.9
LipoCu(DDC)$_2$-2%PEG3% HA17000	209 ± 2	0.108	−20.7 ± 0.9	91.0 ± 4.2
LipoCu(DDC)$_2$-5%HA17000	226 ± 2	0.107	−38.7 ± 1.9	91.4 ± 3.9

Table 7.2. Characteristics of plain and HA-liposomes containing DSF and Cu (DDC)2. Values are the means ± SEM of three independent experiments each performed in triplicate. Entrapment efficiency: ratio between drug/lipid molar ratio after purification and drug/lipid molar ratio after extrusion.

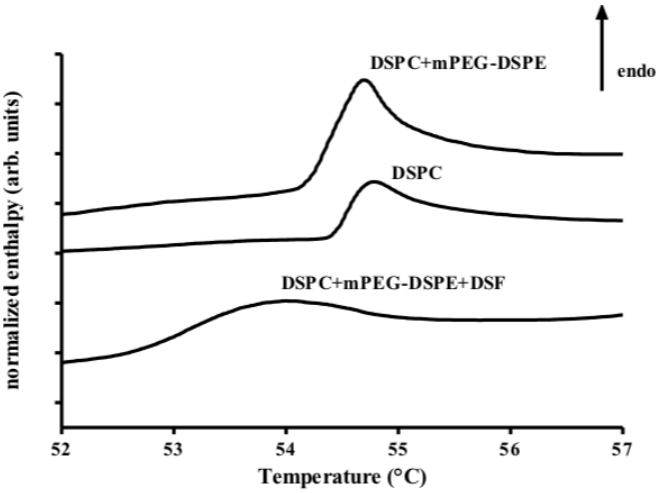

	ONSET (°C)
DSPC	54.3
DSPC+mPEG-DSPE	54.0
DSPC+mPEG-DSPE+DSF	52.8

Figure 7.2: DSC thermograms of pure DSPC, DSPC + mPEG-DSPE and DSPC + mPEG – DSPE + DSF.

7.3.2.4. Cryogenic transmission electron microscopy (cryo-TEM)

The morphology of Cu (DDC)2 liposomes was evaluated by cryo-TEM analysis. In Figure 7.3, the images relative to the empty (A) or loaded non- decorated formulations (Figure 7.3 B-F) are shown. It is possible to note the presence of unilamellar and multilamellar liposomes, probably due to the limited number of extrusion cycles performed. Liposomes showed the typical spherical shape or, in few cases, elongated shape due to the pressure exerted by ice layer, and presented slightly different sizes. The most interesting observation was the presence of needle-shaped structures (Figure 7.3 C-F) representing stacked Cu (DDC)2 complexes precipitated inside the aqueous core of liposomes in the form of crystals.

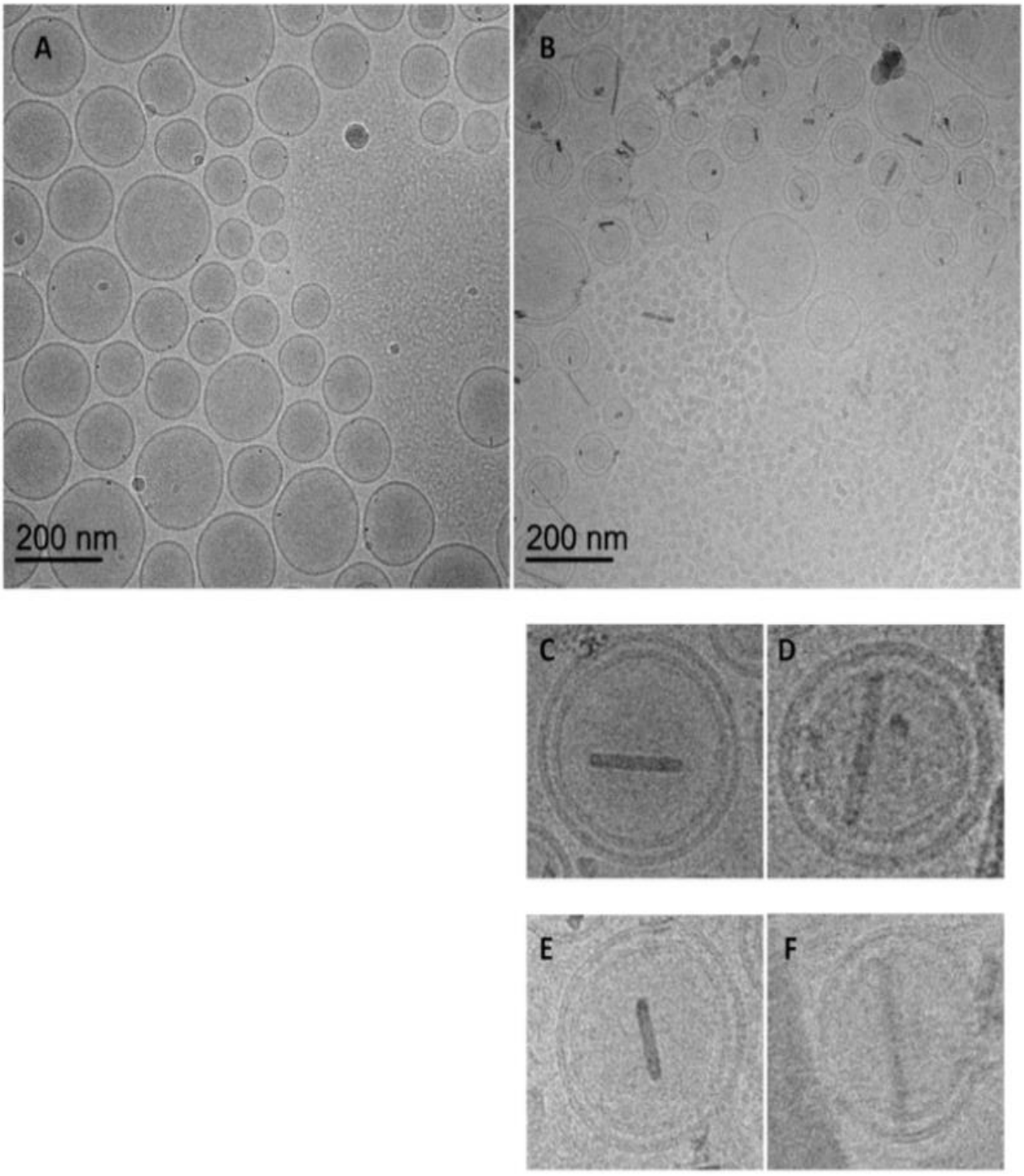

Figure 7.3: Cryo-TEM images of empty liposomes (A) and Cu(DDC)2 loaded liposomes (B–F).

.

7.3.3. Studies on cells

7.3.3.1. Cu (DDC)2 containing liposomes possess a strong anti-proliferative activity on Panc1 cells and Panc1 CSCs

The liposomal formulation containing DSF (LipoDSF-5%PEG) was significantly more active than free DSF, only after 72 h of treatment, in both cell lines, as shown by the IC50 values in Table 1 and by the cell growth curve in Supplementary material Figure S1 Moreover, Panc1 CSCs were more sensitive than Panc1 to LipoDSF-5 % PEG treatment at both incubation times (Table 1). Loading of Cu (DDC)2 into the liposomes strongly increased the anti-proliferative effect of Cu (DDC)2. As reported in Figure 7.4, LipoCu (DDC) 2 – 5 % PEG showed a higher anti-proliferative activity than Cu (DDC)2 in Panc1 and Panc1 CSCs, resulting in a con- centration dose-dependent reduction of cell growth and lower IC50 values (Table 7.1). To investigate the targeting ability of HA towards CD44-expressing tumor cells, the anti-proliferative effect of Cu (DDC)2 loaded in liposomes coated with HA with two different MW and/or with different percentage of PEG was evaluated. Liposomal formulations containing either PEG or HA determined a similar inhibition of cell proliferation, whereas the presence of both PEG and HA17000 further increased the anti-proliferative activity of Cu(DDC)2 at 24 h (Figure 7.4 and Table 7.1), in both cell lines. Furthermore, after 72 h of treatment, Panc1 CSCs were more sensitive to liposome formulations with HA17000 and/ or PEG compared to Panc1 cells (Table 7.1). Interestingly, when the anti- proliferative effect was examined at a concentration of the Cu (DDC)2 as low as 0.1μM, Panc1 CSCs were highly sensitive to liposomal formulations, with HA coated liposomes being more active than the plain ones, while Panc1 cells were completely resistant (Figure 7.5). Altogether, these results demonstrate that liposomes coated with 2 % PEG and 3 % HA17000 are the most effective tested formulation on both cell lines, with a higher efficacy on CSCs markedly at low Cu (DDC)2 concentration, suggesting that it could be used in PDAC therapy.

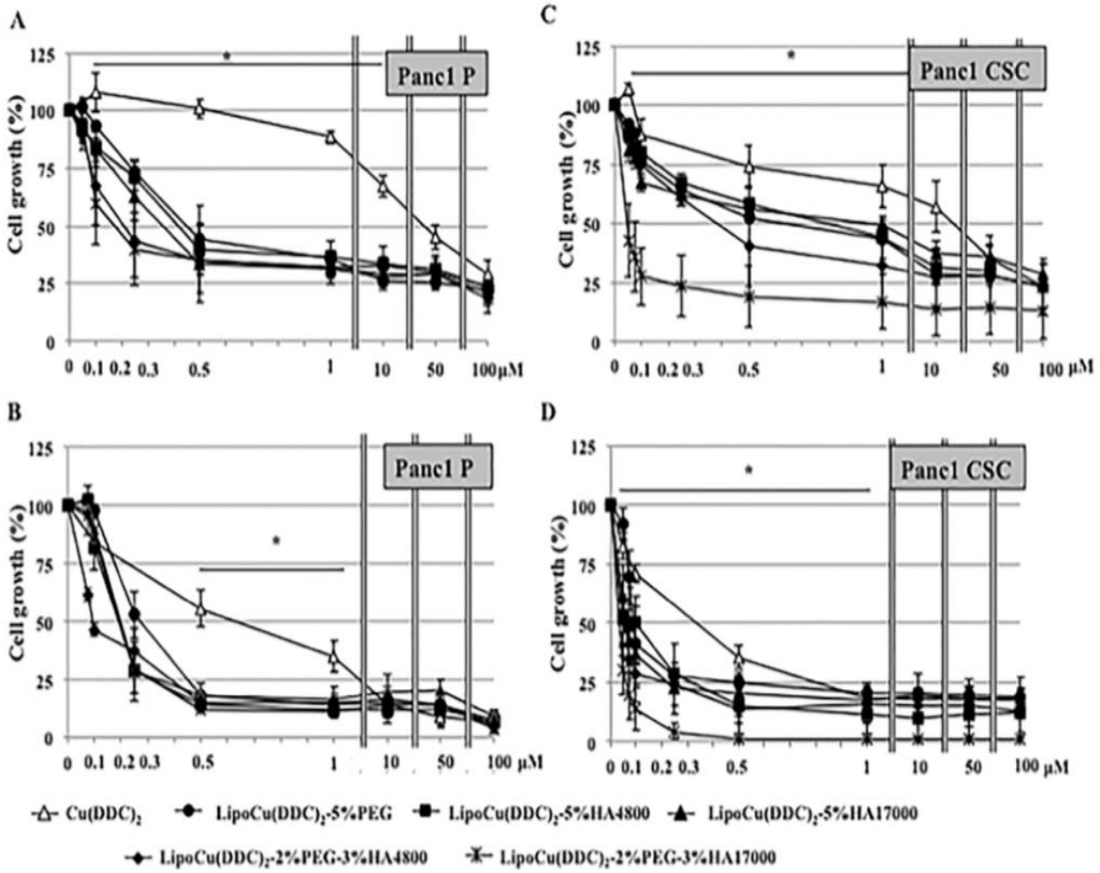

Figure 7.4: Effect of Cu (DDC)2 and of liposome formulations LipoCu (DDC) 2–5 % PEG, LipoCu (DDC) 2 – 5 % HA4800, LipoCu (DDC) 2 – 5 % HA17000, LipoCu (DDC) 2 – 2 % PEG – 3 % HA4800, LipoCu (DDC) 2 – 2 % PEG – 3 % HA17000 on Panc1 parental (P) (A and B) and Panc1 CSCs (C and D) cell growth. Cells were seeded in 96 - well plates and treated after 24 h with increasing concentrations of Cu (DDC)2 formulations for 24 h (A and C) or 72 h (B and D). Cell growth was determined using the resazurin cell viability assay. Values are the means ± SEM of three independent experiments each performed in triplicate. Statistical analysis: liposome formulations versus Cu (DDC)2, * $p < 0.05$.

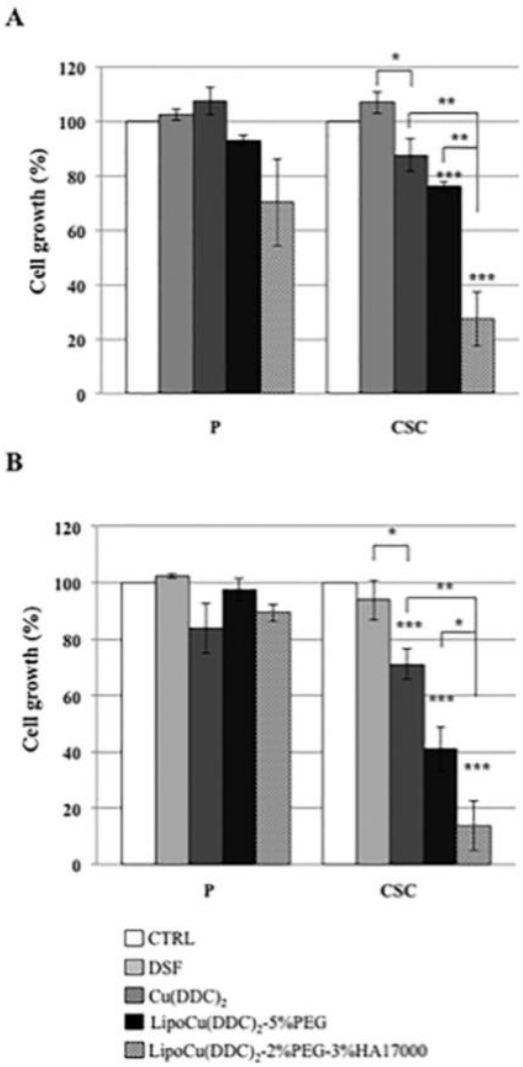

Figure 7.5: Effect of DSF, Cu (DDC)2, LipoCu (DDC)2–5%PEG and LipoCu (DDC) 2 – 2 % PEG -3 % HA17000 on Panc1 parental (P) and Panc1 CSCs cell growth. Cells were treated with 0.1 μM of compounds for 24 h (A) or 72 h (B). Statistical analysis: CTRL *versus* treated, or as indicated in figure * $p < 0.05$, ** $p < 0.01$, *** $p < 0.001$.

7.3.3.2. Reactive oxygen species (ROS) are responsible for the higher anti- proliferative activity of LipoCu (DDC) 2 – 2 % PEG – 3 % HA17000 on Panc1 CSCs compared to parental cells

Cu (DDC)2 has been described as an ionophore complex able to in- duce a copper-mediated ROS increase that can promote a mitochondrial-mediated cell death program. To verify whether ROS were responsible for the higher anti-proliferative activity of LipoCu (DDC)2–2%PEG-3%HA17000 on Panc1 CSCs compared to parental cells, we measured ROS production on Panc1 cells and Panc1 CSCs at the constitutive level and after treatment with LipoCu (DDC)2–2%PEG-3% HA17000 containing 0.1 μM of Cu (DDC)2. In parallel, we determined the effect of ROS neutralization on cell growth. Figure 6 shows that constitutive ROS levels were significantly higher in CSCs compared to parental cells (Figure 6A) and they increased after treatment only in CSCs (Figure 6B). Neutralization of ROS with *N*-acetyl-L-cysteine (NAC) almost completely recovered cell viability (Figure 6C), indicating that ROS play a major role in CSC growth inhibition by LipoCu (DDC)2–2%PEG-3% HA17000.

The observation that constitutive ROS levels were higher in Panc1 CSCs compared to parental cells prompted us to investigate the cellular status of GSH/glutathione disulphide, the major redox couple in animal cells. Figure 6 D indicates that the ratio GSH/GSSG is lower in Panc1 CSCs, consistently with the higher amount of ROS compared to parental cells. This result strongly suggests that Panc1 CSCs are more susceptible to the oxidative stress induced by Cu (DDC)2 probably because of an alteration of their metabolism leading to increased ROS and the con- sequential increased consumption of GSH. Indeed, we have recently published that Panc1 CSCs display, compared to Panc1 parental cells, a more glycolytic phenotype (Brandi et al., 2017), which is known to maintain a high non-toxic oxidative stress in cancer cells (Sabharwal et al., 2014).

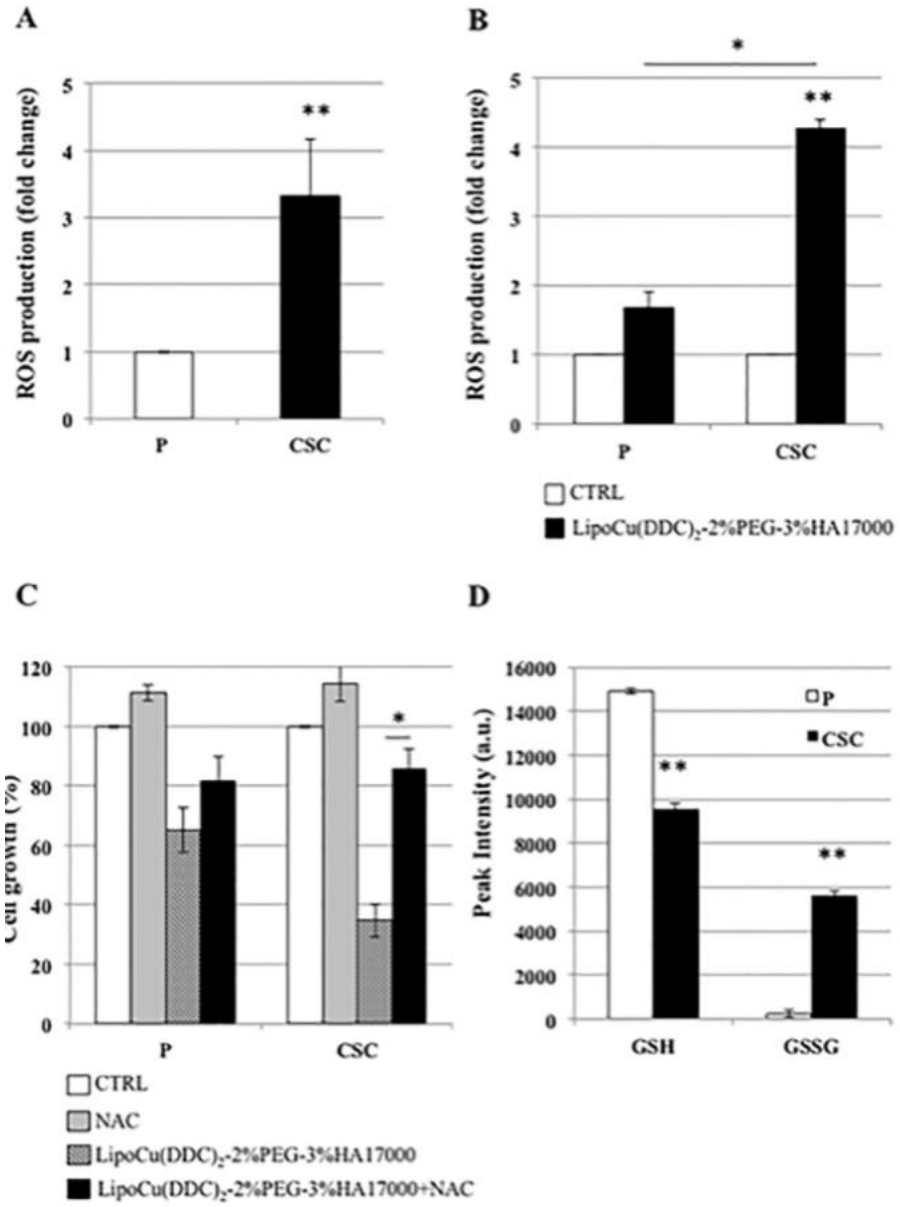

Figure 6: Analyses of intracellular ROS production on Panc1 parental cells and Panc1 CSCs at the constitutive level (A) and after treatment with LipoCu (DDC) 2 – 2 % PEG – 3 % HA17000 containing 0.1 μM of the active compound for 24 h treatment (B). Effect of 5 mM NAC and/or 0.1 μM LipoCu (DDC) 2 – 2 % PEG – 3 % HA17000 on Panc1 parental and Panc1 CSC cell growth after 24 h treatment (C). Absolute glutathione quantification (arbitrary ion counts) in Panc1 cells (P; white histogram) and Panc1 CSCs (black histogram) (D). Values are presented as mean ± SEM. Statistical analysis: P cells *versus* CSCs, or as indicated in figure * $p < 0.05$, ** $p < 0.01$.

7.3.3.3. Cu(DDC)2 containing liposomes possess a strong anti-proliferative activity on cells derived from PDAC patients

To evaluate whether the liposome formulations were active also on a cellular context clinically relevant, we tested their anti-proliferative activity in comparison to DSF and Cu (DDC)2 on pancreatic cancer cells directly obtained from patients affected by PDAC. The primary cells 12556, A6L, C75, C76, and C102 were cultured as spheres, as described in Materials and Methods, and treated with 0.1 μM of the formulations mentioned above. Cell viability was evaluated after 24 h of treatment. As shown in Figure 7, the liposome formulations containing Cu (DDC)2 were more effective than free compounds on first generation spheres and even more on second generation spheres. These data are particularly interesting since they show a strong anti-proliferative effect of Cu (DDC)2 containing liposomes on cells derived from PDAC patients having stem like features. Furthermore, they open the way to the clinical use of Cu (DDC)2 liposomal formulations due to their suitability for intravenous administration.

7.3.4. Effect of DSF and DSF containing liposomes on sphere formation capability

In the context of CSC features, the sphere formation capability is generally studied *in vitro* and used to identify new ways for targeting CSCs (Lonardo et al., 2015). A specific method for culturing primary human pancreatic cancer cells from tissues resected during surgery was used in order to obtain tumor spheres of first or second generation. In Figure 8, the effect of DSF, Cu (DDC)2, LipoCu (DDC) 2 – 5 % PEG and LipoCu (DDC) 2 – 2 % PEG – 3 % HA17000 on the *in vitro* sphere formation capability is shown. Liposome formulations at 0.1 μM of Cu (DDC)2 decreased the number of first generation spheres, while DSF and Cu (DDC)2 treatment slightly affected or did not affect sphere number. Also the cellular morphology was affected by liposome formulation treatment (Supplementary material Figure S2), as shown by the loss of the typical shape of the spheres, which appeared similar to small cell aggregates. The first generation spheres were subsequently passage into second generation spheres and also the formation of these spheres was drastically reduced (Figure 8). Thus, our data demonstrate a significant inhibitory effect of liposome formulations on the capacity of primary pancreatic cancer

stem like cells to form spheres, which is a typical feature of these cells.

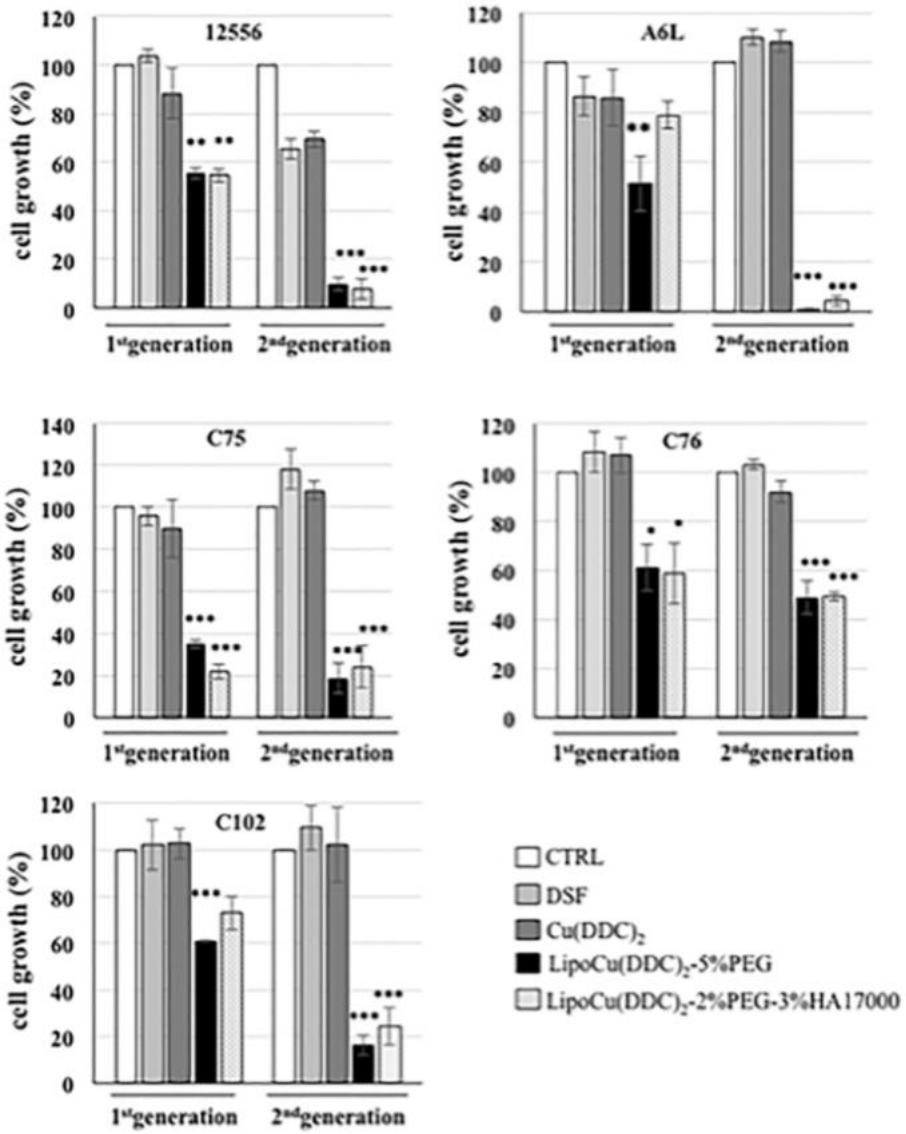

Figure 7: Effect of DSF, Cu(DDC)2, LipoCu(DDC)2–5%PEG and LipoCu(DDC)2–2%PEG-3%HA17000 on cell growth of primary PDAC cells (12556, A6L, C75, C76, C102) cultured as first and second generation spheres. Cells were treated with 0.1 μM compounds for 24 h. Cell growth was determined using the resazurin cell viability assay. Values are the means ± SEM of three independent experiments each performed in triplicate. Statistical analysis: CTRL *versus* treated, * $p < 0.05$, ** $p < 0.01$, *** $p < 0.001$.

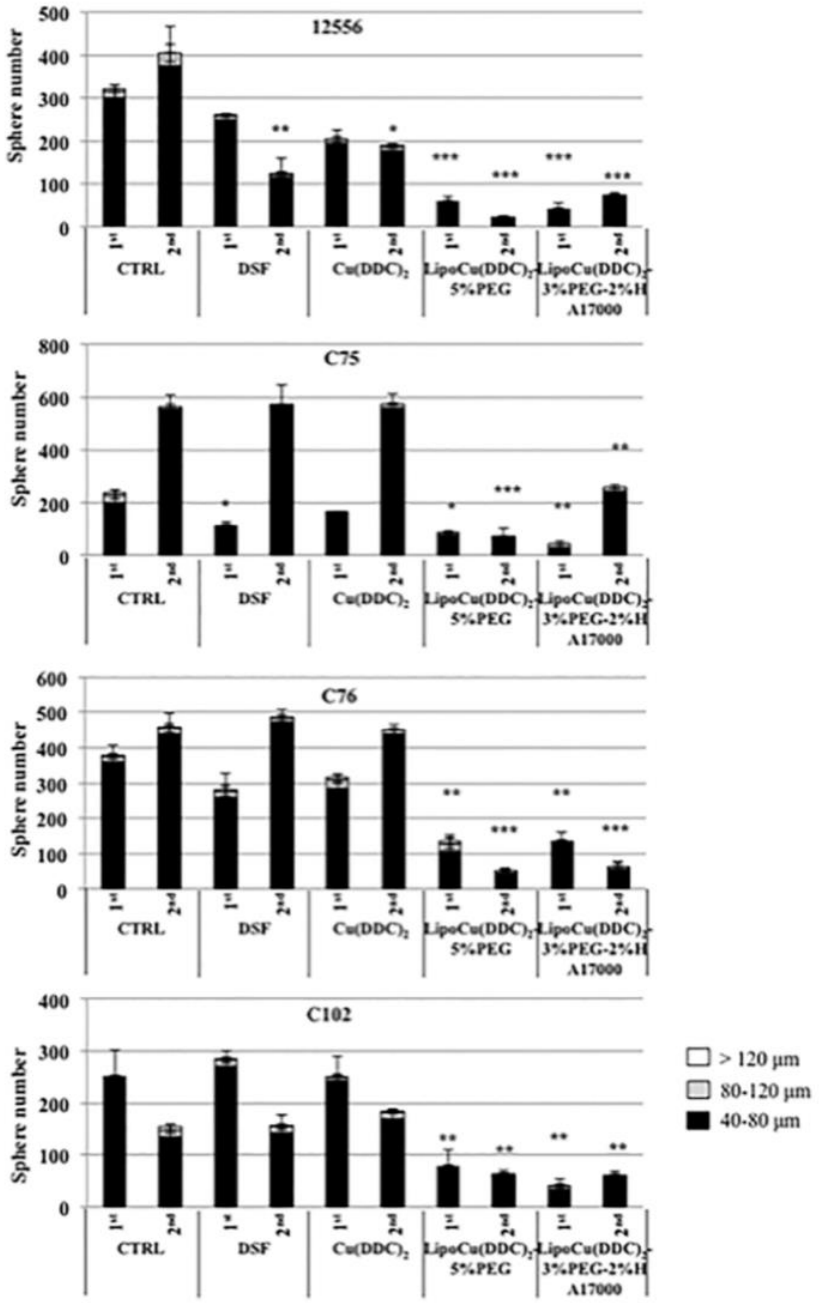

Figure 8: Effect of DSF, Cu(DDC)2, LipoCu (DDC)2–5%PEG and LipoCu (DDC)2–2%PEG-3%HA17000 on 12556, C75, C76, and C102 spheres formation capability. Cells were seeded in 24-well plates for first or second generation spheres and treated after 3 days with 0.1 µM compounds for 4 days. Spheres number was determined through sphere formation assay performed by CASY Counter and reported as spheres of 40–80 µm, 80–120 µm and > 120 µm of diameter. Statistical analysis: CTRL *versus* treated, * $p < 0.05$, ** $p < 0.01$, *** $p < 0.001$.

CONCLUSIONS

7.4 Conclusions

The results described in this paper are of great relevance from clinical point of view since, for the first time to our knowledge, they open the way to consider liposomes decorated with HA and encapsulating the potent anti-proliferative Cu (DDC)2 complex as a potent therapeutic tool against PDAC. Indeed, it has been widely reported that PDAC initiation, growth, metastasis and resistance to therapy are driven by CSCs and our impressive data on primary cells with a stem like phenotype directly derived from PDAC patients show the high capacity of Cu (DDC)2 liposomal formulations to inhibit the proliferation and the sphere forming capability of these cells.

Acknowledgements

Funding from Italian Ministry for University and Research (MIUR) - University of Torino, "Fondi Ricerca Locale (ex-60%)" are kindly acknowledged. This work was supported by Joint Projects program 2017 from University of Verona to M. Palmieri. Ilaria Dando is a fellow of Fondazione Umberto Veronesi. Authors would like to thank Mehrez Sghaier for help with DSC experiments. The present work has benefited also from the core facilities of Imagerie-Gif, (http://www.i2bc.paris- saclay.fr), member of IBiSA (http://www.ibisa.net), supported by "France-BioImaging" (ANR-10-INBS-04-01), and the Labex "Saclay Plant Science" (ANR-11-IDEX-0003-02). Institut Galien Paris-Sud is a member of the Laboratory of Excellence LERMIT supported by a grant from ANR (ANR-10-LABX-33).

Appendix A. Supplementary data

Supplementary data to this article can be found online at https://doi.org/10.1016/j.bbagen.2018.09.018.

8. Conclusion

In conclusion in my thesis applies omics science to analyze the variation of Panc CSCs cellular metabolism. Firstly, through proteomics and metabolomics control cells and Panc CSC were compared to identified the altered metabolic pathways of pancreatic cancer cells. To better understand the altered metabolic pathways of pancreatic cancer stem cells (CSCs), a comprehensive proteomic analysis and metabolite profiling investigation of Panc and Panc CSCs were carried out. The findings obtained indicate that Panc CSCs are characterized by upregulation of glycolysis, pentose phosphate pathway, pyruvate-malate cycle, and lipidmetabolismand by downregulation of Krebs cycle, spliceosome and non-homologous end joining. Moreover, fatty acid synthesis and mevalonate pathways are shown to play a critical contribution to the survival of pancreatic cancer stem cells. This study is helpful for broadening the knowledge of pancreatic cancer stem cells and could accelerate the development of novel therapeutic strategies.

Subsequently, a time course analysis was performed at different time-points (2, 4, 8 weeks) and the changes were highlighted both at a phenotypic and at a metabolic level. CSCs shown, over time, variation of some metabolites that play a key role in the regulation of energy metabolism. Moreover, the results show an increased of tumorsphere – forming ability associated with high expression of stamness markers. CSCs ranging from quiescent phase after 8 weeks to survival and response at changes in the local environment. For the first time, an in vitro model is shown which is closer to the characteristics of stem cells in patients with PDAC. Moreover the evidence of quiescent state acquisition, it is useful to improve the research of novel therapeutic agents that specifically target on dormant CSCs.

Finally, in order to develop CSC-targeted therapies, new liposomal diethyldithiocarbamate/copper ($Cu(DDC)_2$) formulations were investigated demonstrating their high capacity to inhibit the proliferation and the sphere forming capability of CSCs. In vitro testing on pancreatic CSCs derived from PDAC cell lines or patients showed high ROS mediated anticancer activity of hyaluronic acid (HA) decorated liposomes. The sphere formation capability of CSCs obtained from patients was drastically reduced by

liposomal formulations containing Cu $(DDC)_2$. The results obtained show that the encapsulation of Cu $(DDC)_2$ complex in HA decorated liposomes strongly increases its anti-proliferative activity on pancreatic CSCs.

References

1. Abbruzzese JL, Hess KR. New option for the initial management ofmetastatic pancreatic cancer? J. Clin. Oncol. 2014, 32, 2405–2407.
2. Abdullah LN, Chow EK. Mechanisms of chemoresistance in cancer stem cells. Clin. Transl. Med. 2013, 2, 3.
3. Adamska A, Elaskalani O, Emmanouilidi A, Kim M, Abdol Razak NB, Metharom P, Falasca M. Molecular and cellular mechanisms of chemoresistance in pancreatic cancer. Adv. Biol. Regul. 2018, 68, 77-87.
4. Akbarzadeh A, Rezaei-Sadabady R, Davaran S, Joo SW, Zarghami N, Hanifehpour Y, Samiei M, Kouhi M, Nejati-Koshki K. Liposome: classification, preparation, and applications. Nanoscale Res. Lett. 2013, 8, 102.
5. Allensworth JL, Evans MK, Bertucci F, Aldrich AJ,. Festa RA, Finetti P, Ueno NT, Safi R, McDonnell DP, Thiele DJ, Van Laere S, Devi GR. Disulfiram (DSF) acts as a copper ionophore to induce copper-dependent oxidative stress and mediate anti-tumor efficacy in inflammatory breast cancer. Mol. Oncol. 2015, 9, 1155–1168.
6. Amini S, Fathi F, Mobalegi J, Sofimajidpour H, Ghadimi T. The expressions of stem cell markers: Oct4, Nanog, Sox2, nucleostemin, Bmi, Zfx, Tcl1, Tbx3, Dppa4, and Esrrb in bladder, colon, and prostate cancer, and certain cancer cell lines. Anat. Cell Biol. 2014, 47(1),1-11.
7. Ansari D, Chen BC, Dong L, Zhou MT, Andersson R. Pancreatic cancer: translational research aspects and clinical implications. World J. Gastroenterol. 2012, 18(13), 1417-24.
8. Arpicco S, Lerda C, Dalla Pozza E, Costanzo C, Tsapis N, Stella B, Donadelli M, Dando I, Fattal E, Cattel L, Palmieri M. Hyaluronic acid-coated liposomes for active targeting of gemcitabine. Eur. J. Pharm. Biopharm. 2013, 85, 373–380.
9. Baenke F, Peck B, Miess H, Schulze A. Hooked on fat: the role of lipid synthesis in cancer metabolism and tumour development. Dis. Model. Mech. 2013, 6(6), 1353-63.

10. Bailey P et al. Genomic analyses identify molecular subtypes of pancreatic cancer. Nature. 2016, 531(7592), 47–52.
11. Bao B, Ahmad A, Azmi AS, Ali S, Sarkar FH. Overview of cancer stem cells (CSCs) and mechanisms of their regulation: implications for cancer therapy. Curr. Protoc. Pharmacol. 2013, Chapter 14
12. Bartholin L. Pancreatic cancer and the tumor microenvironment: Mesenchyme's role in pancreatic carcinogenesis. Grippo PJ, Munshi HG ed. Transworld Research Network, 2012. Chapter 4.
13. Bartlett GR. Phosphorus assay in column chromatography. J. Biol. Chem. 1959, 234 466–468.
14. Beloribi-Djefaflia S, Vasseur S, Guillaumond F. Lipid metabolic reprogramming in cancer cells. Oncogenesis. 2016, 5, e189.
15. Bian Y, Yu Y, Wang S, Li L. Up-regulation of fatty acid synthase induced by EGFR/ERK activation promotes tumor growth in pancreatic cancer. Biochem. Biophys. Res. Commun. 2015, 463, 612–617.
16. Blackford A, Parmigiani G, Kensler TW, et al. Genetic mutations associated with cigarette smoking in PDAC. Cancer Res. 2009, 69, 3681–8.
17. Boja ES, Kinsinger CR, Rodriguez H, Srinivas P, on behalf of Omics Integration Workshop Participants. Integration of omics sciences to advance biology and medicine. Clin. Proteomics. 2014, 11(1), 45.
18. Brandi J, Dalla Pozza E, Dando I, Biondani G, Robotti E, Jenkins R, Elliott V, Park K, Marengo E, Costello E, Scarpa A, Palmieri M, Cecconi D. Secretome protein signature of human pancreatic cancer stem-like cells. J. Proteomics . 2016, 16, 30020-3.
19. Brandi J, Dando I, Pozza ED, Biondani G, Jenkins R, Elliott V, Park K, Fanelli G, Zolla L, Costello E, Scarpa A, Cecconi D, Palmieri M. Proteomic analysis of pancreatic cancer stem cells: Functional role of fatty acid synthesis and mevalonate pathways. J. Proteomics. 2017, 150, 310–322.
20. Bruenderman E, Martin RC 2nd. A cost analysis of a pancreatic cancer screening protocol in high-risk populations. Am. J. Surg. 2015, 210(3), 409–416.7

21. Buac D, Schmitt S, Ventro G, Kona FR, Dou Q.P. Dithiocarbamate-based coordination compounds as potent proteasome inhibitors in human cancer cells. Mini Rev. Med. Chem. 2012, 12, 1193–1201.
22. Calle EE, Rodriguez C, Walker-Thurmond K, Thun MJ. Overweight, obesity, and mortality from cancer in a prospectively studied cohort of U.S. adults. N. Engl. J. Med. 2003, 348(17), 1625-38.
23. Cecconi D, Zamo A. Proteomics of human cancer tissues and cells. TrAC Trends Anal. Chem. 2011, 30, 346–359.
24. Cen D, Gonzalez RI, Buckmeier JA, Kahlon RS, Tohidian NB, Meyskens FL. Disulfiram induces apoptosis in human melanoma cells: a redox-related process. Mol. Cancer Ther. 2002, 1, 197–204.
25. Chae YC, Kim JH. Cancer stem cell metabolism: target for cancer therapy. BMB Rep. 2018, 51(7), 319-326.
26. Chakraborty S, Singh S. Surgical resection improves survival in pancreatic cancer patients without vascular invasion—a population based study. Ann. Gastroenterol. 2013, 26(4), 346–352
27. Chen D, Cui QC, Yang H,. Dou QP. Disulfiram, a clinically used anti-alcoholism drug and copper-binding agent, induces apoptotic cell death in breast cancer cultures and xenografts via inhibition of the proteasome activity. Cancer Res. 2006, 66, 10425–10433.
28. Chen Q, Jin M, Zhu J, Xiao Q, Zhang L. Functions of heterogeneous nuclear ribonucleoproteins in stem cell potency and differentiation. Biomed. Res. Int. 2013, 2013, 623978.
29. Chen W, Dong J, Haiech J, Kilhoffer MC, Zeniou M. Cancer Stem Cell Quiescence and Plasticity as Major Challenges in Cancer Therapy. Stem Cells Int. 2016, 1740936.
30. Chen X, Zhang L, Hu X, Lin X, Zhang Y, Tang X. Formulation and preparation of a stable intravenous disulfiram-loaded lipid emulsion. Eur. J. Lipid Sci. Technol. 2015, 117, 869–878.

31. Cheng Y, Chen G, Hong L, Zhou L, Hu M, Li B, et al. How does hypoxia inducible factor-1alpha participate in enhancing the glycolysis activity in cervical cancer? Ann. Diagn. Pathol. 2013, 17, 305–311.
32. Cho HJ, Lee TS, Park JB, Park KK, Choe JY, Sin DI, Park YY, Moon YS, Lee KG, Yeo JH, Han SM,. Cho YS, Choi MR, Park NG, Lee YS, Chang YC. Disulfiram suppresses invasive ability of osteosarcoma cells via the inhibition of MMP-2 and MMP-9 expression. J. Biochem. Mol. Biol. 2007, 40, 1069–1076.
33. D'Alessandro A, Amelio I, Berkers CR, Antonov A, Vousden KH, Melino G, et al. Metabolic effect of TAp63alpha: enhanced glycolysis and pentose phosphate pathway, resulting in increased antioxidant defense. Oncotarget. 2014, 5, 7722–7733.
34. D'Alessandro A, Gevi F, Zolla L. A robust high resolution reversed-phase HPLC strategy to investigate various metabolic species in different biological models. Mol.BioSyst. 2011, 7, 1024–1032.
35. Dalla Pozza E, Dando I, Biondani G, Brandi J, Costanzo C, Zoratti E, Fassan M, Boschi F, Melisi D, Cecconi D, Scupoli MT, Scarpa A, Palmieri M. Pancreatic ductal adenocarcinoma cell lines display a plastic ability to bi-directionally convert into cancer stem cells. Int. J. Oncol. 2015, 46, 1099-1108.
36. Dalla Pozza E, Lerda C, Costanzo C, Donadelli M, Dando I, Zoratti E, Scupoli MT, Beghelli S, Scarpa A, Fattal E, Arpicco S, Palmieri M. Targeting gemcitabine containing liposomes to CD44 expressing pancreatic adenocarcinoma cells causes an increase in the antitumoral activity. Biochim. Biophys. Acta. 2013, 1828, 1396–1404.
37. Dando I, Dalla Pozza E, Biondani G, Cordani M, Palmieri M, Donadelli M. The metabolic landscape of cancer stem cells. IUBMB Life. 2015, 67(9), 687-93.
38. Daniëls VW, Smans K, Royaux I, Chypre M, Swinnen JV, Zaidi N. Cancer cells differentially activate and thrive on de novo lipid synthesis pathways in a low-lipid environment. PLoS One. 2014, 9(9), e106913.
39. Delphine T.M, Ines L, Richard P.H. Cancer stem cells, the epithelial to mesenchymal transition (EMT) and radioresistance: Potential role of hypoxia. Cancer Lett. 2013, 63-72.

40. Deng T, Lyon C.J, Bergin S, Caligiuri M.A. Hsueh W.A. Obesity, Inflammation, and Cancer. Annu. Rev. Pathol. 2016, 11(1), 421-449.

41. Deshpande PP, Biswas S, Torchilin VP. Current trends in the use of liposomes for tumor targeting. Nanomed. (Lond., Engl.) 2013, 8, 1509–1528.
42. Dettmer K, Aronov PA, Hammock BD. Mass spectrometry-based metabolomics. Mass Spectrom. Rev. 2007, 26(1), 51-78.
43. Di Gangi I.M, Vrhovsek U, Pazienza V, Mattivi F. Analytical metabolomics-based approaches to pancreatic cancer. Elsevier, Trends in Analytical Chemistry 2014, 55, 94–116.
44. Di Girolamo F, Lante I, Muraca M, Putignani L. The Role of Mass Spectrometry in the "Omics" Era. Curr. Org. Chem. 2013, 17(23), 2891-2905.
45. Dong C, Yuan T, Wu,Y Wang Y, Fan TW, Miriyala S, et al. Loss of FBP1 by snailmediated repression providesmetabolic advantages in basal-like breast cancer. Cancer Cell. 2013, 23, 316–331.
46. Eskander MF, Bliss LA, Tseng JF. Pancreaticadenocarcinoma. Curr.Probl.Surg. 2016, 53, 107–154.
47. Fan J, Ye J, Kamphorst JJ, Shlomi T, Thompson CB, Rabinowitz JD. Quantitative flux analysis reveals folate-dependent NADPH production. Nature. 2014, 510,298–302.
48. Fendt SM, Bell EL, Keibler MA, et al. Reductive glutamine metabolism is a function of the α-ketoglutarate to citrate ratio in cells. Nat. Commun. 2013, 4, 2236.
49. Gevi F, D'Alessandro A, Rinalducci S, Zolla L. Alterations of red blood cell metabolome during cold liquid storage of erythrocyte concentrates in CPD-SAGM. J. Proteome. 2012, 76, 168-80.
50. Giovannetti E, Giaccone G. CYB5A and autophagy-mediated cell death in pancreatic cancer. Autophagy. 2014, 10(4), 697-8.
51. Giovannetti E, van der Borden CL, Frampton AE, Ali A, Firuzi O, Peters GJ. Never let it go: Stopping key mechanisms underlying metastasis to fight pancreatic cancer. Semin. Cancer. Biol. 2017, 44, 43-59

52. Goodwin PJ, Chlebowski RT. Obesity and Cancer: Insights for Clinicians. J. Clin. Oncol. 2016, 34(35), 4197-4202.
53. Griffiths WJ, Wang Y. Mass spectrometry: from proteomics to metabolomics and lipidomics. Chem. Soc. Rev. 2009, 38(7), 1882-96.
54. Guo X, Xu B, Pandey S, Goessl E, Brown J, Armesilla AL Darling JL, Wang W. Disulfiram/copper complex inhibiting NFkappaB activity and potentiating cytotoxic effect of gemcitabine on colon and breast cancer cell lines. Cancer Lett. 2010, 290, 104–113.
55. Gygi SP, Rochon Y, Franza BR, Aebersold R. Gene expression:correlation between protein and mRNA abundance in yeast. Mol. Cell. Biol. 1999, 19, 1720–1730.
56. Han J, Liu L, Yue X, Chang J, Shi W, Hua Y. A binuclear complex constituted by diethyldithiocarbamate and copper(I) functions as a proteasome activity inhibitor in pancreatic cancer cultures and xenografts. Toxicol. Appl. Pharmacol. 2013, 273, 477–483.
57. Han X, Gross RW. Shotgun lipidomics: electrospray ionization mass spectrometric analysis and quantitation of cellular lipidomes directly from crude extracts of biological samples. Mass Spectrom. Rev. 2005, 24(3), 367-412.
58. Hassa PO. The molecular "Jekyll and Hyde" duality of PARP1 in cell death and cell survival. Front. Biosci. 2009, 14, 72–111.
59. Hermann PC, Huber SL, Herrler T, Aicher A, Ellwart JW, Guba M, Bruns CJ, Heeschen C. Distinct populations of cancer stem cells determine tumor growth and metastatic activity in human pancreatic cancer. Cell Stem Cell 2007, 1, 313–323.
60. Hidalgo M. Pancreatic cancer. N. Engl. J. Med. 2010, 362(17), 1605–161.
61. Hirschhaeuser F, Sattler UG, Mueller-Klieser W. Lactate: a metabolic key player in cancer. Cancer Res. 2011, 71(22), 6921-5.
62. Hong SP, Wen J, Bang S, Park S, Song SY. CD44-positive cells are responsible for gemcitabine resistance in pancreatic cancer cells. Int. J. Cancer. 2009, 125(10), 2323–2331.
63. Hosein A.N, Beg M.S. Pancreatic Cancer Metabolism: Molecular Mechanisms and Clinical Applications. Gastrointestinal. 2018, 20, 56.

64. Iacobuzio-Donahue CA, Fu B, Yachida S, Luo M, Abe H, Henderson CM, Vilardell F, Wang Z, Keller JW, Banerjee P, Herman JM, Cameron JL, Yeo CJ, Halushka MK, Eshleman JR, Raben M, Klein AP, Hruban RH, Hidalgo M, Laheru D. DPC4 gene status of the primary carcinoma correlates with patterns of failure in patients with pancreatic cancer. J. Clin. Oncol. 2009, 27(11), 1806–1813.
65. Ilmer M, Horst D. Pancreatic CSCs and microenvironment. Genes Cancer, 2015, 6, 9-10.
66. Ishiguro T, Ohata H, Sato A, Yamawaki K, Enomoto T, Okamoto K. Tumor-derived spheroids: Relevance to cancer stem cells and clinical applications. Cancer Sci. 2017, 108(3), 283-289.
67. Islam F, Qiao B, Smith RA, Gopalan V,. Lam AK. Cancer stemcell: fundamental experimental pathological concepts and updates. Exp. Mol. Pathol. 2015, 98, 184–191.
68. Javier A. Menendez & Ruth Lupu. Fatty acid synthase and the lipogenic phenotype in cancer pathogenesis. Nature Rev. Cancer. 2007, 7, 763–777.
69. Jiang L, Wang H, Li J, Fang X, Pan H, Yuan X, et al., Up-regulated FASN expression promotes transcoelomic metastasis of ovarian cancer cell through epithelial-mesenchymal transition. Int. J. Mol. Sci. 2014, 15, 11539–11554.
70. Jiang P, Mukthavaram R, Chao Y, Nomura N, Bharati IS, Fogal V, et al., In vitro and in vivo anticancer effects of mevalonate pathway modulation on human cancer cells. Br. J. Cancer. 2014, 111, 1562–1571.
71. Jiang Y-X, Yang S-W, Li P-A, Luo X, Li Z-Y, Hao Y-X & -W Yu P. The promotion of the transformation of quiescent gastric cancer stem cells by IL-17 and the underlying mechanisms. Oncogene. 2017, 36, 1256–1264.
72. Jimeno A, Feldmann G, Suarez-Gauthier A, Rasheed Z, Solomon A. Zou GM, Rubio-Viqueira B, Garcia-Garcia E, Lopez-Rios F, Matsui W, Maitra A, Hidalgo M. A direct pancreatic cancer xenograft model as a platform for cancer stem cell therapeutic development. Mol. Cancer Ther. 2009, 8, 310–314.
73. Johansson B. A review of the pharmacokinetics and pharmacodynamics of disulfiram and its metabolites. Acta Psychiatr. Scand. Suppl. 1992, 369, 15–26.

74. Kaddurah-Daouk R, Kristal BS, Weinshilboum RM. Metabolomics: a global biochemical approach to drug response and disease. Annu Rev Pharmacol Toxicol. 2008, 48, 653-83.
75. Kaur P, Sheikh K, Kirilyuk A, Kirilyuk K, Singh R, Ressom HW, Cheema A.K. Metabolomic profiling for biomarker discovery in pancreatic cancer. International Journal of Mass Spectrometry. 2012, 310, 44-51.
76. Kim H. DNA repair Ku proteins in gastric cancer cells and pancreatic acinar cells. Amino Acids 2008, 34, 195–202.
77. Kim JY, Cho Y, Oh E, Lee N, An H, Sung D, Cho TM, Seo JH. Disulfiram targets cancer stem-like properties and the HER2/Akt signaling pathway in HER2-positive breast cancer. Cancer Lett. 2016, 379, 39–48.
78. Kinlaw WB, Baures PW, Lupien LE, Davis WL, Kuemmerle NB. Fatty acids and breast Cancer: make them on site or have them delivered. J Cell Physiol. 2016, 231(10), 2128–41.
79. Le N, Sund M, Vinci A, on behalf of the GEMS collaborating group of Pancreas 2000. Prognostic and predictive markers in pancreatic adenocarcinoma. Digestive and Liver Disease 2016, 48, 223–230.
80. Lee CJ, Dosch J, and Simeone DM. Pancreatic cancer stem cells. J Clin Oncol 2008, 26, 2806-12.
81. Lee JH, Han YS, Lee SH. Long-duration three-dimensional spheroid culture promotes Angiogenic activities of adipose-derived Mesenchymal stem cells. Biomol. Ther 2016, 24, 260–267.
82. Li C, Heidt DG, Dalerba P, Burant CF, Zhang L, Adsay V, Wicha M, Clarke MF. Simeone DM. Identification of pancreatic cancer stem cells. Cancer Res. 2007, 67, 1030–1037.
83. Li J, Dong L, Wei D, Wang X, Zhang S, Li H. Fatty acid synthase mediates the epithelial-mesenchymal transition of breast cancer cells. Int. J. Biol. Sci. 2014, 10, 171–180.
84. Li XP, Zhang XW, Zheng LZ, Guo WJ. Expression of CD44 in pancreatic cancer and its significance. Int. J. Clin. Exp. Pathol. 2015, 8, 6724–6731.

85. Liu P, Brown S, Goktug T, Channathodiyil P, Kannappan V, Hugnot JP, Guichet PO, Bian X, Armesilla AL, Darling JL, Wang W. Cytotoxic effect of disulfiram/copper on human glioblastoma cell lines and ALDH-positive cancer-stem-like cells. Br. J. Cancer 2012, 107,1488–1497.
86. Liu X, Fan D. The epithelial-mesenchymal transition and cancer stem cells: functional and mechanistic links. Curr. Pharm. Des. 2015, 21, 1279-91.
87. Lonardo E, Cioffi M, Sancho P, Crusz S, Heeschen C. Studying pancreatic cancer stem cell characteristics for developing new treatment strategies. J. Vis. Exp. 2015, e52801.
88. Lonardo E,. Hermann PC, Mueller MT, Huber S, Balic A, Miranda-Lorenzo I, Zagorac S, Alcala S, Rodriguez-Arabaolaza I, Ramirez JC, Torres-Ruiz R, Garcia E, Hidalgo M,. Cebrian DA, Heuchel R, Lohr M, Berger F, Bartenstein P, Aicher A, Heeschen C. Nodal/Activin signaling drives self-renewal and tumorigenicity of pancreatic cancer stem cells and provides a target for combined drug therapy. Cell Stem Cell 2011, 9, 433–446.
89. Long J, Zhang CJ, Zhu N, et al. Lipid metabolism and carcinogenesis, cancer development. Am. J. Cancer Res. 2018, 8(5), 778-791.
90. Lovborg H, Oberg F, Rickardson L, Gullbo J, Nygren P, Larsson R. Inhibition of proteasome activity, nuclear factor-Kappa B translocation and cell survival by the antialcoholism drug disulfiram. Int. J. Cancer. 2006, 118, 1577–1580.
91. Luo M, Wicha MS. Metabolic plasticity of cancer stem cells. Oncotarget. 2015, 6,35141–35142.
92. Mancini R, Noto A, Pisanu ME, De Vitis C, Maugeri-Saccà M, Ciliberto G. Metabolic features of cancer stem cells: the emerging role of lipid metabolism. Oncogene. 2018, 37, 18.
93. Mattheolabakis G, Milane L, Singh A, Amiji MM. Hyaluronic acid targeting of CD44 for cancer therapy: from receptor biology to nanomedicine. J. Drug Target. 2015, 23, 605–618.
94. McAllister SS, Weinberg RA. The tumour-induced systemic environment as a critical regulator of cancer progression and metastasis. Nat. Cell Biol. 2014, 16(8), 717–727.

95. Moore PS, Sipos B, Orlandini S, Sorio C, Real FX, Lemoine NR, et al. Genetic profile of 22 pancreatic carcinoma cell lines. Analysis of K-ras, p53, p16 and DPC4/Smad4. Virchows Arch. 2001, 439, 798–802.
96. Mullen GE , Yet L. Progress in the development of fatty acid synthase inhibitors asanticancer targets. Bioorg. Med. Chem. Lett. 2015, 25, 4363–4369.
97. Muntimadugu E, Kumar R, Saladi S, Rafeeqi TA, Khan W. CD44 targeted chemotherapy for coeradication of breast cancer stem cells and cancer cells using polymeric nanoparticles of salinomycin and paclitaxel. Colloids Surf. B Biointerfaces. 2016, 143, 532–546.
98. Neoptolemos JP, Stocken DD, Friess H, Bassi C, Dunn JA, Hickey H, et al., A randomized trial of chemoradiotherapy and chemotherapy after resection of pancreatic cancer. N. Engl. J. Med. 2004, 350, 1200–1210.
99. Nicholson JK, Wilson ID. Opinion: understanding 'global' systems biology: metabonomics and the continuum of metabolism. Nat. Rev. Drug Discov. 2003, 2(8), 668-76.
100. Paranjpe A, Zhang R, Ali-Osman F, Bobustuc GC,. Srivenugopal KS. Disulfiram is a direct and potent inhibitor of human O6-methylguanine-DNA methyltransferase (MGMT) in brain tumor cells and mouse brain and markedly increases the alkylating DNA damage. Carcinogenesis. 2014, 35, 692–702.
101. Parsa N. Environmental factors inducing human cancers. Iran J. Public. Health. 2012, 41(11), 1-9.
102. Pastrana E, Silva-Vargas V, Doetsch F. Eyes wide open: a critical review of sphere-formation as an assay for stem cells. Cell Stem Cell. 2011, 8, 486–98.
103. Peer D, Karp JM, Hong S, Farokhzad OC, Margalit R, Langer R. Nanocarriers as an emerging platform for cancer therapy. Nat. Nanotechnol. 2007, 2, 751–760.
104. Peiris-Pagès M, Martinez-Outschoorn UE, Pestell RG, Sotgia F and Lisanti MP. Cancer stem cell metabolism. Breast Cancer Res. 2016, 18, 55.

105. Perusina Lanfranca M, Thompson JK, Bednar F, Halbrook C, Lyssiotis C, Levi B, Frankel TL. Metabolism and Epigenetics of Pancreatic Cancer Stem Cells. Seminars in Cancer Biology 2018.

106. Philip B, Roland C.L, Daniluk J, Liu Y, Chatterjee D, Gomez S.B, Ji B, Haojie H, Wang H, Fleming J.B, Logsdon C.D and Cruz-Monserrate Z. Abstract C61: High fat triggers oncogenic K-Ras activity and a COX2 dependent feed-forward loop to induce pancreatic ductal adenocarcinoma development. American Association for Cancer Research, 2013, 6, C61.

107. Pietrocola F, Galluzzi L, Bravo-San Pedro JM, Madeo F, Kroemer G. Acetyl coenzyme A: a central metabolite and second messenger. Cell. Metab. 2015, 21, 805–821.

108. Porporato PE, Filigheddu N, Bravo-San Pedro JM, Kroemer G& Galluzzi L. Mitochondrial metabolism and cancer. Cell Res. 2018, 265–280.

109. Porta M, Fabregat X, Malats N, Guarner L, Carrato A, de Miguel A, Ruiz L, Jariod M, Costafreda S, Coll S, Alguacil J, Corominas JM, Solà R, Salas A, Real FX. Exocrine pancreatic cancer: symptoms at presentation and their relation to tumour site and stage. Clin. Transl. Oncol. 2005, 7(5), 189-197.

110. Prigione A, Rohwer N, Hoffmann S, Mlody B, Drews K, Bukowiecki R, et al. HIF1alpha modulates cell fate reprogramming through early glycolytic shift and upregulation of PDK1-3 and PKM2. Stem Cells. 2014, 32, 364–376.

111. Puebla-Osorio N, Kim J, Ojeda S, Zhang H, Tavana O, Li S, et al. A novel Ku70 function in colorectal homeostasis separate fromnonhomologous end joining. Oncogene. 2014, 33, 2748–2757.

112. Rahib L, Smith BD, Aizenberg R, Rosenzweig AB, Fleshman JM, Matrisian LM. Projecting cancer incidence and deaths to 2030: the unexpected burden of thyroid, liver, and pancreas cancers in the United States. Cancer Res. 2014, 74(11), 2913-2921

113. Rao CV and Mohammed A. New insights into pancreatic cancer stem cells. World. J. Stem Cells. 2015, 7(3), 547-55.

114. Rasheed ZA, Yang J, Wang Q, Kowalski J, Freed I, Murter C, Hong SM, Koorstra JB, Rajeshkumar NV, He X, Goggins M, Iacobuzio-Donahue C, Berman DM, Laheru D, Jimeno A, Hidalgo M, Maitra A, Matsui W. Prognostic significance of tumorigenic cells with mesenchymal features in pancreatic adeno-carcinoma. J. Natl. Cancer Inst. 2010, 102, 340–351.

115. Renehan AG, Tyson M, Egger M, Heller RF, Zwahlen M. Body-mass index and incidence of cancer: a systematic review and meta-analysis of prospective observational studies. Lancet. 2008, 371(9612), 569-78.

116. Rhim AD, Mirek ET, Aiello NM, Maitra A, Bailey JM, McAllister F, Reichert M, Beatty GL, Rustgi AK, Vonderheide RH, Leach SD, and Stanger BZ. EMT and Dissemination Precede Pancreatic Tumor Formation. Cell. 2012, 148, 349–361.

117. Rohrig F, Schulze A. The multifaceted roles of fatty acid synthesis in cancer. Nat. Rev. Cancer 2016, 16, 732–749.

118. Sabharwal SS, Schumacker PT. Mitochondrial ROS in cancer: initiators, amplifiers or an Achilles' heel? Nat. Rev. Cancer 2014, 14, 709–721.

119. Salem AA, Mackenzie GG. Pancreatic cancer: A critical review of dietary risk. Nutr .Res. 2018, 52, 1-13.

120. Sana TR, Waddell K, Fischer SM. A sample extraction and chromatographic strategy for increasing LC/MS detection coverage of the erythrocyte metabolome. J. Chromatogr. B Anal. Technol. Biomed. Life Sci. 2008, 871, 314–321.

121. Sancho P, Barneda D, Heeschen C. Hallmarks of cancer stem cell metabolism. Br. J. Cancer. 2016, 114(12), 1305-12.

122. Santos CR, Schulze A. Lipid metabolism in cancer. FEBS J. 2012, 279(15), 2610-23.

123. Schulze A, Harris AL. How cancer metabolism is tuned for proliferation and vulnerable to disruption. Nature 2012, 491, 364–373.

124. Sheahan AV, Biankin AV, Parish CR, Khachigian LM. Targeted therapies in the management of locally advanced and metastatic pancreatic cancer: a systematic review. Oncotarget. 2018, 9(30),21613-21627.

125. Shen YA, Wang CY, Hsieh YT, ChenYJ, Wei YH. Metabolic reprogramming orchestrates cancer stem cell properties in nasopharyngeal carcinoma. Cell Cycle 2015, 14, 86–98.

126. Shi C, Hruban RH, Klein AP. Familial pancreatic cancer. Arch Pathol. Lab. Med. 2009, 133(3), 365-74.

127. Shian SG, Kao YR, F.Y Wu, Wu C.W. Inhibition of invasion and angiogenesis by zinc-chelating agent disulfiram. Mol. Pharmacol. 2003, 64, 1076–1084.

128. Shilov IV, Seymour SL, Patel AA, Loboda A, Tang WH, Keating SP, et al., The paragon algorithm, a next generation search engine that uses sequence temperature values and feature probabilities to identify peptides from tandem mass spectra, Mol. Cell. Proteomics 2007, 6, 1638–1655.

129. Siegel RL, Miller KD, Jemal A. Cancer statistics. Cancer J. Clin. 2016, 66,7–30.

130. Son J, Lyssiotis CA, Ying H, Wang X, Hua S, Ligorio M, et al. Glutamine supports pancreatic cancer growth through a KRAS-regulatedmetabolic pathway. Nature. 2013, 496, 101–105.

131. Spaderna S, Schmalhofer O, Hlubek F, Jung A, Kirchner T, Brabletz T. Epithelial-mesenchymal and mesenchymal-epithelial transitions during cancer progression. Verh. Dtsch. Ges. Pathol. 2007, 91, 21-8.

132. Stark A, Eib G. Pancreatic Ductal Adenocarcinoma. Pancreapedia: Exocrine Pancreas Knowledge Base. 2015.

133. Steeg PS. Targeting metastasis, Nat. Rev. Cancer 2016, 16(4), 201–218.

134. Sumner LW, Mendes P, Dixon RA.Plant metabolomics: Large-scale phytochemistry in the functional genomics era. Phytochem. 2003, 62, 817– 836.

135. Sunami Y, Rebelo A, Kleeff J. Lipid Metabolism and Lipid Droplets in Pancreatic Cancer and Stellate Cells. Cancers (Basel). 2017, 10(1), 3.

136. Swierczynski J, Hebanowska A, Sledzinski T. Role of abnormal lipid metabolism in development, progression, diagnosis and therapy of pancreatic cancer. World J Gastroenterol. 2014, 20(9), 2279-303.

137. Taguchi R, Hayakawa J, Takeuchi Y, Ishida M. Two-dimensional analysis of phospholipids by capillary liquid chromatography/electrospray ionization mass spectrometry. J Mass Spectrom. 2000, 35, 953–966.

138. Tang WH, Shilov IV, Seymour SL. Nonlinear fitting method for determining local false discovery rates from decoy database searches. J. Proteome Res. 2008, 7, 3661–3667.

139. Tenori L, Oakman C, Claudino WM, et al. Exploration of serum metabolomic profiles and outcomes in women with metastatic breast cancer: a pilot study. Mol Oncol. 2012, 6(4), 437-44.

140. Tomita M, Kami K. Cancer. Systems biology, metabolomics, and cancer metabolism. Science. 2012, 336(6084), 990-1.

141. Torchilin V. Antibody-modified liposomes for cancer chemotherapy. Expert Opin. Drug Deliv. 2008, 5, 1003–1025.

142. Tucker ON, Dannenberg AJ, Yang EK, Fahey III TJ. Bile acids induce cyclooxygenase-2 expression in human pancreatic cancer cell lines. Carcinogenesis. 2004, 25, 419–23.

143. Ulmer CZ, Yost RA, Chen J, Mathews CE and Garrett TJ. Liquid Chromatography-Mass Spectrometry Metabolic and Lipidomic Sample Preparation Workflow for Suspension-Cultured Mammalian Cells using Jurkat T lymphocyte Cell. J Proteomics Bioinform. 2015, 8, 6.

144. Upadhyay M, Samal J, Kandpal M, Singh OV, Vivekanandan P. The Warburg effect: insights from the past decade. Pharmacol. Ther. 2013, 137(3), 318-30.

145. Valcourt JR, Lemons JM, Haley EM, Kojima M, Demuren OO, Coller HA. Staying alive: metabolic adaptations to quiescence. Cell Cycle. 2012, 11(9), 1680-96.

146. Valle S, Martin-Hijano L, Alcalá S, Alonso-Noceloand M, Sainz Jr B. The Ever-Evolving Concept of the Cancer Stem Cell in Pancreatic Cancer. Cancers 2018, 10, 33.

147. Vigneau-Callahan KE, Shestopalov AI, Milbury PE, Matson WR, Kristal BS. Characterization of diet-dependent metabolic serotypes: analytical and biological variability issues in rats. J Nutr. 2001, 131(3), 924S-932S.

148. Villas-Boˆas SG, Mas S, kesson MA, Smedsgaard J and, Nielsen J. Mass spectrometry in metabolome analysis. Mass Spectrom Rev. 2005, 24(5), 613-46.

149. Visvader JE, Lindeman GJ. Cancer stem cells: current status and evolving complexities. Cell Stem Cell. 2012, 10, 717–728.

150. Wang B, Rong X, Palladino END, Wang J, Fogelman AM, Martín MG, Tontonoz P. Phospholipid Remodeling and Cholesterol Availability Regulate Intestinal Stemness and Tumorigenesis. Cell Stem Cell. 2018, 22(2), 206–220.

151. Wang H, Agarwal P, Zhao S,. Xu RX, Yu J, Lu X, He X. Hyaluronic acid-decorated dual responsive nanoparticles of Pluronic F127, PLGA, and chitosan for targeted co-delivery of doxorubicin and irinotecan to eliminate cancer stem-like cells. Biomaterials. 2015, 72, 74–89.

152. Wang ML, Chiou SH, Wu CW. Targeting cancer stem cells: emerging role of Nanog transcription factor. Onco Targets Ther. 2013, 6, 1207-20.

153. Wang T, Fahrmann JF, Lee H, Li YJ, Tripathi SC, Yue C, Zhang C, Lifshitz V, Song J, Yuan Y, et al. JAK/STAT3-regulated fatty acid beta-oxidation is critical for breast Cancer stem cell self-renewal and Chemoresistance. Cell Metab. 2018, 27(1), 136–50.

154. Wanyin Chen, Jihu Dong, Jacques Haiech, Marie-Claude Kilhoffer, and Maria Zeniou. Cancer Stem Cell Quiescence and Plasticity as Major Challenges in Cancer Therapy. Hindawi Publishing Corporation Stem Cells Int. Volume 2016, 1-16.

155. Warita K, Warita T, Beckwitt CH, Schurdak ME, Vazquez A, Wells A, et al. Statininduced mevalonate pathway inhibition attenuates the growth of mesenchymallike cancer cells that lack functional E-cadherin mediated cell cohesion. Sci. Rep. 2014, 4, 7593.

156. Wehbe M, Anantha M, Backstrom I, Leung A, Chen K, Malhotra A, Edwards K, Bally MB. Nanoscale reaction vessels designed for synthesis of copper-drug complexes suitable for preclinical development, PLoS One 2011, 11, e0153416.

157. Wehbe M, Anantha M, Shi M, Leung AW, Dragowska WH, Sanche L, Bally MB. Development and optimization of an injectable formulation of copper diethyldithiocarbamate, an active anticancer agent. Int. J. Nanomedicine. 2017, 12, 4129–4146.

158. Weiswald LB, Bellet D, Dangles-Marie V. Spherical cancer models in tumor biology. Neoplasia. 2015, 17(1), 1-15.

159. Wolin KY, Carson K, Colditz GA. Obesity and cancer. Oncologist. 2010, 15(6), 556-65.

160. World Cancer Research Fund/American Institute for Cancer Research. Food, Nutrition, Physical Activity, and the Prevention of Cancer: a Global Perspective. Washington DC: AICR, 2007.

161. Woutersen RA, Appel MJ, van Garderen-Hoetmer A, Wijnands MV. Dietary fat and carcinogenesis. Mutat. Res. 1999, 443, 111–27.

162. Xie D, Xie K. Pancreatic cancer stromal biology and therapy. Genes Dis. 2015, 2(2), 133-143.

163. Yachida S, White CM, Naito Y, et al. Clinical significance of the genetic landscape of pancreatic cancer and implications for identification of potential long-term survivors. Clin. Cancer. Res. 2012, 18(22), 6339-47.

164. Yi M, Li J, Chen S, Cai J, Ban Y, Peng Q, Zhou Y, Zeng Z, Peng S, Li X, Xiong W, Li G, Xiang B. Emerging role of lipid metabolism alterations in Cancer stem cells. J. Exp. Clin. Cancer Res. 2018, 37(1), 118.

165. Yin T, Wei H, Gou S, Shi P, Yang Z, Zhao G, & Wang C. Cancer stem-like cells enriched in Panc-1 spheres possess increased migration ability and resistance to gemcitabine. Int. J.Mol.Sci. 2011, 12(3), 1595-604.

166. Yu Z, Pestell TG, Lisanti MP, Pestell RG. Cancer stem cells. Int. J.Biochem. Cell. Biol. 2012, 44(12), 2144-51.

167. Zaidi N, Lupien L, Kuemmerle NB, Kinlaw WB, Swinnen JV, Smans K. Lipogenesis and lipolysis: the pathways exploited by the cancer cells to acquire fatty acids. Prog Lipid Res 2013, 52, 585-589.

168. Zaytseva YY, Rychahou PG, Gulhati P, Elliott VA, Mustain WC, O'Connor K, et al. Inhibition of fatty acid synthase attenuates CD44-associated signaling and reduces metastasis in colorectal cancer. Cancer Res. 2012, 72, 1504–1517.

169. Zhang A, Sun H, Yan G, Wang P, Wang X. Metabolomics for Biomarker Discovery: Moving to the Clinic. Biomed. Res. Int. 2015, 2015, 354671.

170. Zhao X, Gao S, Ren H, Sun W, Zhang H, Sun J, et al., Hypoxia-inducible factor-1 promotes pancreatic ductal adenocarcinoma invasion and metastasis by activating transcription of the actin-bundling protein fascin. Cancer Res. 2014, 74, 2455–2464.

Acknowledgments

Firstly, I would like to express my gratitude to my advisor Prof. Lello Zolla who gave me permission to work in his laboratory and to use the facilities available for my research. Special words of thanks should also go to my research co-guides Prof.ssa Timperio Anna Maria and Prof.ssa Rinalducci Sara for the continuous support of my Ph.D. Their guidance helped me in all the time of research and writing of this thesis.

I am grateful to Dott.ssa Gevi Federica for introducing me to this exciting field of science and for her dedicated help, advice and continuous encouragement throughout my Ph.D. I thank my fellow lab mates, Dott.ssa Michaletti Anna, Dott. Belardo Antonio, Dott.ssa Lelli Veronica and my colleague/friend Dott. Balzerano Alessio for the stimulating discussions, support and for all the fun we have had in the last four years. Their constant support has always kept me going.

My gratitude also goes to Prof.ssa Palmieri Marta and her research group and for accepting to collaborate with us. A very special thanks goes out to Dot.ssa Dando Ilaria for all help and suggestions during my thesis. I am grateful for your help both at professional and personal levels.

I would like to thank Prof.ssa Roberta Cimmaruta for their guidance and for carefully coordinating the XXXI PhD course.

I would like to thank my family: my parents and Loretta, Roberto, Francesco Irene for supporting me for everything and especially I can't thank you enough for encouraging me throughout this experience. I would like to thank my niece Francesca, for the joy she brought to my family. This accomplishment would not have been possible without them. Thank you. I would also like to thank all my relatives, my grandmother, my mother-in-law, nieces and nephew, uncles, cousins, the brothers-in-law and friends for always being close to me.

Last but not the least, I would like to express my special thanks to my boyfriend Giacomo and in this case there is no need to add anything else!

Giuseppina